Experimental investigation and modeling of hot machining operation using high-strength material

A THESIS SUBMITTED IN PARTIAL FULFILLMENT OF THE
REQUIRMENTS FOR THE DEGREE OF

Master of Technology
(By Research)
In
Mechanical Engineering

By

SHALINI SINGH
Roll No. 611 ME 308

Department of Mechanical Engineering
National Institute of Technology
Rourkela

DEPARTMENT OF MECHANICAL ENGINEERING
National Institute of Technology
Rourkela, India
July, 2014

Experimental investigation and modeling of hot machining operation using high-strength material

A THESIS SUBMITTED IN PARTIAL FULFILLMENT OF THE
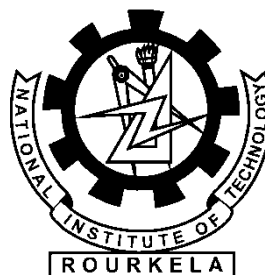REQUIRMENTS FOR THE DEGREE OF

Master of Technology
(By Research)
In
Mechanical Engineering

By

SHALINI SINGH
Roll No. 611 ME 308

Under the supervision of

Dr.K. P. Maity
Professor
Department of Mechanical Engineering
National Institute of Technology
Rourkela

DEPARTMENT OF MECHANICAL ENGINEERING
National Institute of Technology
Rourkela, India
July, 2014

National Institute of Technology
Rourkela

C E R T I F I C A T E

This is to certify that the thesis entitled *"Experimental investigation and modeling of hot machining operation using high-strength material"* submitted by **SHALINI SINGH** toNational Institute of Technology, Rourkela for the award of the degree of**Master of Technology (Research)** in *Mechanical Engineering* is anauthentic record of research work carried out by her under my guidance and supervision.

The work incorporatedin this thesis has not been, to the best of my knowledge, submitted to any other University or Institute for the award of a degree or diploma.

Dr. K. P. Maity
Professor
Department of Mechanical Engineering,
National Institute of Technology
Rourkela

Acknowledgement

Abstract

High strength work materials have tremendous applications in the field of aerospace, nuclear, biomedical, automotive, etc. It is a challenging task to machine these high strength materials. Costly cutting tools are required to machine those materials. Hot machining is another alternative approach for hot machining those hard material using low cost cutting tools. Basic concept behind the hot machining is to soften the material by heating technique which reduces the shear strength of the workpiece as well as reduces the forces required to machine the workpiece at the time of machining. In the present investigation, experimental investigation of hot machining operation has been carried out using flame heating for machining high manganese steel using ordinary carbide insert.

Hot machining operation has been investigated to study the advantages of hot machining operation over conventional machining operation. Tool wear, surface roughness, chip reduction coefficient, tool life and power consumption have been measured as per the design of response surface methodology technique. This technique has been used to determine the optimum conditions for the desired responses (minimum tool wear, minimum surface roughness, minimum chip reduction coefficient, minimum power consumption and maximum tool life). Principal component analysis (PCA) coupled with Grey relational analysis (GRA) and weighted principal component analysis (WPCA) have been used for optimizing the multi-performance characteristics. WPCA has been proved to provide better results as compared to PCA coupled with GRA with the help of confirmatory test. Fuzzy TOPSIS approach has been used for optimizing performance characteristics namely, tool life and power consumption. It has been proved that Fuzzy TOPSIS is an alternative approach for practical based problems using the decisions that have been taken by decision maker based on experience and skill. FEM modelling has been carried out to determine temperature at the chip/tool interface and validated by experimental results.

Contents

List of tables

List of Figures

List of Acronyms

HM	Hot machining
TW	Tool wear
TL	Tool life
P	Power consumption
T	Temperature
V	Cutting speed
f	Feed rate
d	Depth-of-cut
gm	Gram
RSM	Response surface methodology
CCD	Central composite design
C+	Closeness Coefficient Index
ANOVA	Analysis of Variance
DF	Degree of freedom
FPIS	Fuzzy Positive Ideal Solution
FNIS	Fuzzy Negative Ideal Solution
GRA	Grey relational analysis
HTB	Higher-The-Better
LTB	Lower-The-Better
NTB	Nominal-The-Better
PCA	Principal Component analysis
PCS	Principal Component Scores
PCBN	Polycrystalline Cubic Boron Nitride
PPI	Process Performance Index
TOPSIS	Technique for Order of Preference by Similarity to Ideal Solution
FMADM	Fuzzy Multi Attribute Making Decision
FEM	Finite element method
ANN	Artificial Neural Network
SEM	Scanning Electron Microscope
S/N	Signal-to-Noise

MPCI	Multi Performance Criteria Index
MPI	Multi-response Performance Index
OQPI	Overall Quality Performance Index
WPCA	Weighted Principal Component Analysis
NORM	Normalized value
v1 and v2	weighted normalized value
V+ and V-	ideal and negative ideal solution
SCEA	Side cutting edge angle
BR	Back rake angle
SR	Side rake angle
HAZ	Heat affected zone
X_{def}	FEM results
X_{exp}	Experimental results

List of Nomenclatures

Ra	Surface roughness
t_2	Deformed chip thickness
ξ	Chip reduction coefficient
r	Nose radius
C+	Closeness coefficient
ζ	Distinguishing coefficient
λ	Inclination angle
γ_0	Orthogonal rake angle
ϕ_e	End clearance angle
ϕ	Side clearance angle
α_0	Auxiliary cutting edge angle
$\alpha_0{}'$	Principal/ side cutting edge angle
α_T	Thermal diffusivity
K_T	Thermal conductivity
ρ	Material density
Cp	heat capacity
T∞	medium temperature
h	Heat transfer coefficient
σ	Flow stress
$\dot{\varepsilon}_0$	Strain rate
θ	Absolute temperature
θ_R	Room temperature
θ_m	Mean temperature
τ	Frictional stress
μ	Coefficient of friction
σ_n	Normal stress
HRC	Rockwell Hardness measured on the C scale
SNMG	Square, zero clearance angle, thickness with cylindrical shape hole

Chapter 1

Introduction

Chapter 1

Introduction

1.1   Background

The materials having high tensile strength and wear resistance such as temperature resisting alloys, high manganese steel, Inconel, quenched steels, etc., which have wide applications in aerospace, nuclear industries, missile industries, etc., are usually difficult to machine. Machining of these high strength materials by conventional methods has to face many problems such as high tool wear, low surface finish, and high power consumption. As a result it increases the cost of manufacturing. To avoid mentioned problems, the costly cutting tools such as ceramic, cubic boron nitride, cermet, etc. are used. The cost of machining increases because of costly tools. Softening of workpiece by heating the workpiece is another alternative approach. The machining can be carried out using low costly cutting tools. The machining becomes economical.

From industrial point of view, the most important aspect of metal cutting is machinability and its influence on the economics of the manufacturing [1]. There are many methods to enhance the machinability of difficult to cut the materials by employing ramping technique, high pressure coolant supply technology, cryogenic machining, use of self-propelled rotary tooling and hot machining [2]. Researchers focussed on improved cutting tools for enhancing machinability of such high strength materials, smoothness of the product, cost of operation and performances.

Hot machining is a suitable method to machine hard workpiece material with high surface quality and good machinability. The main aim of hot machining is to facilitate an effective and easier machining method. The machining of workpiece at elevated temperature using ordinary tool is more effective approach than machining with high strength cutting tools [3]. The basic principle behind hot machining is the reduction in hardness of workpiece material leading to reduction in the component force, with improvement in surface finish and tool life [2]. In hot machining operation workpiece (S355) has been heated above recrystallization temperature where the yields stress of

materials decreased rapidly [2]. The heating gas flame is used to raise the temperature of the workpiece material.
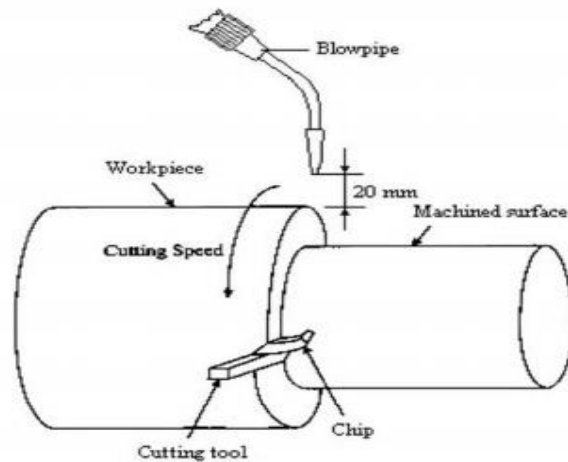
Figure. 1.1 A schematic view of the turning operation [3]

There are many heating techniques such as gas flame heating, arc heating, electric resistance heating, etc. for hot machining operation having their own importance for softening of workpiece material. In different ways these heating techniques affect properties such as micro structure, micro hardness, etc. The use of heating techniques depends on the shape and size of the workpiece materials, cost restriction and accuracy requirement. There are many processes used by industries, among them plasma heating and gas flame heating are the most used methods instead of induction heating, electric resistance heating, etc. [4]. The special features of different heating techniques are given as follows:

(a) Gas flame heating: In this technique, oxygen and LPG is used in an appropriate ratio for concentrated flame on the workpiece material. The set up required for this technique is inexpensive for small jobs. Transfer of energy is also low. But it will be inappropriate for the large size workpiece for large shear zone.

(b) Arc heating: Arc heating can supply high specific heat input. The heat produced is not very constant. It may be hazardous for operator. Its initial set up cost is very high. Maximum temperature range is upto 20,000 K can be generated. Due to high supply of heat, the machining of high speed and depth of cut are possible.

(c) Furnace heating: It is the simplest and cheapest technique with respect to other heating techniques. For machining, a furnace is required at a constant temperature

and the workpiece material is heated inside it, until the workpice attains same temperature. Then the workpiece material is kept out for machining.

(d) Resistance heating: In this heating technique, the workpiece and tool is connected to anode and cathode respectively. The current is supplied to the workpiece material. The potential difference between the tool and workpiece produces same amount of heat for heating the workpiece material. The temperature obtained is limited which is not damaging the bulk material.

(e) Inductive heating: The workpiece materials should be magnetic and is based on transformer action concept. Localisation of heat is not difficult except intrinsic shape workpiece. The set up used for induction heating is relatively costly.

(f) Friction heating: This heating technique is very useful for large shape of workpiece but cannot used for intricate workpiece. Its initial set up cost and maintenance cost are low.

(g) Radio-frequency resistance heating: This heating technique used over a small area. It provides high specific heat and fast temperature rise. Its initial cost as well as maintenance cost is high.

1.2   Working principle of hot machining operation

Hot machining is a process in which workpiece has to be heated below recrystalization temperature [5] but in some cases it has been also heated above recrystalization temperature [6]. High manganese steel and other high wear resistance alloys which are widely used for various applications are having high strain hardening property. The work hardening works on the dislocation phenomenon, which seizes further dislocations and makes the material hard. Hot machining delivers good surface finish with hardening property.

The hot machining operation is based on the softening phenomenon at the vicinity of shear zone (deformation zone). Softening of workpiece at the deformation zone makes the material ductile (reduces shear strength) which helps to reduce cutting force and increment in surface integrity. Heating gas flame used for operation should be in a constant manner, which delivers same temperature throughout the workpiece material. Heating can be done prior or at the time of machining. For constant temperature, the blowpipe should move with the tool holder [7]. The blowpipe direction should be opposite to tool holder for better heating as shown in following Figure 1.1.

There are many controlling factors such as workpiece temperature, cutting speed, feed rate, depth of cut, nose radius, cutting time, etc. which contribute on the performance characteristics. The problem arises may be due to the use of incorrect levels of control parameters such as feed, depth of cut and cutting velocity, etc. Tool life and power consumption have much contribution in cost of manufacturing. Surface finish is the most desired characteristic for good performance of product. Chip reduction coefficient is also an effective measure which evaluates the machinability. The appropriate selection of machining parameters has to be made to achieve the above machinability criteria.

1.3   Applications of hot machining (HM) operation

In general, hot machining can be applied to machine any hard material to manufacture industrial products. Due to external heat supply, the hot machining operations can be applied for different operations such as turning and milling operations [8]. High manganese steel is a potential material for hot machining operation. High manganese steel are, often used for gears, spline shafts, axles, rifle barrels, mining equipment, grinding and crushing machinery, railway track work, cement plants kiln and mill liners, stone crushers jaw and gyratory crushers and ore processing.

1.4   Objectives of the present work

1)   Experimental investigation of hot- machining operation of high-manganese steel using gas flame heating.
2)   Modelling of optimization criteria of hot-machining operation using response surface methodology.
3)   Modelling of hot-machining operation using PCA and WPCA operation.
4)   Modelling of hot-machining operation using fuzzy-TOPSIS.
5)   FEM modelling for prediction of temperature distribution and validated with experimental result.

1.5   Organization of the thesis

The thesis consists of seven chapters. The introduction of thesis and literature is briefly described in Chapter 1. The experimental details have been described in Chapter 2. Chapter 3 discuss the study of influence of the process parameters on the performance characteristics (tool wear, surface roughness, chip reduction coefficient,

tool life and power) with the help of ANOVA test and modelled equations. The influence of the process parameters using the PCA and WPCA in achieving the machinability criteria has been discussed in Chapter 4. The influence of the process parameters has been discussed using Fuzzy TOPSIS in Chapter 5. The prediction of interface temperature using FEM modelling with validations has been described in Chapter 6. Summary of the present work and points to possible directions for future work have been mentioned in Chapter 7.

1.6 Literature Survey

Shah and Gelot [9] have presented a review on the hot machining operation and mentioned application for hot machining operation. They mentioned importance to study the temperature at chip/tool interface. Dawami and Zadshakoyan [2] have conducted experiment on AISI 1060(45 HRC) material with uncoated TNNM 120608 SP10 tool by keeping all the cutting parameters constant. He analysed better surface finish at 300 °C compared to machining at room temperature. Secondly, they analysed the temperature variation on tool by varying the cutting speed at 300 °C and at room temperature. Baili et al. [9] have applied induction heating in hot machining operation for heating Ti-5553 material for reducing mechanical properties which reduces cutting forces. They focused to enhance the machinability of Ti-5553. He observed that there is 13% reduction in cutting force at 500°C where as it reduces to 34% at 700°C. Madhavulu and Basheer Ahmed [1] investigated hot machining operation using plasma as heat source. Stainless steel 410 and other alloys are considered as work material. Kitagawa and Maekawa [10] used plasma heating technique for improving machinability of material such as pyrex, mullite, alumina, zirconia, etc. Plasma heating has been used for converting discontinuous chips to continuous chips. The tool wear was also found to be reduced. Rajopadhye et al. [11] developed an experimental set up for hot machining operation to improve the cutting tool life as well as to reduce the manufacturing cost. Fui [5] studied about hot machining operation for high manganese steel with electric heating. Prediction of tool wear has been done for evaluating tool life. The best combination of process parameters has been taken to provide improved tool life. Wang et al. [12] adopted a new approach to the machining system called hybrid machining. In this technique cryogenic cooling technique was used to reduce tool temperature. The plasma heating technique was used to heat the

workpiece material. Inconel 718 was machined using ceramic inserts (WG-308 and WG 300). There was reduction in surface roughness by 250% and improvement in tool life by 170% than that of the conventional machining operation. Liliana Popa [13] investigated turning operation by using plasma heating for heating workpiece material and observed enhancement in productivity. It was concluded that productivity increased upto 10-15 times and tensile stress was reduced about 60-70%. Deshmukh and Borkar [14] developed mathematical equation for tool life in turning operation on AISI 304 material using carbide cutting inserts. The tool life was predicted using FEM software (ANSYS) and validated with experimental result. Raczkovi [15] studied the mechanism of tool wear on the cutting tool in hard turning over grinding operation. PCBN (Poly Crystalline Boron Nitride) cutting tool has been used and modelling has been carried out for evaluation of tool life. Talib [16] investigated the effect of cutting velocity and feed rate on tool life for turning operation without using any lubricant. Tool wear is based on direct normal load occurred due to interaction between tool and workpiece. Pal and Basu [17] investigated hot machining operation of austenitic manganese steel by shaping. They developed the relationship between tool life and cutting forces with process parameters. Kuljanic [18] presented the comparisons among the tool grades and their geometries for machining high wear resistance materials. Surface roughness, chip formation and tool life were studied for special tools. Ti(C, N) was dispersed to enhance the wear resistance properties of hadfield steel. Kopac [19] discussed about the hardening phenomenon for austenitic manganese steels (12% Mn). Due to the hardening effect, microhardness in cutting zone extremely increases and influences tool life. Jeon et al. [20] discussed about different energies used for machining such as thermal machining, plasma machining, laser machining, gas/induction/furnace preheating method and cryo machining. They focussed mainly on vibration assisted machining for different types of operations.

Ranganathan et al. [21] investigated the influence of cutting parameters using Taguchi technique on tool wear for AISI 316 stainless steel at 200°C, 400°C and at 600°C. They found different parameters are significant at different levels of temperature. At 200°C cutting speed and depth of cut are significant factors, at 400°C feed and depth of cut are significant and at 600C cutting speed and depth of cur are significant. They found low value of error at 200°C and at 400°C and high value for R^2 shows significance of ANOVA table for optimization. Ranganathan and Senthilvelan [22]

conducted experiment using Taguchi design on stainless steel 316 for tool wear by varying temperature keeping other at constant level. Interaction between input factors has been discussed for tool wear using orthogonal array and ANOVA test. Regression equation has been developed for establishing the relationship between input variables and tool wear. Maity and Swain [23] used half factorial design for conducting experiments for tool life using carbide cutting tool on high manganese steel. Expression for tool life has been established from statistical technique. They concluded that the temperature is the most significant factor followed by cutting velocity, feed and depth of cut for tool life. Sahoo and Mohanty [24] applied Taguchi's quality loss function for investigating cutting force and chip reduction coefficient in turning operation. Optimal combination for process parameters has been obtained with satisfying both of the performance characteristics. Lajis et al. [25] conducted experiment in end milling of AISI D2 hardened steel for coated carbide cutting insert. They established regression equation for tool life. Mainly they focussed on machinability by avoiding catastrophic damage of tool by using coated tools and obtained overall enhancement in machinability at higher level of cutting velocity and feed. Lo and Chen [26] applied response surface methodology in hot machining operation for tool life by considering four input parameters named as speed, feed, depth of cut and direct current were applied. Finally, they mentioned that RSM provides highly precision equation for tool life which shows good co-relation between them. Fnides et al. [27] have used full factorial design for conducting experiments on AISI H11 using a mixed ceramic tool for cutting forces (axial, tangential and radial direction). Optimum condition has been obtained by using ANOVA test for the responses. It was concluded that depth of cut was the most influencing factor on the cutting forces. L. Ozler et al.[28] applied factorial regression analysis for accomplishing the experimental work for tool life of sintered carbide inserts with austenitic manganese steel. They considered the cutting parameters named as surface temperature, cutting speed, feed and depth of cut for investigation. It was noticed that as the cutting speed increased tool life decreased. At 600 °C surface temperature, tool life was found maximum as the workpiece material became ductile. It was noticed that as the feed rate increased tool life decreased. Nihat Tosun et al. [29] evaluated mathematical equation for tool life by using regression analysis method and tool life was also estimated by Artificial neural network with back propagation algorithm. Both

experimental result and estimated ANN result was compared. It was found that ANN result was better. Rai et al. [30] conducted experiment on end milling in CNC machine for investigating the effect of cutting parameters on the AISI D2 hardened steel of (52-62 HRC) with TiAlN coated carbide inserts. They found less tool wear and good surface finish at the preheating condition and improvement in machinability by preventing catastrophic damage to tool at higher levels of cutting speed and feed. They predicted surface roughness model by the use of artificial neural network (ANN). They concluded that ANN predicted accurate results. Lajis et al. [31] investigated the effect of induction heating on the surface integrity (microhardness and work hardening). For analysis they varied feed, velocity and pre heating temperature while keeping depth of cut constant. Ranganathan et al. [32] conducted experiments on AISI 316 using carbide tool for surface roughness at 200 °C, 400 °C and at 600 °C. The good fitting has been obtained between the RSM and ANN predicted results with experimental results. Ranganathan et al. [33] accomplished their experiment in hot machining in order to determine tool life and material removal rate of stainless steel (type 316). They applied grey relational analysis (GRA) with Taguchi technique. It was revealed that feed and cutting speed were the dominating factors on multi performance analysis. GRA improved the grey relation of the optimal combination of cutting parameters. Chakravorty et al.[34] discussed about PCA with many different approaches such as GRA, PQLR, TOPSIS and WPC over PCA. They compared the optimal setting for different cases with mentioned approaches. Pradhan [35] investigated tool wear, materials removal rate and radial overcut on AISI D2 tool steel using GRA coupled with PCA. Confirmation test has been done for validating the optimal setting obtained from analysis. Siddique et al.[36] used GRA coupled with PCA for optimizing the cutting parameters in centerless cylindrical grinding. They used L9 orthogonal array for designing the experimental runs. Confirmation test had been done for validating the optimal combination obtaining from the analysis. Lu et al. [37] had optimised the cutting parameters for high speed end milling using GRA coupled with PCA. Confirmation test was carried out for validating the optimal combination obtained for cutting parameters using proposed approach. Tosun and Ozler [38] used the S/N ratio features for obtaining the optimal combination for tool life and surface roughness simultaneously. They used M20 as cutting tool with high manganese steel as workpiece. Olson [39] gave comparison between the results

obtained from weights given in TOPSIS with that of the results obtained from multi attribute technique Sequential Multiple Assignment Randomized Trial (SMART). Wimatsari et al. [40] studied on FMADM (Fuzzy Multi Attribute Making Decision) with TOPSIS on system of scholarships selection for the best alternative. The four criteria considered are as Grade Point Average, income of parents, usage of electrical power and student activities. The maximum value of closeness coefficient is 1 which shows the selected alternative. Jiang et al.[41] used TOPSIS with Group Brief MCDM approach for best alternative and compared with Evidential reasoning approach. Chamodrakas et al. [42] implemented a new class of Fuzzy TOPSIS approach to handle the problem of uncertainty in customer evaluation field. The best solution was having the least distance from ideal solution and the farthest distance from negative ideal solution. Holland [43] described the basics of principal component analysis (PCA). He discussed about the uncorrelation between two axes/vectors which was due to the rotation of the axes. Reduction of data concept was based on the variation of the data.

Xu et al. [44] investigated the effect of cutting parameters on cutting forces using AISI 52100-type bearing steel of hardness 61 HRC in hot machining operation using electric heating technique. The experimental results have been compared with the simulation results in ANSYS. The simulation results have been validated with the experimental results. Tamizharasan et al.[45] investigated the effects of different types of tool geometry for turning operation with multi-responses such as interface temperature, interface pressure, wear depth and cutting forces through FEM analysis. Insert DCMG 15 04 08 with 7^0relief angle and 0.8 mm nose radius was the most optimum condition for workpiece material AISI 1045 steel. Tanase et al. [46] optimized the process parameters on the responses such as productivity, tool wear and residual stresses in turning operation. It was discussed that temperature generation at the cutting operation and so considered thermal phenomenon in the FEM analysis. The flank wear will be less at higher cutting velocity with low feed. Coefficient of friction between chip and rake face depended on the cutting speed, feed and depth of cut. Dissipation of heat generation in primary shear zone was responsible of the less temperature of workpiece material compared to the chip temperature. Bhoyar et al. [47] studied about the cutting force, specific energy and adequate temperature occurring at the chip/tool interface and coating boundary. J. G. Hendri et al. [48]

studied cutting process and chip formation in turning operation. The effect of tool geometry and cutting speed has been studied on the stress and temperature variation in turning operation of AISI 1045 through FEM simulation. Ezilarasan et al. [49] used the FEM software for analysing thermal and mechanical loads such as tangential cutting force, stress, strain, temperature at tool tip at the time of machining for Nimonic C-263super alloy. Simulations have been done according to the designed runs of orthogonal array. Validations of the simulated results have been done with the experimental results by considering 6% error in result. Ghodam [50] used FEM analysis for predicting temperature at the tool chip interface and validated with experimental result. He used thermocouple for measuring temperature at the tool chip interface. Komanduri and Hou [51] discussed some of the temperature measuring techniques while heating the workpiece material such as embedded thermocouple, dynamic thermocouples, thin film thermocouple, transverse thermocouple technique and infrared photographic technique with their applications. Huang and Liang [52] studied for temperature distribution at chip tool interface according to the designed runs. The study has been done by assuming uniform heat partition for the primary shear zone and non-uniform heat partition for secondary shear zone. Adiabatic boundary condition was assumed along chip back side and tool flank face. The validation of the simulated results was done with experimental result. The effects of the interaction between primary and secondary boundary condition on the chip –tool interface was studied. Klocke and Kratz [53] used FEM analysis to determine cutting force and temperature distribution at the tool edge. It resulted that the tool edge modification is an effective approach to obtain surface finish and high materials removal rate. Comparison has been done for validating simulations with the experimental result. Uhlmann et al. [54] studied about segmented chip occurred in Inconel 718 in turning operation by using FEM software. They investigated about stress, strain, temperature distribution. The results obtained from 2D and 3D simulations are well correlated with the experimental results. Yaseen [55] used FEM software for study of temperature distribution and heat flux for transient condition in turning operation. The effect of cutting variables on responses has been investigated. The analysis has been done according to designed runs and the simulated results were validated with the experimental results. Abhang and Hameedullah [56] predicted chip tool interface temperature by using FEM analysis and validated result with

experimental work. Cutting speed, feed and depth of cut are considered for analysis. The temperature measurement was calibrated by using thermocouple technique. The analysis has been done by using factorial design technique. Kawi [57] carried out 3D model for temperature behaviour on AISI 1045, AISI 1030, AISI 4340 and AISI 4140. Polynomial models of third, fourth and fifth orders were studied and studied that maximum temperature at nodes for any operating condition. The validation has been done by comparing simulated result with experimental results. Grzesik et al. [58] determined cutting forces, specific cutting energy and temperature distribution using Thirdwave Advant Edge FEM software for coated and uncoated tools. They also discussed about how friction is effecting temperature distribution at the interface zone. Comparison has been done for simulation result with the experimental result.

Petru et al. [59] have done investigation on micro-structure and micro-hardness for high speed steel ASP 2023 in high speed milling operation. It was noticed that microhardness value increases in high speed milling. Che-Haron and Jawaid [58-4] investigated surface integrity (surface roughness, microhardness and workhardening) of rough machining of Titanium alloy with uncoated tools. Machining is carried out at four different cutting speeds, at constant depth of cut 2.0mm and feed rates at 0.35 and 0.25mm/rev. It has been concluded that higher microhardness at distance 0.01mm from machined surface than at 0.02mm. The highest microhardness obtained at 0.005mm from machined surface. Thakur et al. [60] conducted experiments to study the effect of the process parameters on the microhardness and microstructure of the Inconel 718 in dry turning operation on machinability. Autenrieth et al. [61] studied about properties of AISI 1045 steel with the use of X-ray diffraction, microscopy and microhardness testing. The effect of cutting tool edges concluded to addition of process inherent to the machining processes such as built up edges. Sarikaya [62] used spraying distance, substrate temperature and coating thickness with Al2O3 coatings for analysing the effects of properties of the coatings (hardness, porosity and surface roughness). It was concluded that with increase in the coating layer of Al_2O_3 the hardness value for material as well as its porosity decreases. Jaiswal [63] investigated for microhardness affected from process parameters in submerged arc welding (SAW). It was concluded that with the increase in number of passes of welding, it would decrease the microhardness of the weld metal area as well as heat affected zone. Alrabi and Zumot [64] investigated about microhardness for medium carbon

steel using HSS tools effecting with cutting parameters. It was found that microhardness of chip increases with increase in depth of cut. Microhardness increases upto a certain level with increase in speed and feed rate after that it decreases. Krolczyk et. al., [65] investigated about microhardness DSS after turning operation at different cutting speeds. It was concluded that with the increase in speed microhardness of the material is going to be decreased. Increasing the roundness of the cutting tool increases the microhardness of the material.

It is evident from the literature review that the different aspects of the hot machining have been investigated. It seems that inadequate work has been reported in the field of multi response optimization, multi response optimization has been carried out to determine optimum process parameters in hot machining operation.

Chapter 2

Experimental investigation

2.1 Introduction

High manganese steel is a high strength material. It is very difficult to machine this material at room temperature. The costly cutting tool of high hardness is required to machine this material. By heating the material to elevated temperature, the material can easily be machined. The temperature acts as an additional variable with other cutting variables. In the present investigation, the experimental investigation of hot machining operation of high manganese steel has been carried out with gas flame heating using response surface methodology (RSM). The optimization of the process parameters has been carried out to enhance tool life and to reduce the tool wear, surface roughness, chip reduction coefficient and cutting power.

2.2 Experimental Set up for hot machining

The experiments were accomplished on a three jaw chuck centre lathe machine at Central Workshop of NIT Rourkela. The schematic diagram of the experimental set-up is shown in Figure 2.1. The diameter and length of workpiece are taken as 50mm and 450 mm respectively. The hardness of the workpiece material was measured to be 42 HRC. The insert SNMG 120MG120408 of grade TTR 08 was used as cutting tool for machining. The photograph of the experimental set-up is given in Figure 2.2. The oxygen and LPG are combinedly used for heating. A heating arrangement with automatic temperature controller has been retrofitted with the lathe machine. A mechatronic system has been developed to control the heating arrangement.

The temperature of the workpiece was controlled by automatic movement of the flame torch. The temperature of the workpiece is set to a fixed temperature in a temperature controlling unit. The experiment was performed by keeping 20 mm distance between the gas nozzle and workpiece for heating the workpiece. When the temperature of the workpiece falls below the set temperature, flame torch moves towards to the workpiece. When temperature of workpiece material will reach to the set value, gas nozzle will automatically moves away from the workpiece so that it can maintain the

temperature of workpiece. The maximum movement of the torch is controlled by the limit. The turning operation has been sequentially run for each run. Measurement of tool wear was examined by measuring the flank wear using the Tool maker Microscope. The roughness of the workpiece was measured by Talysurf (Model-Taylor Hobson, Surtronic 3+). The chip reduction coefficient was evaluated by ratio of deformed chip thickness to undeformed chip thickness as described earlier. All the measured values are given in Table 2.7 and Table 2.8. The temperature of the workpiece is sensed by the thermocouple (Nickel − Chromel). The thermocouple is connected to the digital display unit (Figure 2.7). The composition of the workpiece (Figure 2.3) and the specification of insert (Figure 2.4) with holder are given in Table 2.1 and Table 2.2 respectively. The geometry of the cutting insert is shown in Table 2.3.
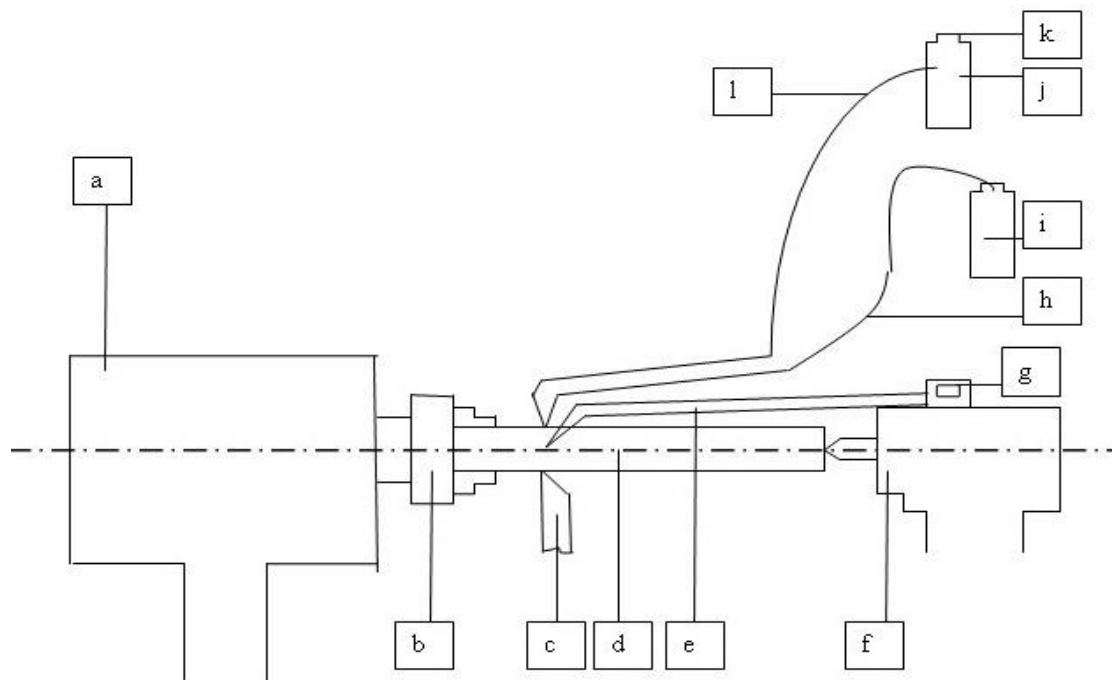
Figure 2.11 Schematic diagram for experimental setup

(a) Lathe head stock (b) Chuck (c) Cutting tool (d) Workpiece (e) Thermocouple wire (f) Tail stock (g) Temperature indicator (h) LPG pipe (i) LPG cylinder(j) Oxygen cylinder (k) Oxygen flow valve (l) Oxygen pipe
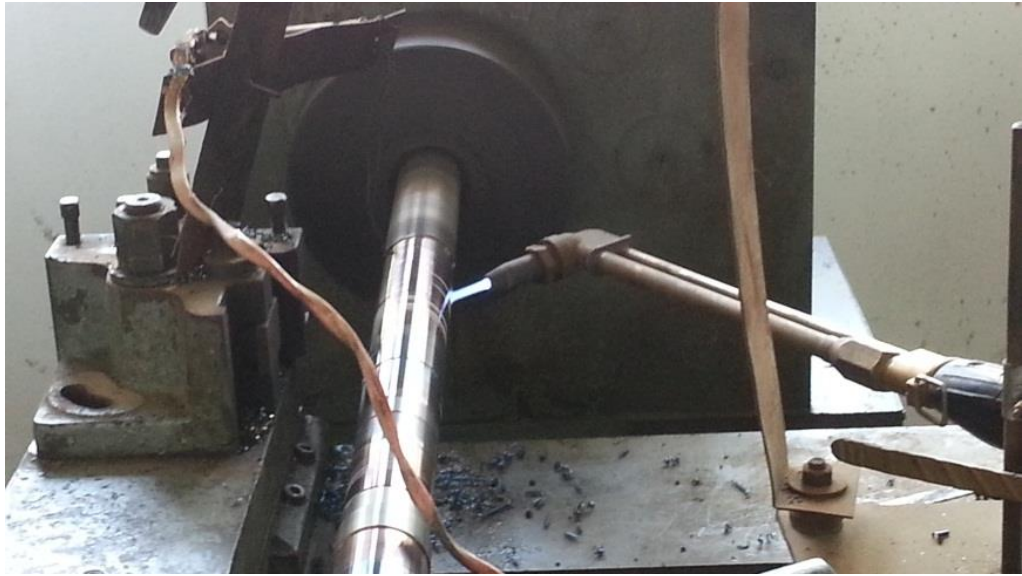
Figure 2.12 Experimental Set up for hot machining

Figure 2.13Workpiece (High manganese steel)

Table 2.3 Composition of high manganese steel by weight percentage (All elements are analysed: Normalized)

Constituents	O	P	S	Cr	Mn	Fe	Mo	W
%	25.21	0.18	0.02	0.21	10.47	63.26	0.15	0.50

Table 2.4 Properties of cutting insert and tool holder

Cutting insert	SNMG 120408
Nose radius	0.8
Edge geometry	Chamfered
Chamfer width	25°
Grade	TTR 08
Tool holder	PSBNR 2525 M12
Approach angle	75°

The tool geometry is shown in Table 2.3.
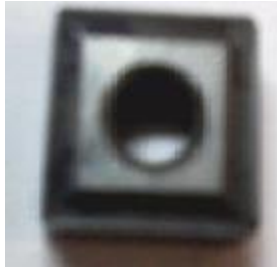
Figure 2.14 Uncoated carb0ide insert (TTR 08)

Table 2.5 Tool geometry of uncoated carbide

Inclination angle	-6°
Orthogonal rake angle	-6°
End relief angle	6°
Side relief angle	6°
Auxiliary cutting edge angle	15°
Principal cutting edge angle	75°
Nose radius	0.8 Mm

2.3   Instruments for measuring performance characteristics

The experiments have been conducted to measure tool wear, surface roughness, chip thickness, tool life and cutting power. The tool wear was measured by using Tool maker's microscope. In order to determine the tool life, the machining continued till the tool wear limit reached a critical limit of 0.3mm.

Tool maker microscope: It isa precision Optical Microscope that consists of single or multiple objective lenses, which magnifies the object and by the help of eyepiece lens the object is focused. Tool wear and chip thickness were measured by using Tool maker microscope (Figure 2.5).
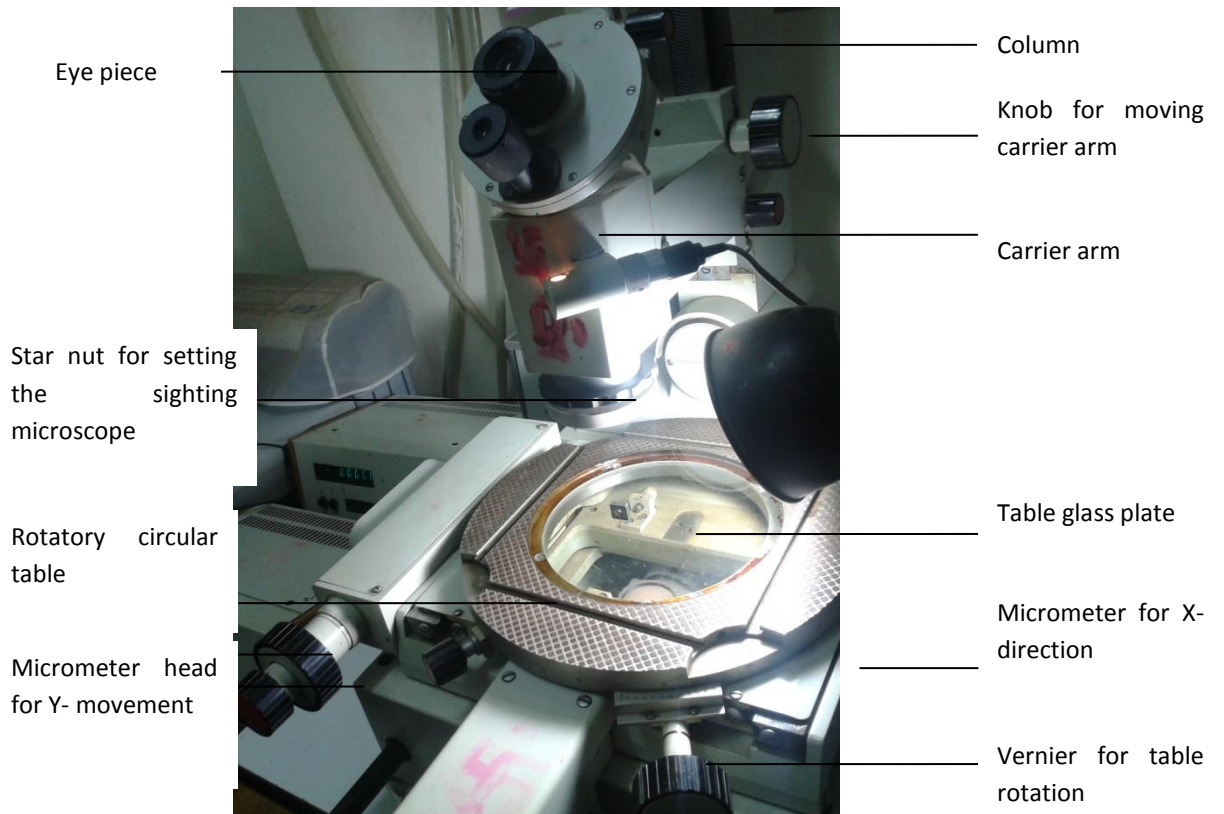
Figure 2.15 Tool maker microscope

Talysurf instrument: It measures the average/mean value for surface roughness (Model- Taylor Hobson, Surtronic 3+) (Figure 2.6). The Talysurfinstrument is facilitated with 2CR ISO (Corrected Phase).

Figure 2.16Talysurf (Model: Taylor Hobson, Surtronic 3+)

Digital power indicator: Power consumed by the lathe machine for accomplishing operation, is indicated digitally on screen (Figure 2.7).

Figure 2.17 Digital energy meter

Digital display unit: Digital display unit for measuring temperature using temperature thermocouple is given in Figure 2.8. The temperature of the workpiece near the tool tip is measured by the thermocouple.

Figure 2.18 Digital display unit

Microhardness tester: The basic principle, for measuring microhardness, is to observe the material's ability to resist plastic deformation from a standard source. The hardness number can be determined by applying load over the surface area of the indentation (Figure 2.9).
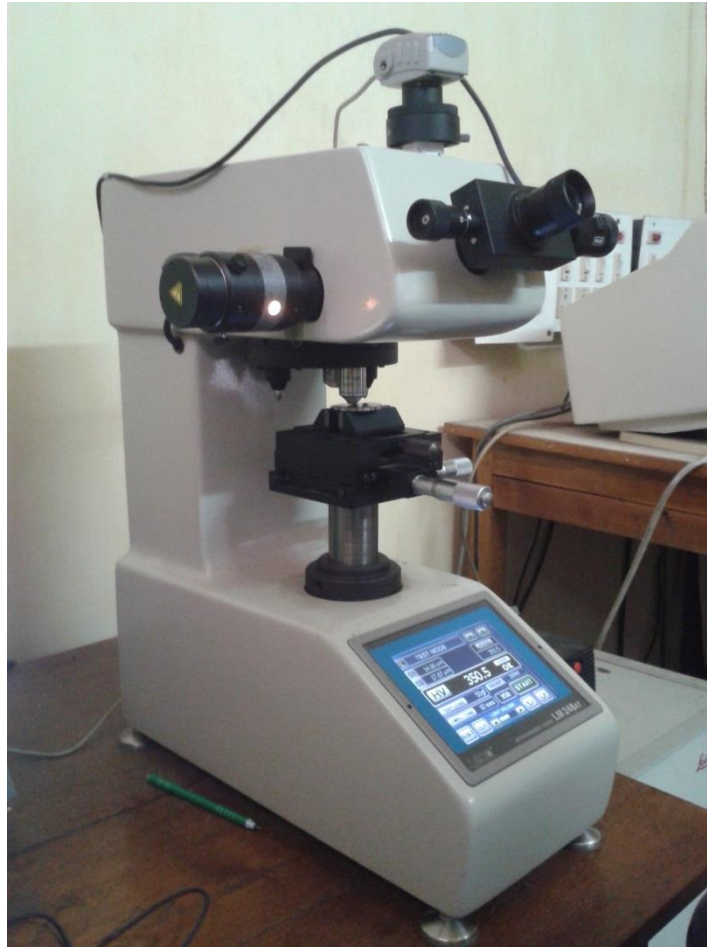
Figure 2.19Microhardness tester

Infra-red Pyrometer: It is also called as laser thermometers or non-contact thermometers or temperature guns or radiation thermometers. It measures the temperature at a spot by knowing the quantity of infrared energy of the object and its emissivity (Figure 2.10).

Figure 2.20 Infra-red Pyrometer

2.4 Results and discussion

Prior to the experiment, the temperature was set to three levels i.e., 200°C, 400°C, 600°C and performed with the three different levels of the cutting speed, feed rate and depth of cut. The material of the workpiece was the high manganese alloy clamped over a chuck and supported using the centre of the tailstock. The experiment was performed by keeping the distance 20mm between gas nozzle and workpiece for heating the workpiece. Afterwards heating is done upto the set temperature in thermocouple.

The tool wear, surface roughness and chip reduction coefficient are measured by heating the workpiece at fixed temperatures 200°C, 400°C and 600°C respectively keeping other parameters at constant level (V= 40m/min, d= 0.5mm). The experiment has been repeated at room temperature. In every case, the machining has been carried out for two minutes. The tool wear for different temperature of workpiece is given in Table 2.4.

Table 2.6 Tool wear (mm) at different feed at four temperatures

Run No.	Feed (mm/rev.)	At 15°C	200°C	400°C	600°C	% Variation		
						15°C-200°C	15°C-400°C	15°C-400°C
1	0.05	0.272	0.199	0.138	0.122	23.75	46.36	53.26
2	0.10	0.272	0.218	0.18	0.16	19.85	33.82	41.18
3	0.20	0.367	0.305	0.29	0.25	16.89	20.98	31.88

Similarly, surface roughness and chip reduction coefficient are given in Table 2.5 and Table 2.6 respectively. Referring to Table 2.4 it is evident that tool wear decreases with increase in temperature. It is also observed that tool wear increases with increase in feed rate. It can be noted that there is maximum reduction of tool wear (53.26%) obtained corresponding to feed 0.05mm/rev. and 600°C temperature.

Table 2.7 Surface roughness (µm) at different feed at four temperatures

Run No.	Feed (mm/rev.)	At 15°C	200°C	400°C	600°C	% Variation		
						15°C-200°C	15°C-400°C	15°C-400°C
1	0.05	3.16	1.9	1.6	1	39.87	49.37	68.35
2	0.10	3.76	2.4	1.9	1.46	36.17	49.47	53.79
3	0.20	5.46	3.6	2.79	3.05	34.07	48.90	44.14

Referring to Table 2.5 it is also observed that the surface roughness decreases with increase in temperature. But some deviations are observed that at high temperature and at high feed, where there is increase in surface roughness. This may be due to change in shape of tool because of high temperature and feed, which induces poor surface finish. Maximum reduction of surface roughness obtained was 68.35% at 0.05mm/rev. and temperature 600°C.

Table 2.8 Chip reduction coefficient at different feed at four temperatures

Run No.	Feed (mm/rev.)	At 15°C	200°C	400°C	600°C	% Variation		
						15°C-200°C	15°C-400°C	15°C-400°C
1	0.05	3.93	3.30	2.44	2.16	15.93	37.91	45.04
2	0.10	3.6	2.34	1.76	1.17	35.06	51.11	67.50
3	0.20	3.05	1.74	1.02	0.85	43.14	66.56	72.13

Referring to Table 2.6, it is observed that chip reduction coefficient decreases with increase in temperature. Minimum chip reduction coefficient is obtained at 600°C temperature and 0.2mm/rev. of feed. It is evident from the above experiment that there is reduction of tool wear, surface roughness and chip reduction coefficient at hot machining operation on comparison to machining at room temperature.
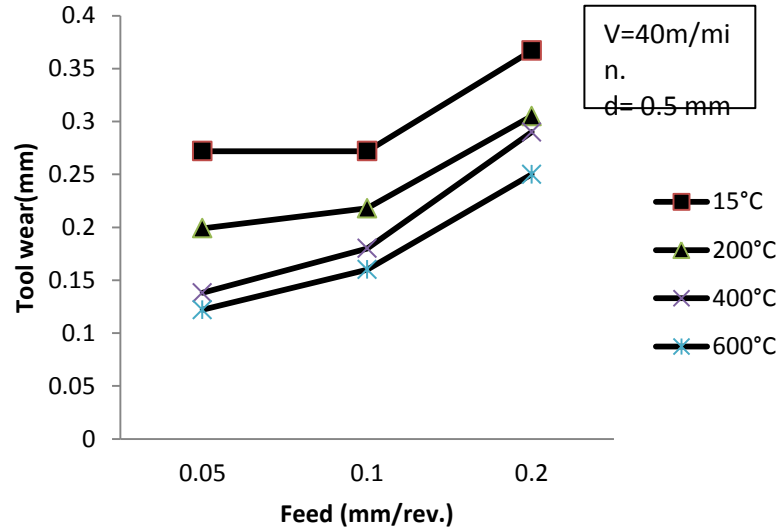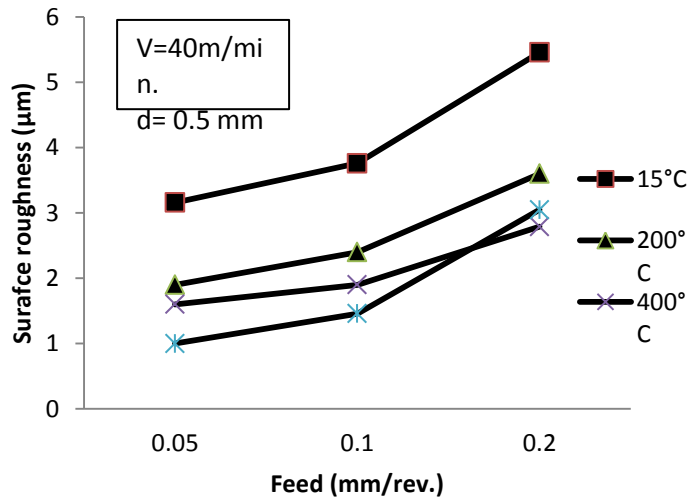
Figure 2.21 Tool wear vs. Feed
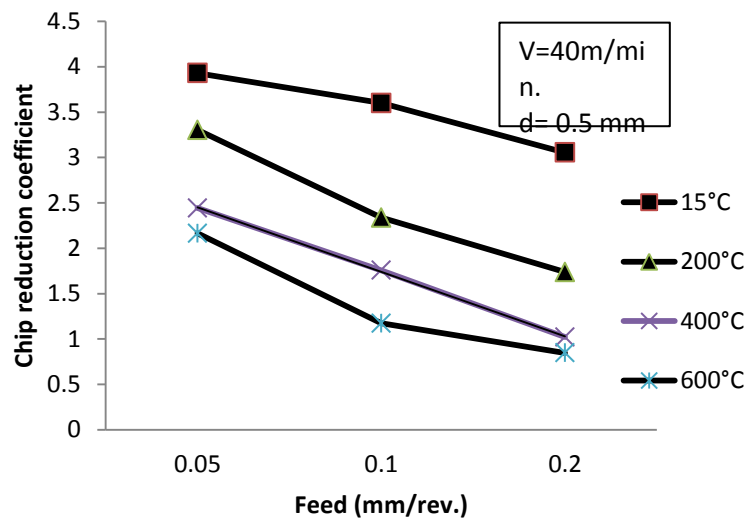

Figure 2.22 Surface roughness vs. Feed

Figure 2.23 Chip reduction coefficient vs. Feed

The variation of tool wear with respect to feed are given Figure 2.11. It is observed that tool wear increases with increase in feed and decreases with increase in temperature.

In order to optimise the process parameters for hot machining operation the experiments have been carried out as per central composite design. The cutting speed, feed rate, depth of cut and temperatures are taken as the variables. The tool wear, surface roughness and chip reduction coefficient are taken as the responses. The temperature is varied at three levels (200°C, 400°C and 600°C). The cutting speed is varied at three levels (24m/min. 45m/min. and 66m/min.). The feed is varied at three levels (0.05mm/rev., 0.125 mm/rev. and 0.2mm/rev.). The depth of cut is also varied at three levels (0.5mm, 1.25mm and 2.0mm). The machining is carried out for two minutes for each run. Experimental results are tabulated in Table 2.7. The chip produced with worn out tool for each combination of cutting variables are given in Figure 2.15. Average flank wear was measured in each case. The chips obtained for each run are collected for determining the effect of the cutting parameters on the chip morphology. It is observed that temperature of the workpiece plays a predominant role influencing the machinability criteria in hot machining operation. The chips morphology obtained with respect to different cutting parameters in hot machining operation have been studied. The chips obtained for each run are collected for determining the effect of the cutting parameters on the chip morphology. It was found that the chips obtained at high speed and low feed rate are mostly continuous. Most of the continuous chips were found at 600°C temperature with range of cutting speed analysed. Continuous chips with tangled shape were also found at medium level of cutting parameters (400°C, 45m/min, 0.125mm/rev and 1.25mm depth of cut). The discontinuous chips were found at 0.5mm depth of cut at 0.05 mm/rev and 0.125mm/rev at any level of temperature and cutting velocity. Formation of built up edge was also found at 600°C, 66m/min, 0.2 mm/rev and for any level of depth of cut.

Table 2.9 Experimental values for tool wear, surface roughness and chip reduction coefficient

| Run Order	T	V	f	d	TW	Ra	t_2	Ξ
1	600	24	0.050	0.50	0.140	1.600	0.097479	2.01840
2	200	66	0.050	0.50	0.280	0.016	0.108760	2.25200
3	200	24	0.200	0.50	0.050	5.350	0.243407	1.26000
4	600	66	0.200	0.50	0.378	5.350	0.414757	2.14700
5	200	24	0.050	2.00	0.132	2.600	0.335843	6.95400
6	600	66	0.050	2.00	0.090	3.200	0.078982	1.63540
7	600	24	0.200	2.00	0.140	3.000	0.377889	1.95615
8	200	66	0.200	2.00	0.301	6.100	0.255964	1.32500
9	400	45	0.125	1.25	0.220	1.800	0.144957	1.20060
10	400	45	0.125	1.25	0.062	0.990	0.186612	1.54560
11	200	24	0.050	0.50	0.076	2.500	0.136675	2.83000
12	600	66	0.050	0.50	0.290	1.000	0.157635	3.26400
13	600	24	0.200	0.50	0.070	4.000	0.195498	1.01200
14	200	66	0.200	0.50	0.098	4.300	0.326667	1.69100
15	600	24	0.050	2.00	0.130	1.400	0.095962	1.98700
16	200	66	0.050	2.00	0.300	1.000	0.114966	2.38050
17	200	24	0.200	2.00	0.327	6.250	0.232009	1.20100
18	600	66	0.200	2.00	0.393	6.500	0.627835	3.25000
19	400	45	0.125	1.25	0.220	1.440	0.168284	1.39380
20	400	45	0.125	1.25	0.210	1.740	0.214104	1.77330
21	200	45	0.125	1.25	0.196	1.400	0.149232	1.23600
22	600	45	0.125	1.25	0.180	1.460	0.141625	1.17300
23	400	24	0.125	1.25	0.062	0.990	0.166618	1.38000
24	400	66	0.125	1.25	0.340	1.700	0.141625	1.17300
25	400	45	0.050	1.25	0.190	1.600	0.175948	3.64319
26	400	45	0.200	1.25	0.280	6.000	0.377889	1.95615
27	400	45	0.125	0.50	0.044	1.560	0.306673	2.54000
28	400	45	0.125	2.00	0.178	2.200	0.702813	5.82100
29	400	45	0.125	1.25	0.183	1.980	0.127028	1.05210
30	400	45	0.125	1.25	0.062	0.990	0.316574	2.62200

(i)

(ii)

(iii)

(iv)

(v)

(vi)

(vii)

(viii)

(ix)

(x)

(xi)

(xii)

(xiii)

(xiv)

(xv)

(xvi)
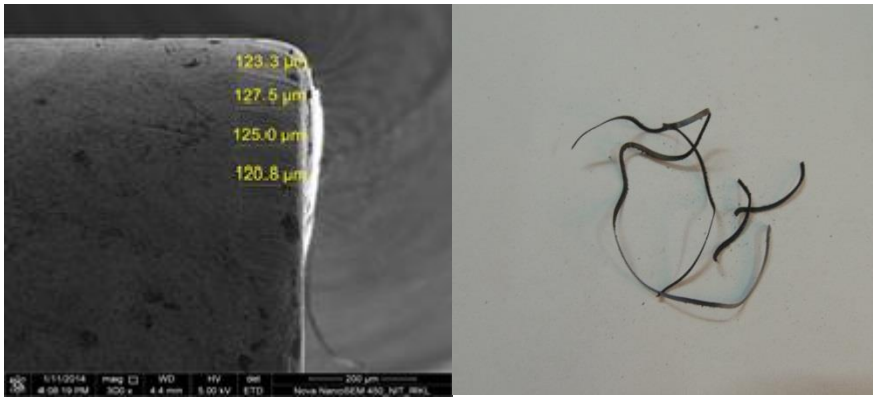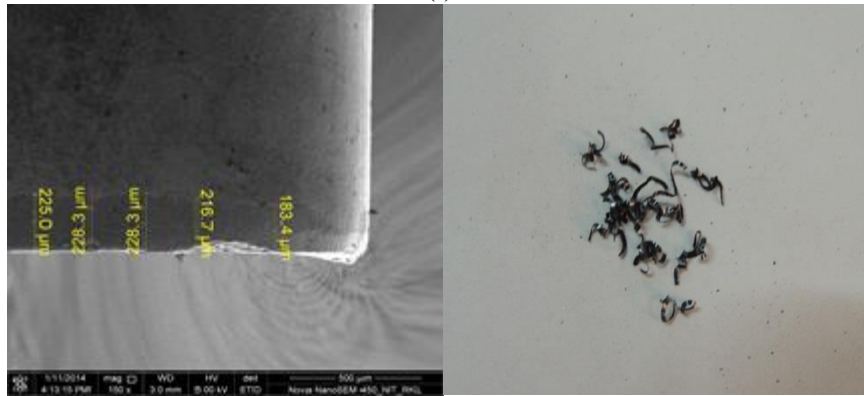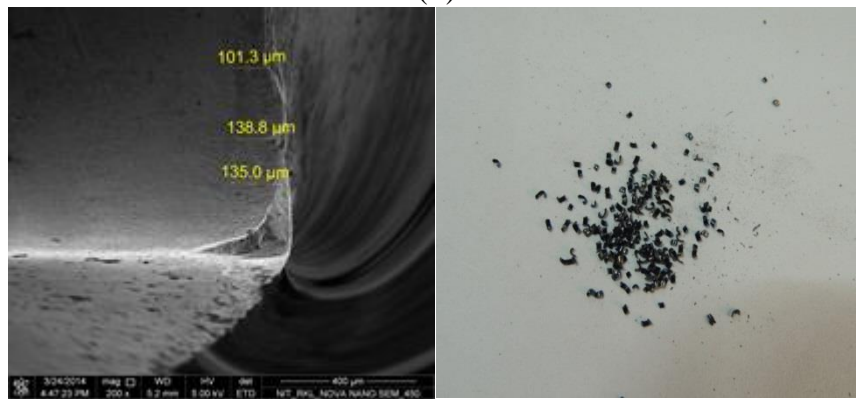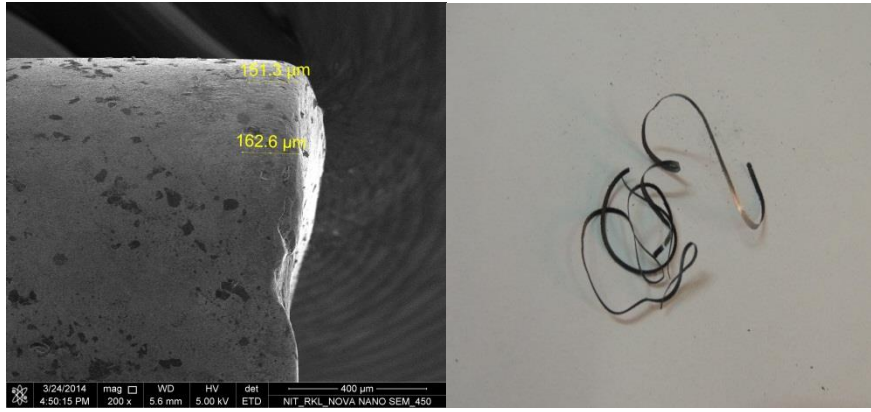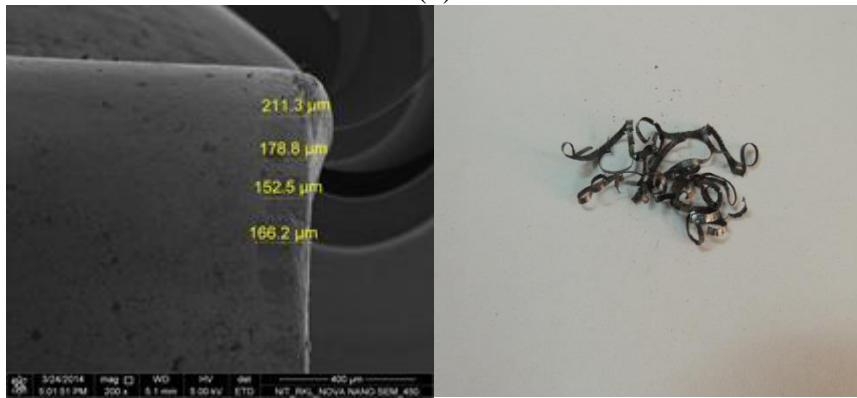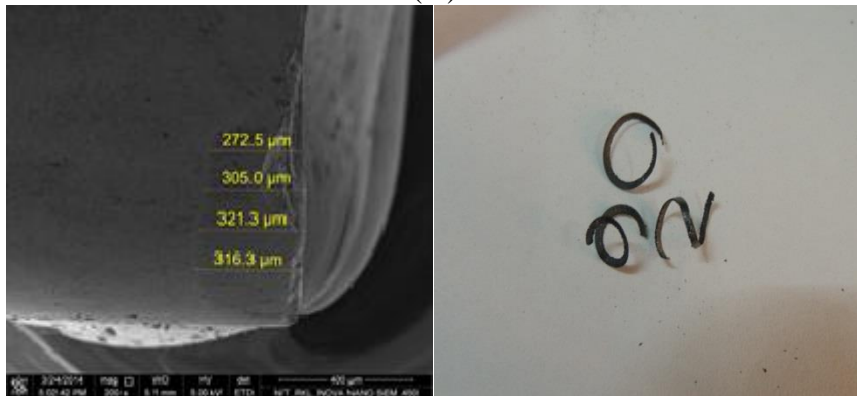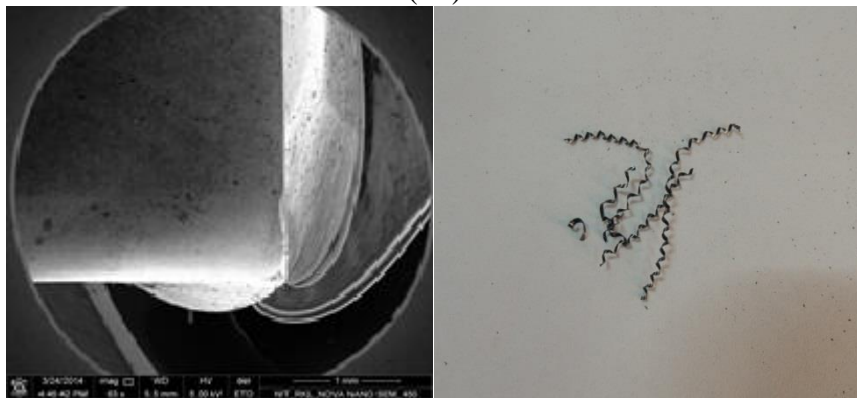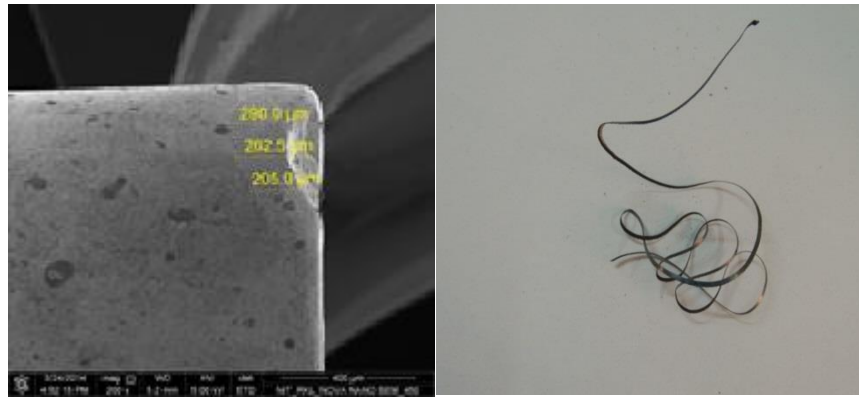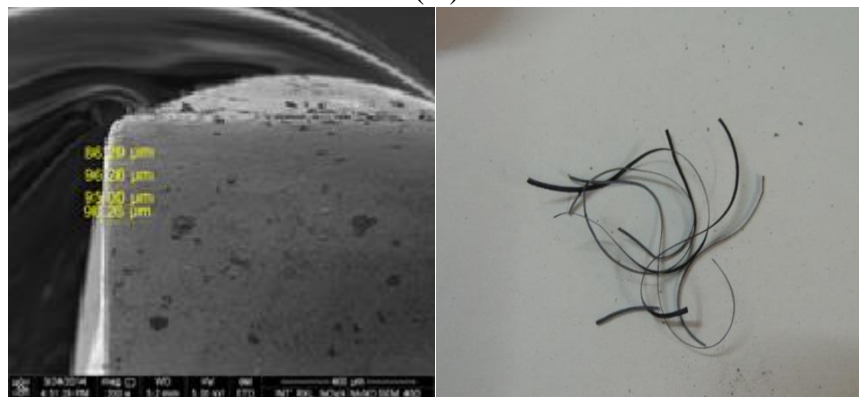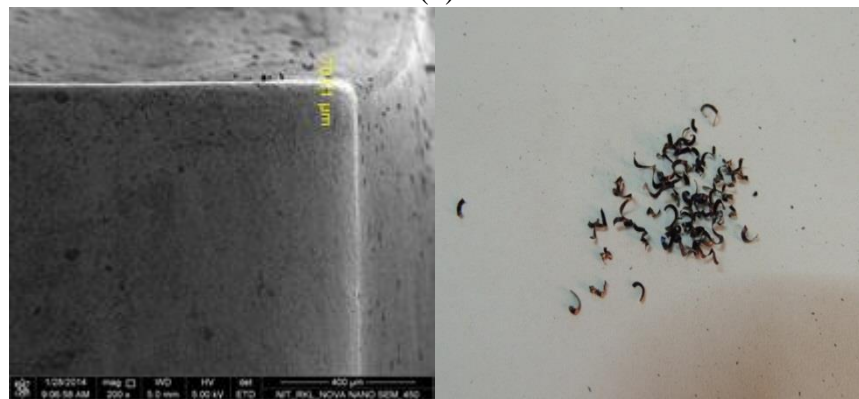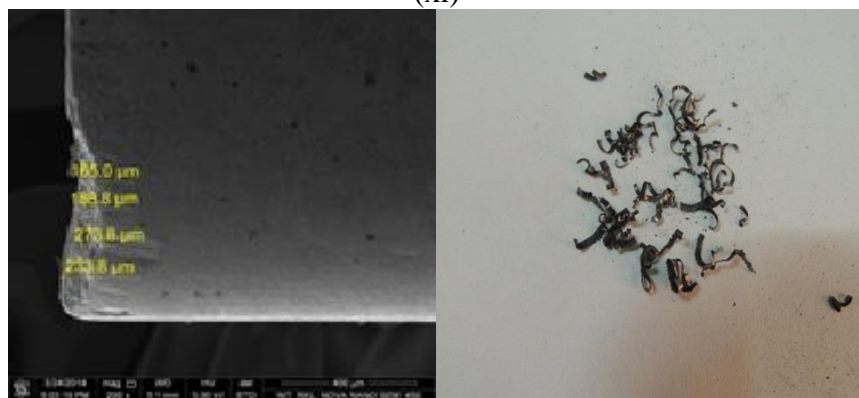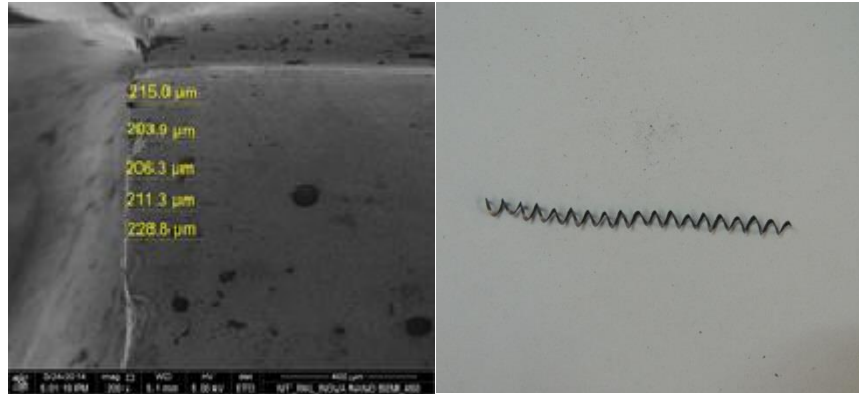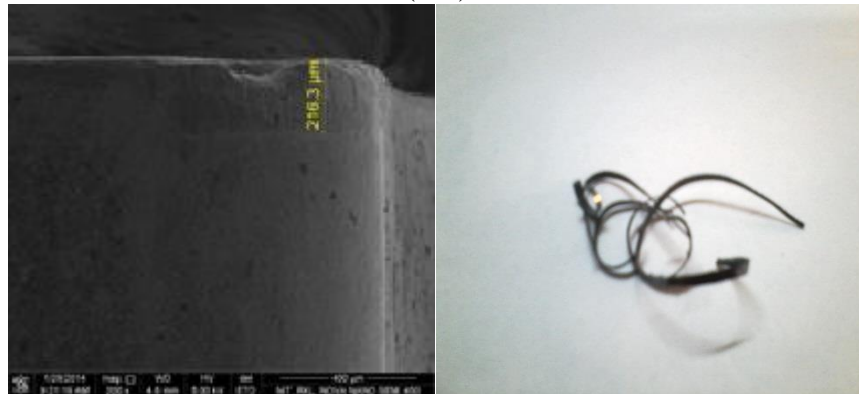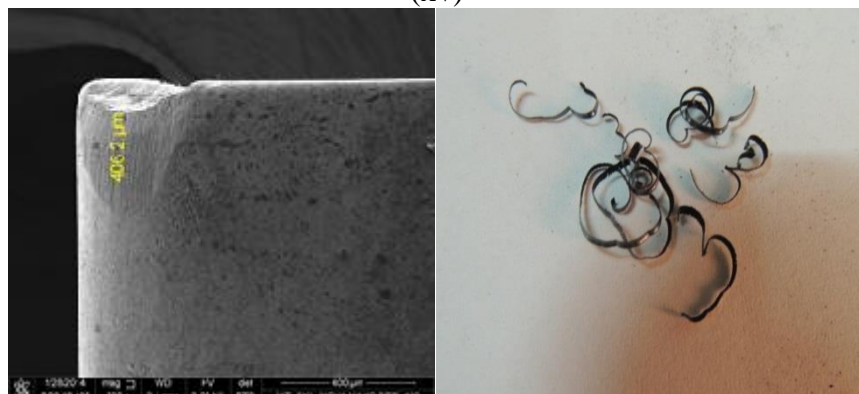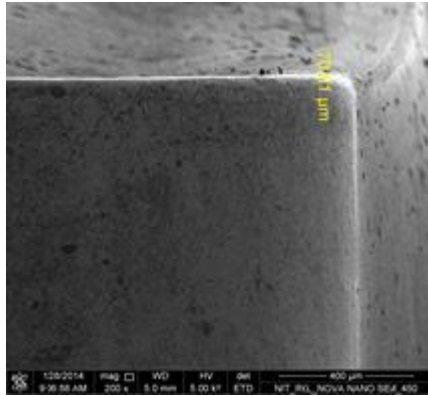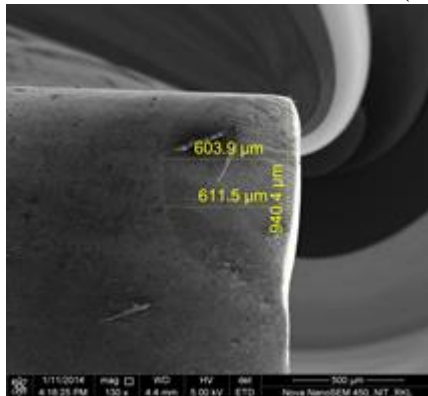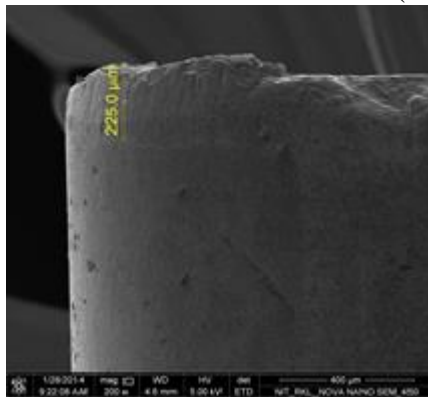
(xvii)

(xviii)

(xix)
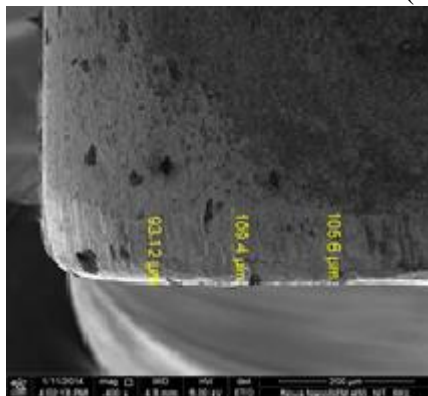
(xx)
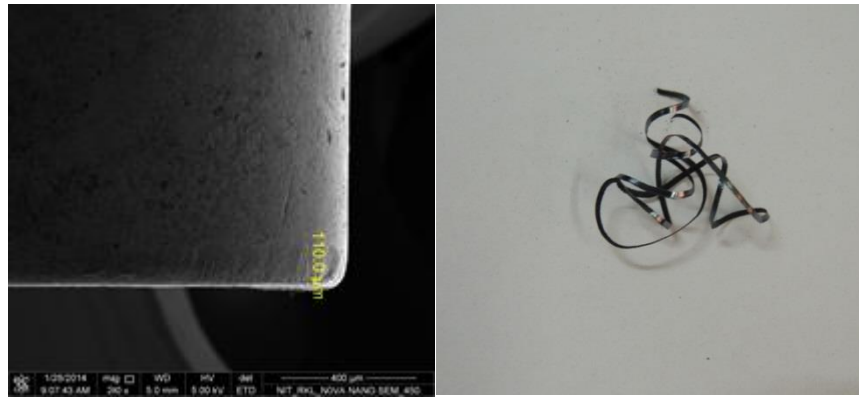
(xxi)
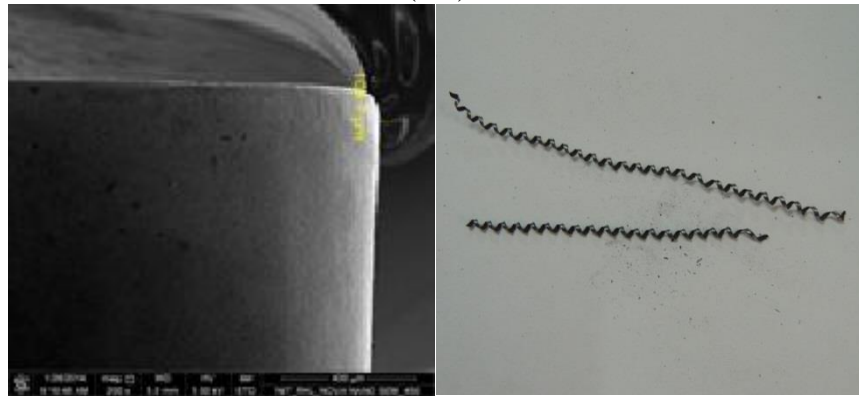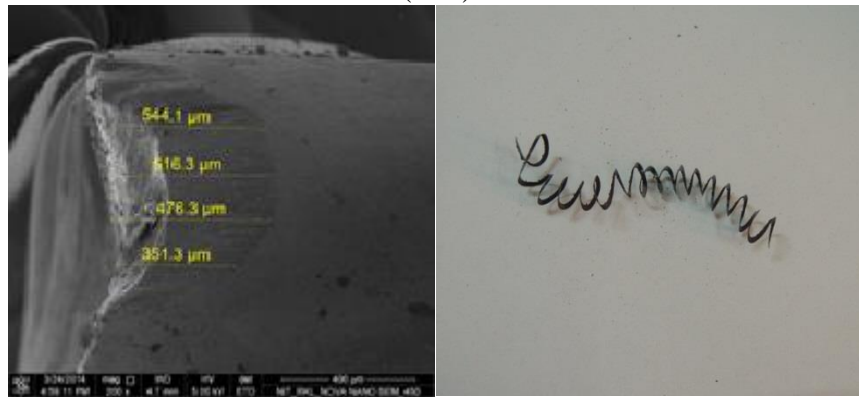
(xxii)

(xxiii)
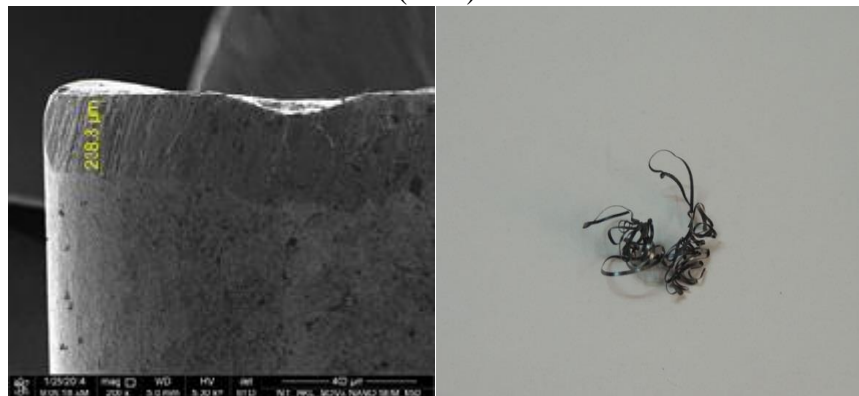
(xxiv)
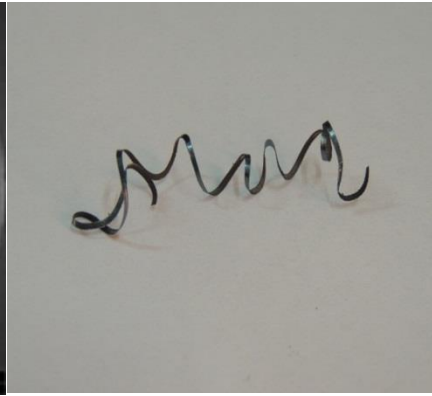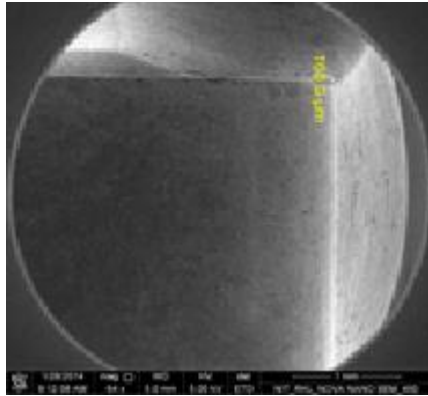
(xxv)

(xxvi)

(xxvii)

(xxviii)

(xxix)

(xxx)
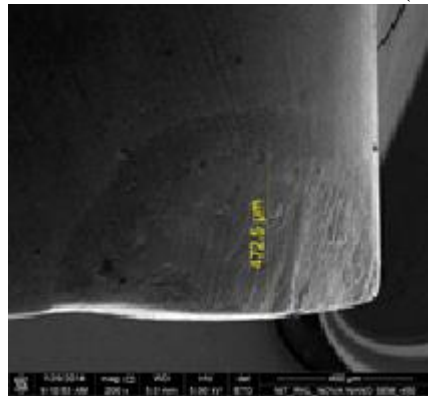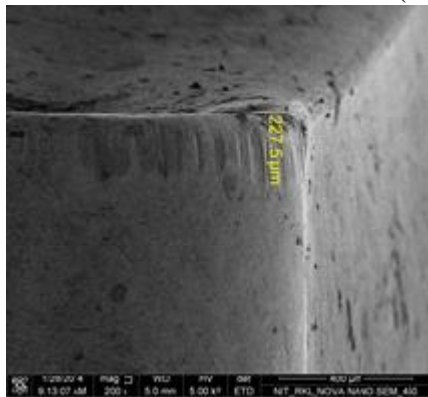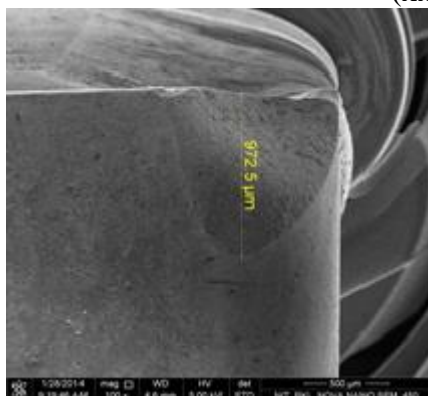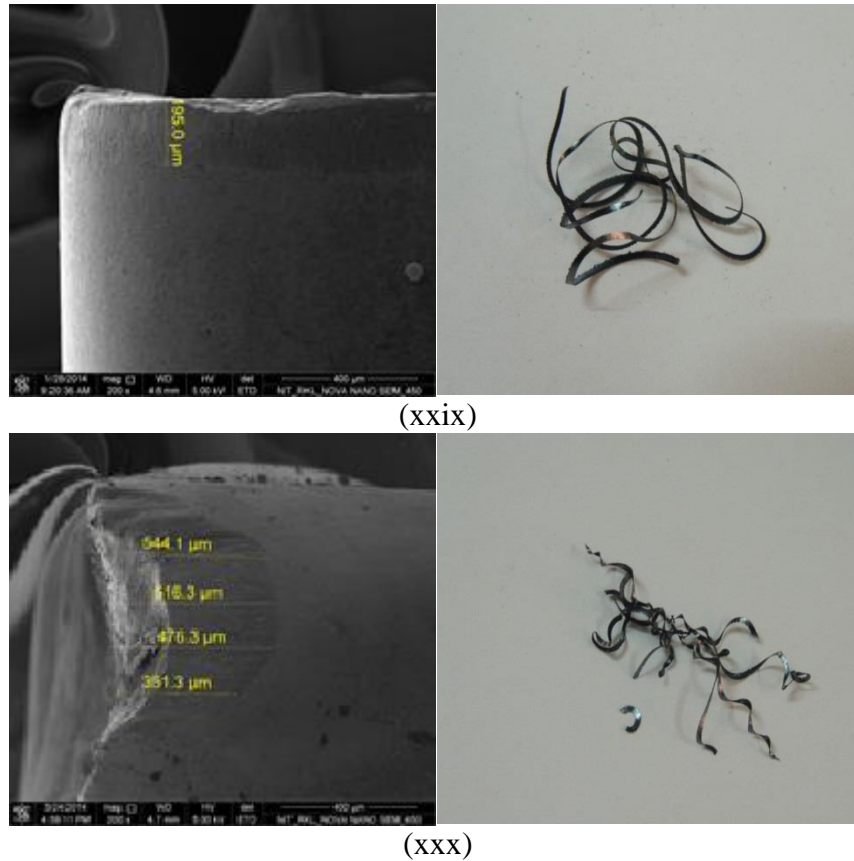
Figure 2.24 Tool wear with their respective chip morphology

The optimization of the process parameters has been carried out to determine optimum process parameters for maximizing tool life and minimizing cutting power. The temperature, cutting velocity, feed and depth of cut are taken as the process parameters. Tool life and power are taken as the response variables. 0.3 mm tool wear was taken as the criteria for tool life. The flank wear was measured under a tool maker microscope after machining for two minutes. The experiment is repeated till the flank wear limit reached 0.3mm. The power is measured from power meter. All the process parameters are varied at three levels. The temperature is varied at three levels (200°C, 400°C and 600°C). The cutting speed is varied at three levels (8m/min., 21.5m/min. and 35m/min.). The feed is varied at three levels (0.05mm/rev., 0.075mm/rev. and 0.10mm/rev.). The depth of cut is varied at three levels (0.5mm, 0.75mm and 1.0mm). The tool life and power as per layout of experimental design has been given in Table 2.8. The variations of flank wear with respect to time for different combinations of process parameters are shown in Figure 2.15. The tool life in each case is determined for taking the limit of flank wear as 0.3mm.

Table 2.10 Experimental results for tool life and power consumption

| Runs	T(˚C)	V(m/min.)	f(mm/rev.)	d(mm)	tl(min.)	Power(W)
1	600	8.0	0.050	0.50	39	603
2	200	35.0	0.050	0.50	9	719
3	200	8.0	0.100	0.50	25	558
4	600	35.0	0.100	0.50	8	782
5	200	8.0	0.050	1.00	29	562
6	600	35.0	0.050	1.00	12	732
7	600	8.0	0.100	1.00	24	599
8	200	35.0	0.100	1.00	5	839
9	400	21.5	0.075	0.75	38	694
10	400	21.5	0.075	0.75	35	695
11	200	8.0	0.050	0.50	31	570
12	600	35.0	0.050	0.50	19	664
13	600	8.0	0.100	0.50	23	588
14	200	35.0	0.100	0.50	11	760
15	600	8.0	0.050	1.00	24	578
16	200	35.0	0.050	1.00	12	714
17	200	8.0	0.100	1.00	23	574
18	600	35.0	0.100	1.00	7	824
19	400	21.5	0.075	0.75	53	708
20	400	21.5	0.075	0.75	62	716
21	200	21.5	0.075	0.75	5	678
22	600	21.5	0.075	0.75	28	715
23	400	8.0	0.075	0.75	40	554
24	400	35.0	0.075	0.75	42	727
25	400	21.5	0.050	0.75	52	709
26	400	21.5	0.100	0.75	35	712
27	400	21.5	0.075	0.50	7	684
28	400	21.5	0.075	1.00	5	701
29	400	21.5	0.075	0.75	43	720
30	400	21.5	0.075	0.75	39	724

(i)

(ii)

(iii)

(iv)

(v)

(vi)

(vii)

(viii)

(ix)

(x)

(xi)

(xii)

(xiii)

(xiv)

(xv)

(xvi)

(xvii)

(xviii)

(xix)

(xx)

(xxi)

(xxii)
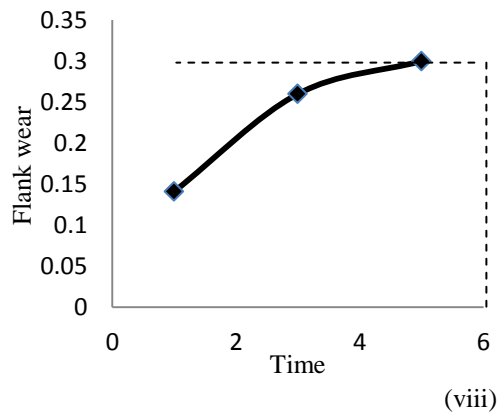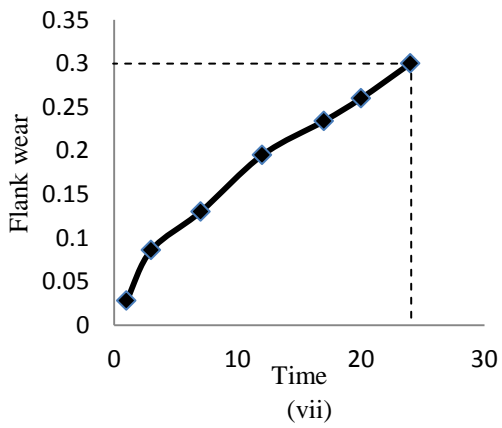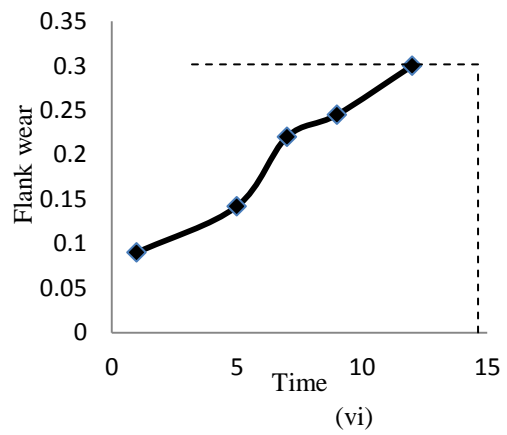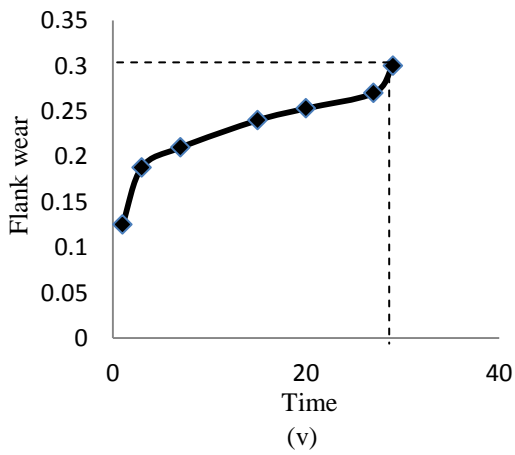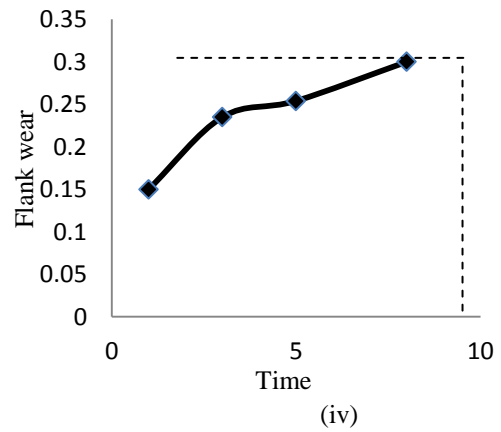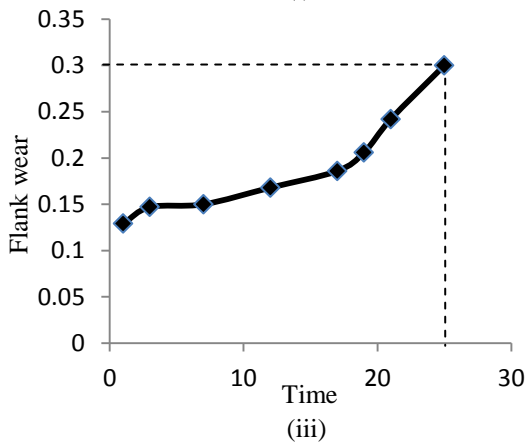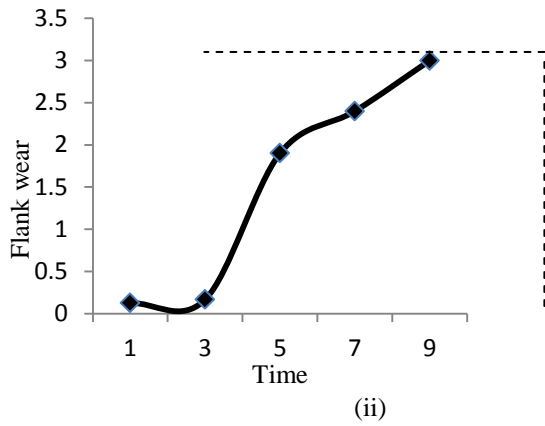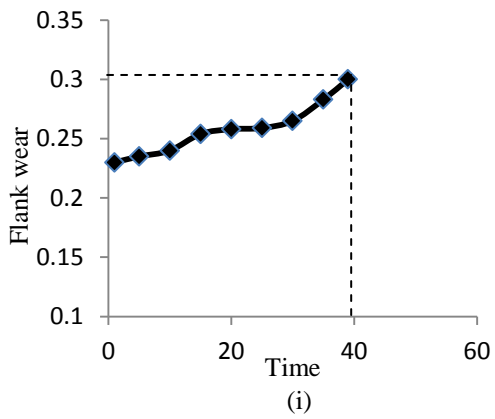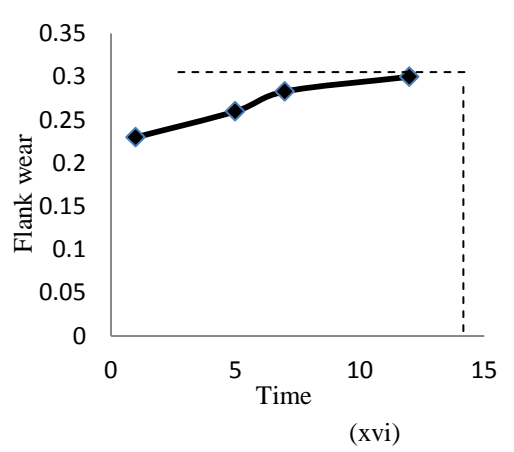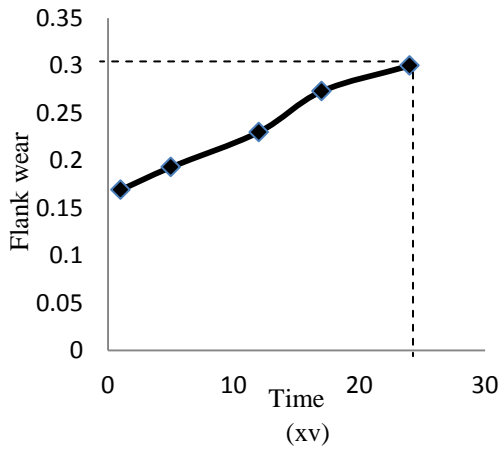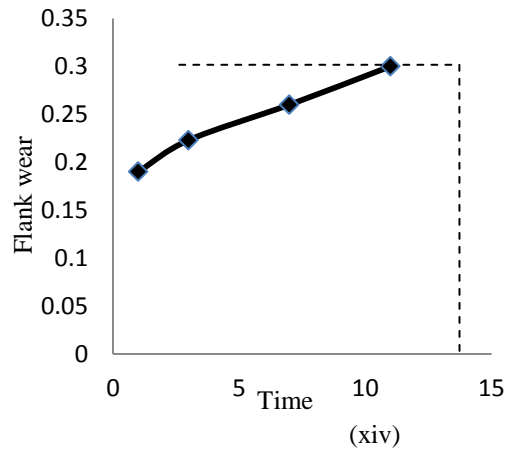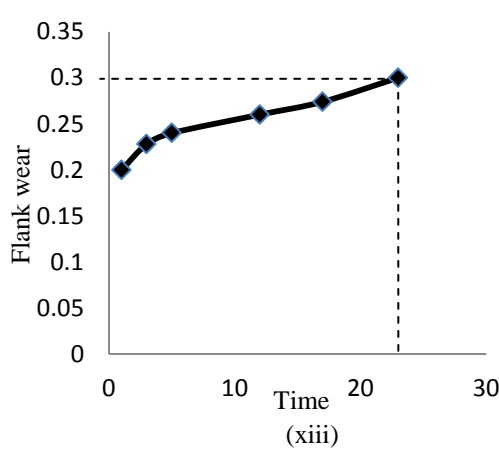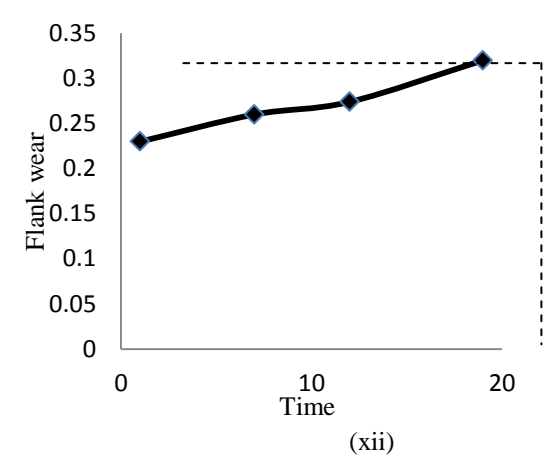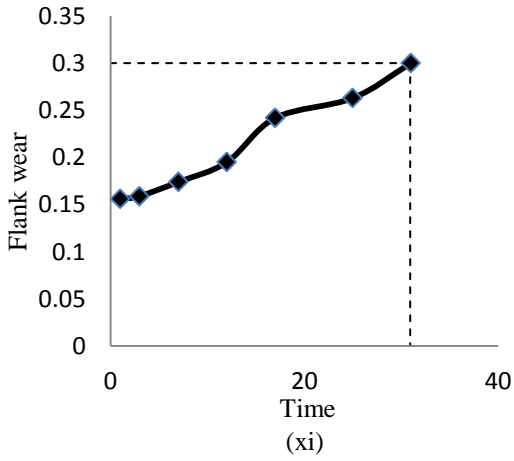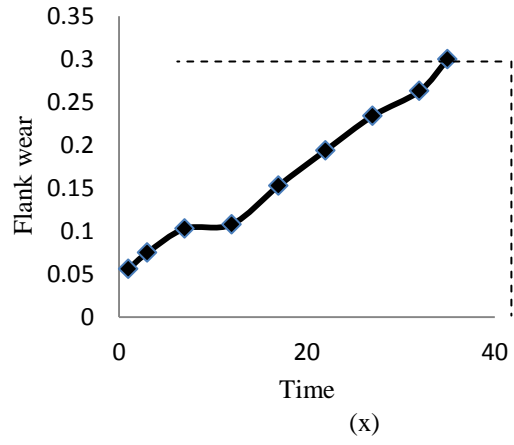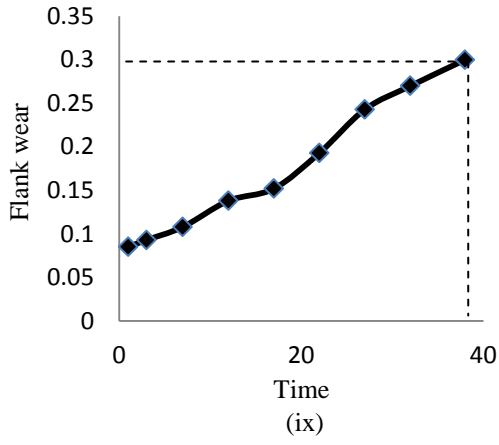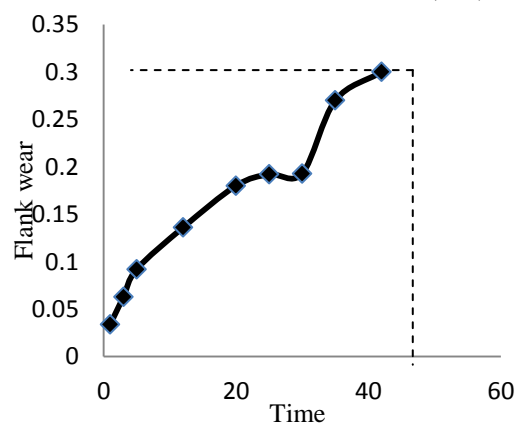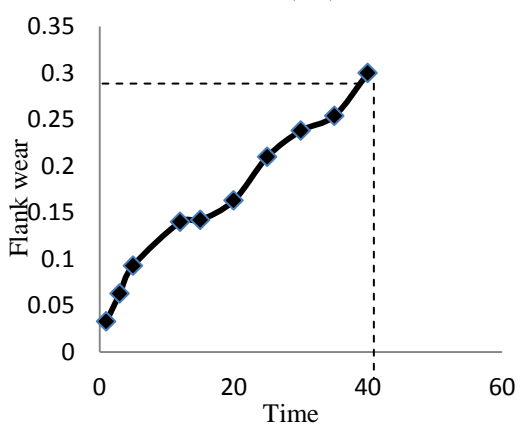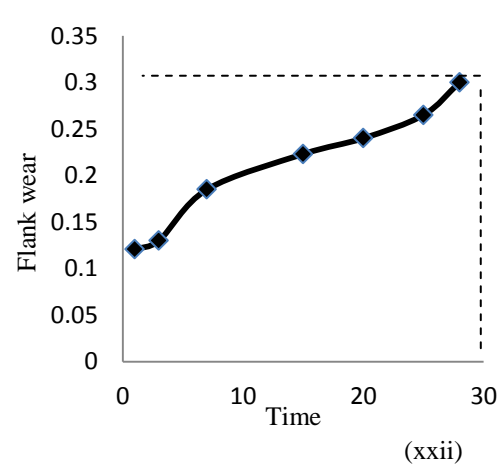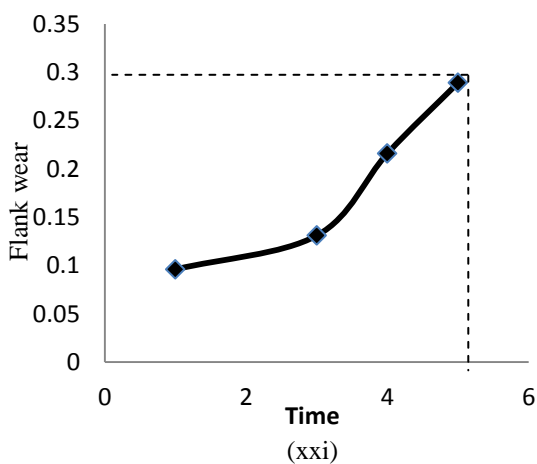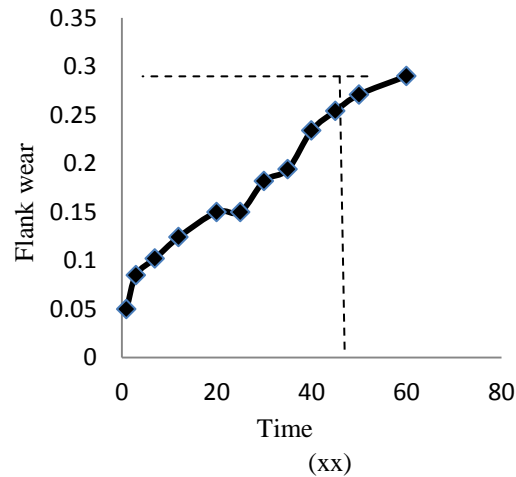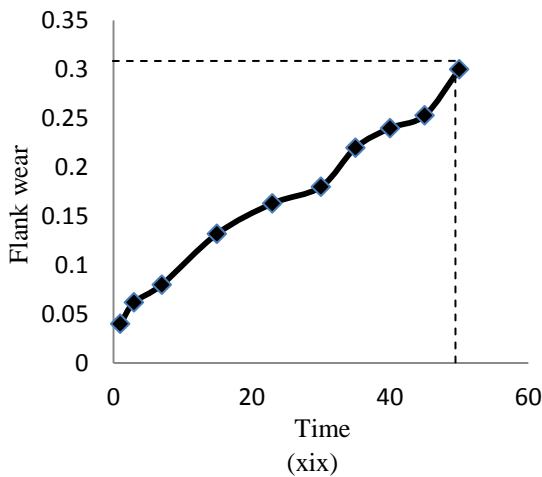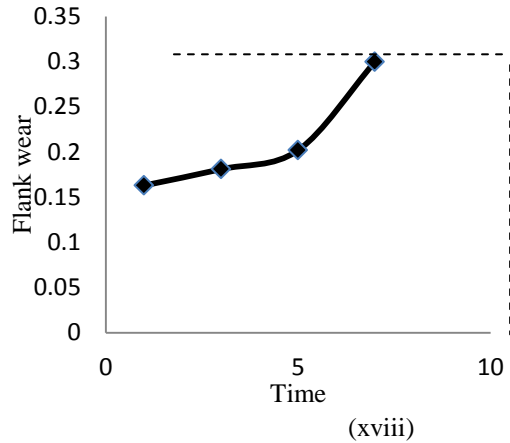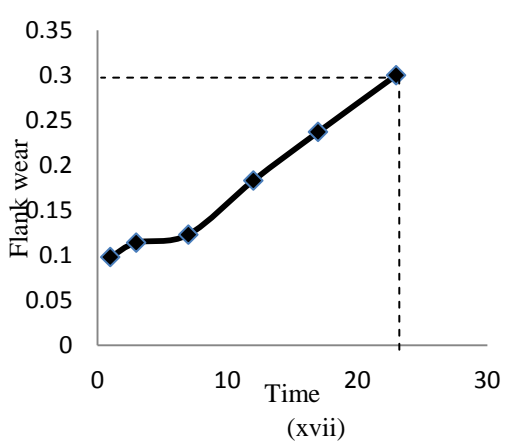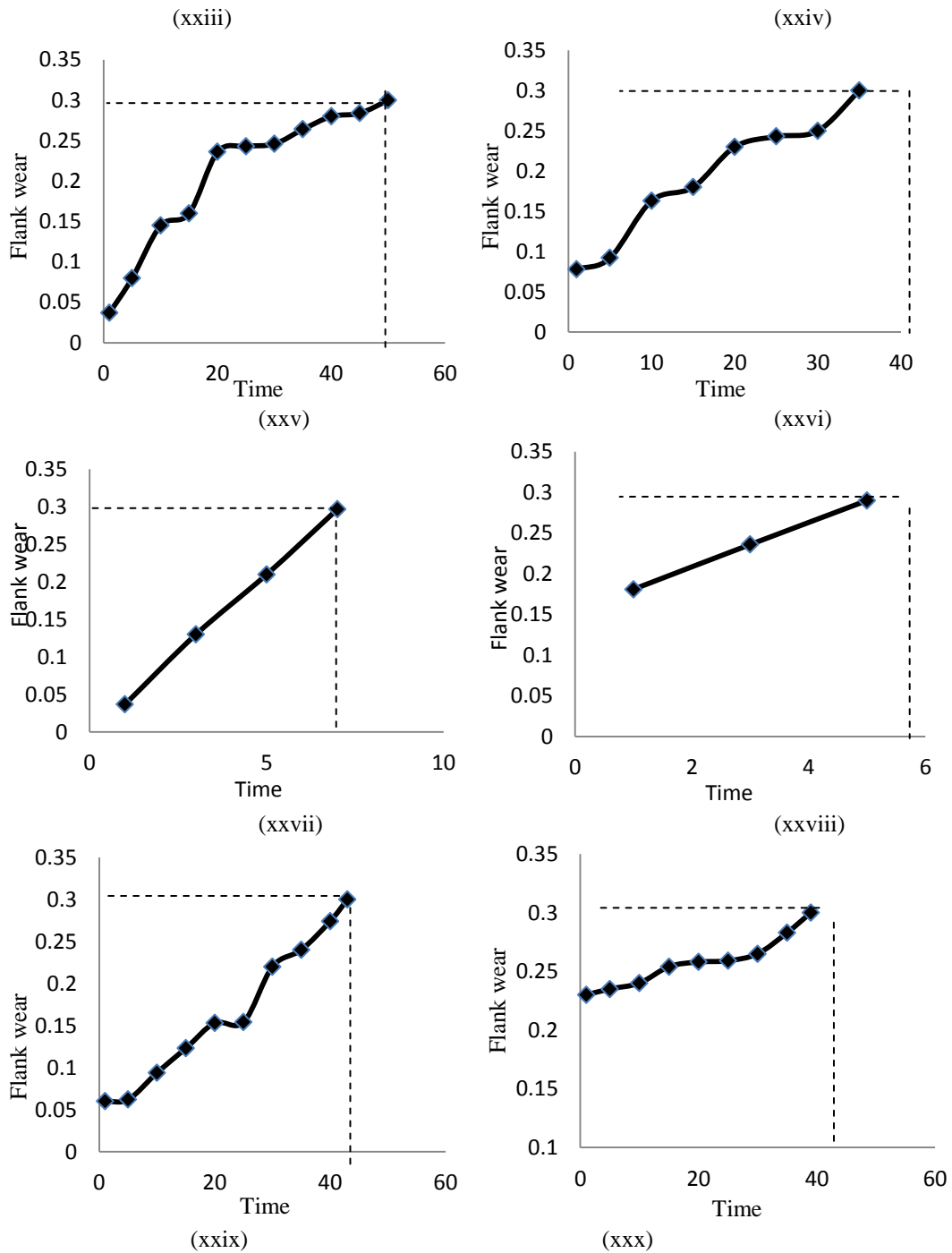
Figure 2.25 Flank wear (mm) vs Time (sec.)

- **Measurement of chip/tool interface temperature**

The chip/tool interface temperature has been measured by using infrared pyrometer having a maximum limit of measurement of temperature uptu 1250°C. The experiment (Figure 2.16) has been conducted by varying the temperature, cutting speed, feed and depth of cut as per L9 orthogonal array. The machining was done for one minute for each experimental run. The parameters are varied at three levels. The temperature is

varied at three levels (23°C, 200°C and 400°C). The cutting speed is varied at three levels (11m/min., 32m/min. and 55m/min.). The feed is varied at three levels (0.05mm/rev., 0.07mm/rev. and 0.1mm/rev.). The depth of cut is also varied at three levels (0.5mm, 0.7mm and 1.0mm). The temperature measured for different combinations of input parameters is mentioned in Table 2.9. The results are validated with FEM modelling.

Figure 2.26 Measurement of temperature

Table 2.11 Taguchi Design for temperature distribution with their experimental values

Run Order	T(°C)	V(m/min.)	f(mm/rev.)	d(mm)	Temperature measured(°C)
1	23	11	0.05	0.5	255
2	23	32	0.07	0.7	264
3	23	55	0.10	1.0	306
4	200	11	0.07	1.0	469
5	200	32	0.10	0.5	476
6	200	55	0.05	0.7	435
7	400	11	0.10	0.7	558
8	400	32	0.05	1.0	615
9	400	55	0.07	0.5	524

The micro-hardness is a measure of surface integrity of the workpiece. The micro-hardness of the workpiece has been determined experimentally under hot machining condition. For this case, the operation was carried out at feed rate 0.05mm/rev.,

0.10mm/rev. and 0.2 mm/rev. at a cutting velocity of 35m/rev. and depth of cut of 0.5mm with workpiece heated at constant temperature of 400°C. The diameter of the workpiece is 30mm. The samples are prepared for analysis with axial thickness of 5mm. The cross-sectional plane obtained for each sample after cutting has been polished by using polishing papers of decreasing grades.

Figure 2.27 Three samples of workpiece at three different feed rates

The measurements are taken at the distance interval at 0.5mm between the points. Measurements of hardness were made by hardness tester with a Vicker indenter on the material. Vickers indenters are more symmetric and better suited for particle hardness measurements [66]. The diamond indenter is pressed on the workpiece material with load 100gms with 10s loading time. D1 (horizontal length) and D2 (vertical length) of the impression were measured using optical microscope with 400× magnification. Samples are shown in Figure 2.17. The hardness, HV, is defined as the maximum applied load using the indentation test, P, divided by the maximum contact area of the indentation immediately before unloading.

$$HV = \frac{P}{A}$$ (1)

The values of micro-hardness at three cutting velocity are given in Table 2.10.It can be observed from Figure 2.19 that values of D1and D2 going to be reduced as the distance increased from the centre and value of D1 and D2 are shown in Table 2.7. The size of impression of indentation on the workpiece shows the value of the hardness (resistance for load). It is observed that the hardness decreases with increase

in distance from the centre. This is due to softness of the surface because of heating the workpiece material.

Table 2. 12 Micro-hardness values at three feed rates

Feed rate (mm/rev.)	D1	D2	HV
0.05	13.64	15.79	532.6
	18.24	18.66	544.8
	18.66	18.66	537.6
0.15	18.69	18.69	530.9
	18.68	18,68	531.4
	17.56	17.56	601.4
0.2	12.04	12.94	600.3
	17.86	17.23	602.4
	17.23	16.77	641.7

It is reported that maximum hardness obtained at 0.15 mm/rev among all the microhardness measured and lowest at 0.1 mm/rev. It is observed that with the increase in feed rate the microhardness value is increasing. It may be due to excess increase in the heat at the machined surface material due to plastic deformation. As the heat input increases, the grain refinement occurs and which increases the microhardness at the layers near to machined surface.
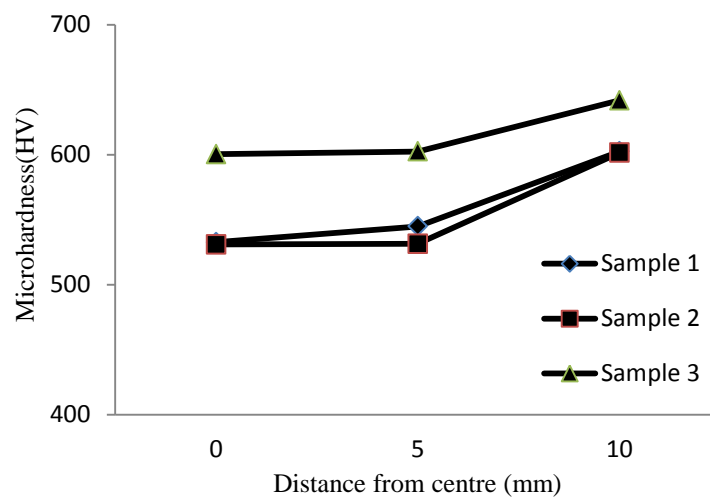
Figure 2. 28 Microhardness variation at different feed rate
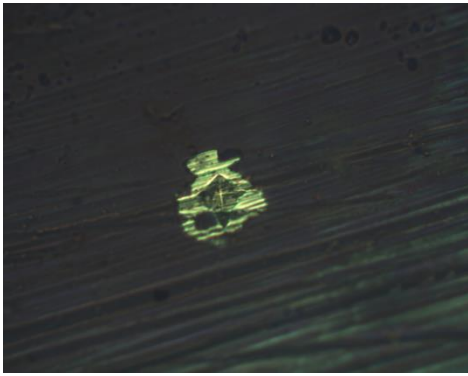
(i) At centre of the workpiece   (ii) At distance of 0.5mm from centre
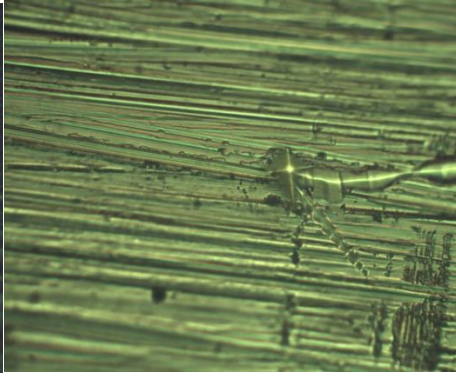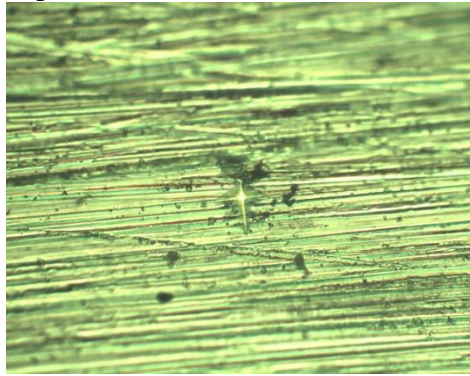
(iii)At the distance of 1.0mm from the centre

(a) Sample 1
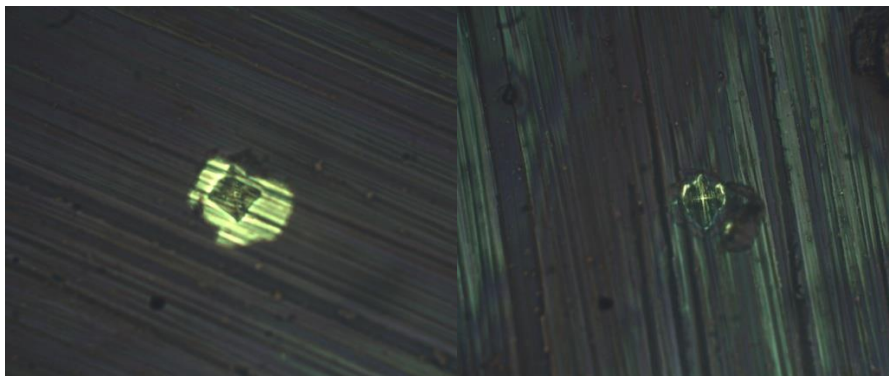
(i) At centre of the workpiece   (ii) At distance of 0.5mm from centre
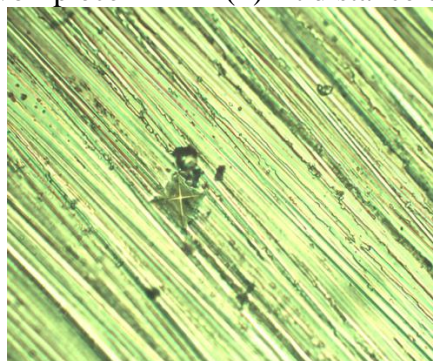
(iii) At the distance of 1.0mm from the centre

(b) Sample 2

(i) At centre of the workpiece   (ii) At distance of 0.5mm from centre

(iii) At the distance of 1.0mm from the centre

(c) Sample 3
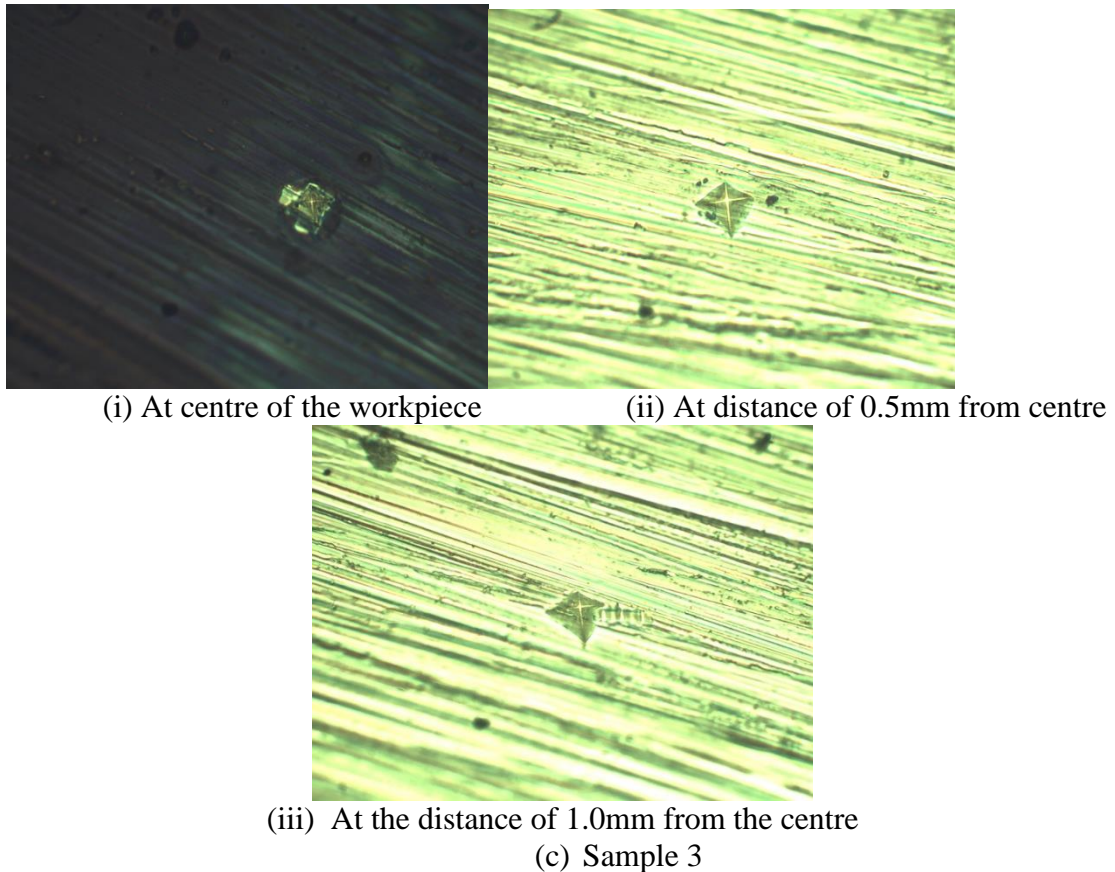
Figure 2. 29 Optical microhardness images of indentations on the workpiece (a) at 24 m/min cutting velocity (b) at 45 m/min cutting velocity and (c) at 66 m/min cutting velocity by keeping other factors at constant level

The variation of microhardness with distance from centre (mm) is shown in Figure 2.18. It is observed that the hardness increases with increase in distance from the centre. It is also observed that microhardness obtained is maximum at feed rate 0.15mm/rev. this is may be due to increase in plastic deformation. As the heat input increases, the grain refinement occurs and which increases the microhardness at the layers near to the machined surface. The optical microhardness images of indentations on the workpiece are shown in Figure 2.19 for different locations from the centre of the workpiece. There is a change in responses while varying the process parameters. So, it is necessary to study about the trend of variation of responses while varying parameters at different levels.

Trend analysis refers to predict trend of responses while varying the levels of the cutting parameters.

Table 2. 13 Tool wear, surface roughness, chip thickness and chip reduction coefficient

Run No.			TW		Ra		t_2		ξ	
			At 200C	At 600C	At 200C	At 600C	At 200C	At 600C	At 200C	At 600C
1	Low V (8m/min.)	Low f(0.05mm/rev.)	Low d(0.5mm)	0.076	0.140	2.500	1.600	0.137	0.097	2.830	2.018
2	Low V(8m/min.)	Low f(0.05mm/rev.)	High d(1.0mm)	0.132	0.130	2.600	1.400	0.336	0.096	6.954	1.987
3	Low V(8m/min.)	High f(0.05mm/rev.)	Low d(0.5mm)	0.050	0.070	5.350	4.000	0.243	0.195	1.260	1.012
4	Low V(8m/min.)	High f(0.05mm/rev.)	High d(1.0mm)	0.327	0.140	6.250	3.000	0.232	0.378	1.201	1.956
5	High V(66m/min.)	Low f(0.10mm/rev.)	Low d(0.5mm)	0.280	0.290	0.016	1.000	0.109	0.158	2.252	3.264
6	High V(66m/min.)	Low f(0.10mm/rev.)	High d(1.0mm)	0.300	0.090	1.000	3.200	0.115	0.079	2.381	1.635
7	High V(66m/min.)	High f(0.10mm/rev.)	Low d(0.5mm)	0.098	0.378	4.300	5.350	0.327	0.415	1.691	2.147
8	High V(66m/min.)	High f(0.10mm/rev.)	High d(1.0mm)	0.301	0.393	6.100	6.500	0.256	0.628	1.325	3.250

Some experiments have been done for analysing the trends of tool wear, surface roughness and chip reduction coefficient by varying temperature. The setting for cutting velocity, feed and depth of cut are shown in Table 2.11. Figure 2.20 (i) shows the trend for responses when the cutting parameters have been changed. The changes came in responses due to increase in temperature from 200°C to 600°C. As the temperature increases from 200°C to 600°C the tool wear increases from 0.076 to 0.14 mm. it shows that the effect of temperature is not more effective at less cutting velocity, less feed and less depth of cut. In case of surface roughness, same setting the surface roughness decreases from 2.5 to 1.6 μm, it indicates that temperature is significant for surface roughness. Similarly in case of deformed chip thickness and chip reduction coefficient, the experimental value changes from 0.13668 to 0.09748 and from 2.83 to 2.0184 respectively. At low cutting velocity, feed and at high depth of cut when temperature is increasing from 200°C to 600 °C. The trend of tool wear, surface roughness, chip thickness and chip reduction coefficients are shown in Figure 2.20 (ii). The slope of chip reduction coefficient is more compared with surface roughness, chip thickness and tool wear. It indicates that as the temperature increases from 200 to 600°C the tool wear, surface roughness, deformed chip thickness and chip

reduction coefficient tends to decrease. Figure 2.20 (iii) shows the trend of changing for tool wear, surface roughness, deformed chip thickness and chip reduction coefficient. It was noticed that at high feed and other parameters are at low levels there is a high slope in surface roughness while other tool wear, deformed chip thickness and chip reduction coefficient are slightly decreasing. Figure 2.20 (iv) shows the change in tool wear, surface roughness, deformed chip thickness and chip reduction coefficient. At high feed and depth of cut surface roughness is decreasing fast and followed by chip reduction coefficient and tool wear. It was observed that there is no remarkable change in deformed chip thickness. At high cutting velocity with low feed and depth of cut, the trend of changing of tool wear, surface roughness, deformed chip thickness and chip reduction coefficient are shown in Figure 2.20 (v). It was observed that there is high decrease in chip reduction coefficient and surface roughness while no change observed in tool wear and deformed chip thickness. Figure 2.20 (vi) shows the change in tool wear, surface roughness, deformed chip thickness and chip reduction coefficient at high velocity, depth of cut and low feed rate.
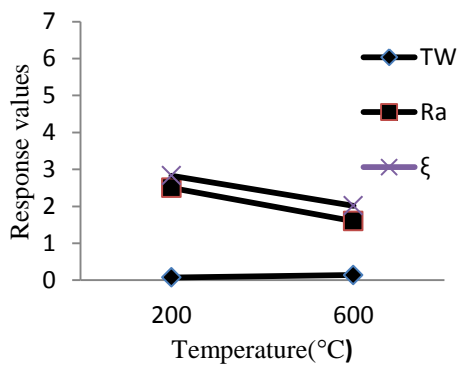
Figure (i)
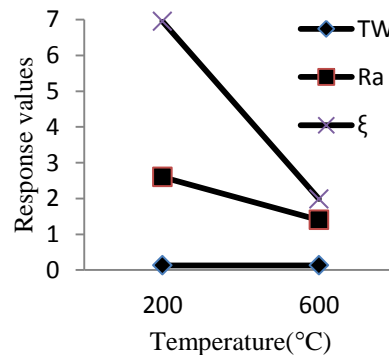
(Figure (ii)
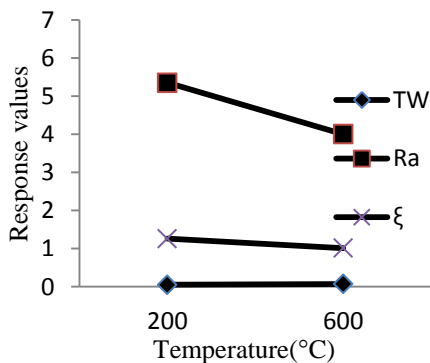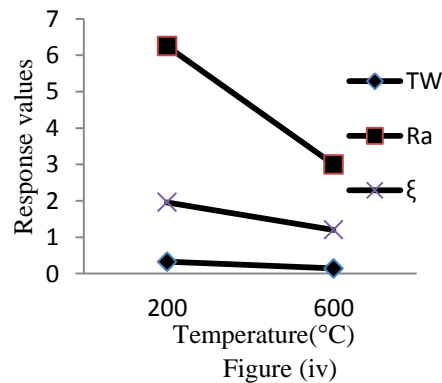
Figure (iii)
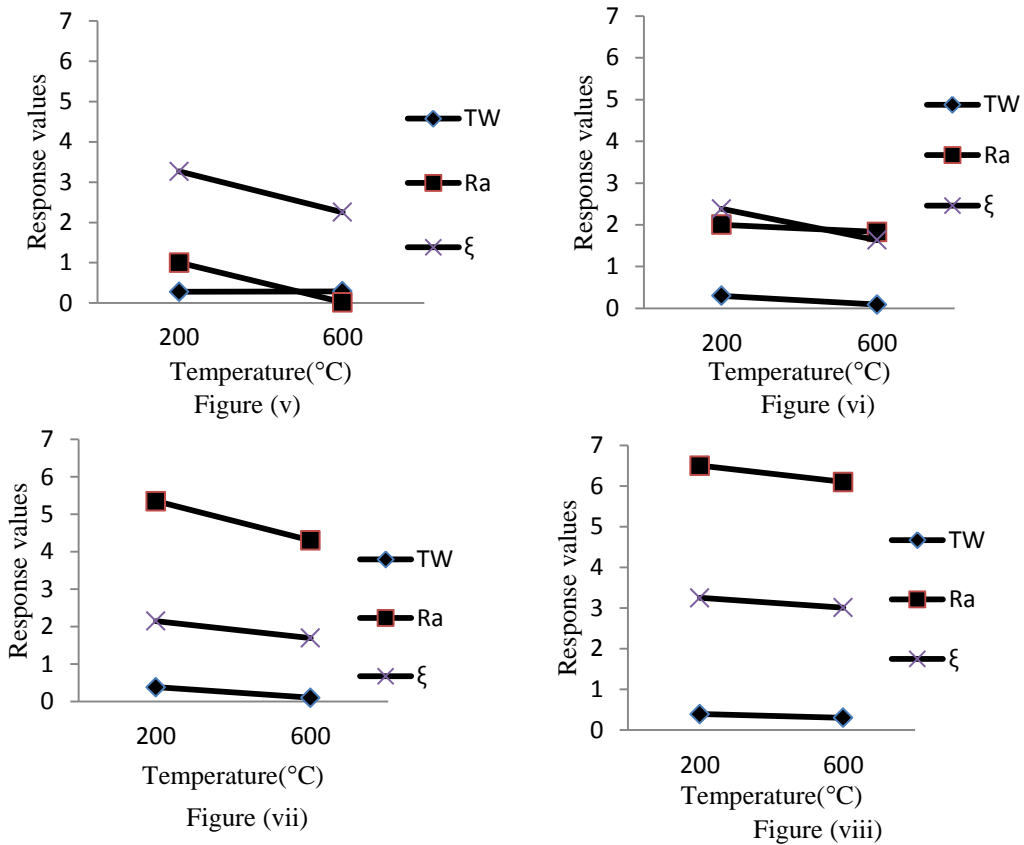
Figure (iv)

Figure 2. 30 Variation of tool wear, surface roughness and chip reduction coefficient while varying temperature

It was observed that trend of changing of tool wear, surface roughness and chip reduction coefficient are decreasing while increasing the temperature. It may possibly due to reduction in hardness of the workpiece.

2.5   Conclusions

It is observed that the temperature plays a significant role in reducing tool wear, surface finish and cutting power in hot machining operation.

Chapter 3

Single optimization techniques for performances characteristics using response surface methodology (RSM)

Chapter 3

Single optimization techniques for performances characteristics using response surface methodology (RSM)

3.1 Introduction

There is a growing trend to use appropriate design for conducting experimentsto attain optimal combination of process parameters.In recent decades many methods have been used such as Taguchi, Response surface methodology, Factorial design, etc. for many experimental works. Ranganathan et al. [1] compared the tool wear at three different temperatures (200°C, 400°C and 600°C) by applying Taguchi technique for stainless steel. They modelled equations for tool wear. Wenji et al. [2] used L_{16}orthogonal array for modelling of hot machining operation to determine surface roughness. The highest temperature obtained at chip formation zone. Tosun et al. [9] applied Taguchi method for tool life and surface roughness for high manganese steel in hot machining. They concluded that cutting speed and feed rate were the dominating factors followed by depth-of-cut and workpiece temperature for both of responses. Maity and Swain [23] modelled an equation for tool life by employing regression analysis.

In present investigation, a statistical model were developed for performance characteristics (tool wear, surface roughness, chip reduction coefficient, tool life and power consumption) usingresponse surface methodology.

3.2 Methodology

Response surface methodology (RSM) consists of a group of mathematical and statistical techniques used in the development of an adequate functional relationship between a response of interest, y, and a number of associated control (or input) variables denoted by x_1, x_2, ... , x_k [67]. The most widespread application of the RSM is in situation where input variables potentially influence some quality characteristics of a process. RSM was used to analyse the main medium constituents influencing process parameters of the hot machining operation on the performances

characteristics. The relationship between process parameters and performance characteristics are represented in form of equations.

RSM consists of a group of mathematical and statistical techniques that can be used to define the relationships between the response and the independent variables. In addition to analysing the effects of the independent variables as well as interactions of the process parameters (independent parameters), this experimental methodology also generates a mathematical model. The relation between process parameters with response parameters can be shown by using second order equation as follows:

$$Z=\lambda_0+\sum_{i=1}^{k}\lambda_i A_i+\sum_{i=1}^{k}\lambda_{ii} A_i^2+\sum_{i,j=1,i^!j}^{k}\lambda_{ij}A_i A_j+\mu \qquad (3.1)$$

where, Z is the respective response, λ_0, λ_i, λ_{ii} and λ_{ij} are the regression coefficients, A_i, is the process variable, A_i^2, $A_i A_j$ are the square and interaction terms for respective process variables and μ is the error in the model. μ was considered as having zero mean and zero variance.

Central composite rotatable design has been divided into three parts:

- Factorial points (2^k)

- Star points positioned at a distance α from origin on both sides of the co-ordinate axes. Star points are evaluated by 2k. For k < 5, α can be evaluated by $2^{k/4}$, value of α is evaluated as 2.

- Some more points are added at the centre known as centre points (n) to give rough equal precision to response Z. For four parameters, six additional runs are required at the origin.

  The total number of runs required as 4+16+8+6 = 30.

ANOVA test is a statistical tool used to understand the experimental data, and it is extensively used to set up the performance of a number of parameters under analysis. In this study, ANOVA was assessed for inspecting the significant factors and their effects on the responses. Probability (p-value) was used for recognising the significant factors and pattern of related interactions among process parameters. The smaller p-value reveals a very significant correlation coefficient. The fitting of the model was determined by the coefficient of determination (R-sq.) and its statistical significance was analysed by using F test. The R-sq. value shows the amount of variation observed in valuesthat is explained by input factors.

In the present investigation, Response surface methodology (RSM) is applied to

optimize the process parameters to reduce the tool wear, surface roughness and chip reduction coefficient in hot machining of high manganese steel using carbide insert. The tool wear for different combination of process parameters as per RSM are obtained from experimental investigation as shown in Table 2.7.

3.3   Results and discussion

The high manganese steel tested in the experimentation section. The tooling and the hot machining cutting conditions were described in same section. The test showed some results on the basis of RSM.

3.3.1   Effects of process parameters on tool wear (TW)

The corresponding ANOVA test for tool wear is represented in Table 3.1 with their percentage contributions. The main effect plot for tool wear is shown in Figure 3.1. The peak tool wear is obtained at 600°C, 66m/min, 0.2 mm/rev. and 2 mm depth of cut. The tool wear value increases with the increase in cutting velocity, feed rate and depth of cut. All the interaction factors affecting tool wear are shown in Figure 3.2. The interaction between feed and depth of cut is found to be the significant term among all parameters at 95% confidence level. The effects of temperature on tool wear are nominal. Tool wear first decreases then it starts to increase after 400°C.The minimum tool wear was obtained at 400°C. It may possibly be due to increase in temperature at shear zone which reduces the shear strength of material that intends to reduce tool wear. The tool wear appears as an incremental function of cutting velocity. With cutting velocity tool wear is increasing because of more abrasion at rake face with respect to time. The tool-chip contact area decreases with increasing cutting speed and contact time in conventional cutting region. It was observed that tool wears out more at the nose area with increase in cutting velocity. The minimum tool wear was obtained at 24m/min. Further tool wear slightly decreased up to 0.125mm/rev. It increased after 0.125mm/rev. due to built-up-edge formation at the nose area. The tool wear also increased with increase in depth of cut due to increase in the contact area at interface.

Table 3. 1 ANOVA test for tool wear

Source	DF	Seq SS	Adj SS	Adj MS	F	p	% Contribution
T	1	0.000144	0.000144	0.000144	0.02	0.883	0.04519
V	1	0.100203	0.100203	0.100203	15.69	0.002*	**31.445**
f	1	0.009293	0.009293	0.009293	1.46	0.249	2.9163
d	1	0.017735	0.017735	0.017735	2.78	0.120	5.56548
T×T	1	0.002185	0.000328	0.000328	0.05	0.824	0.685682
V×V	1	0.001489	0.001507	0.001507	0.24	0.635	0.467268
f×f	1	0.004532	0.008647	0.008647	1.35	0.265	1.422201
d×d	1	0.010936	0.010936	0.010936	1.71	0.213	3.43186
T×V	1	0.004796	0.004796	0.004796	0.75	0.402	1.50505
T×f	1	0.007353	0.007353	0.007353	1.15	0.303	2.30747
T×d	1	0.028985	0.028985	0.028985	4.54	0.053	9.09588
V×f	1	0.000638	0.000638	0.000638	0.10	0.757	0.200213
V×d	1	0.007877	0.007877	0.007877	1.23	0.287	2.471906
f×d	1	0.030538	0.030538	0.030538	4.78	0.048*	**9.583225**
Lack-of-Fit	10	0.063162	0.063162	0.006316	0.95	0.586	
Total	29	0.318661					

S = 1.00176   R-Sq = 75.33%   R-Sq(adj) = 44.96%

* = Significant term

(i)   (ii)

(iii)   (iv)
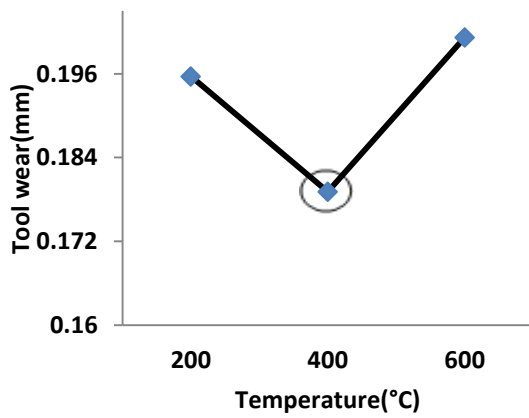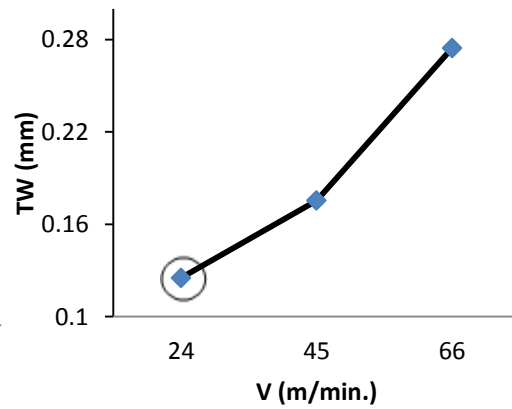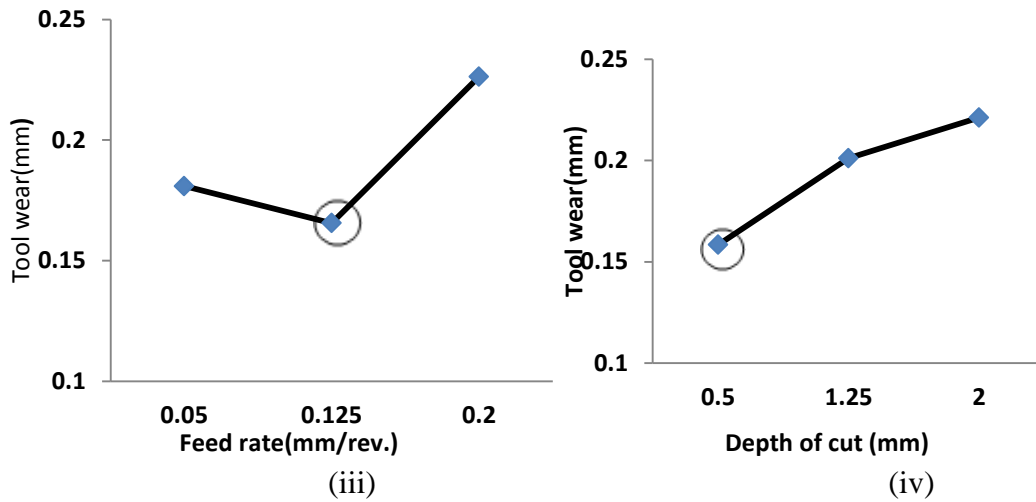
Figure 3. 11 Main effect plot for TW

The second order model for tool wear shown by Equation 3.2.:

$$TW = 0.170327 + 0.002833\ T + 0.074611\ V + 0.022722 \times f + 0.031389 \times d + 0.011364 \times T \times T + 0.024364 \times V \times V + 0.058364 \times f \times f - 0.065636\ d \times d + 0.017313 \times T \times V + 0.021438 \times T \times f - 0.042563 \times T \times d + 0.006313 \times V \times f - 0.022188 \times V \times d + 0.043688 \times f \times d \qquad (3.2)$$

The value of R-sq for tool wear is 75.33% which shows model ability to predict the response. The standard deviation of errors (S) for tool wear is 1.00176. This shows the significance of model for tool wear. The percentage contribution of each parameter affecting responses is shown in Table 3.1. It can be seen that V is the most significant factor with 31.445%.

(i)   (ii)
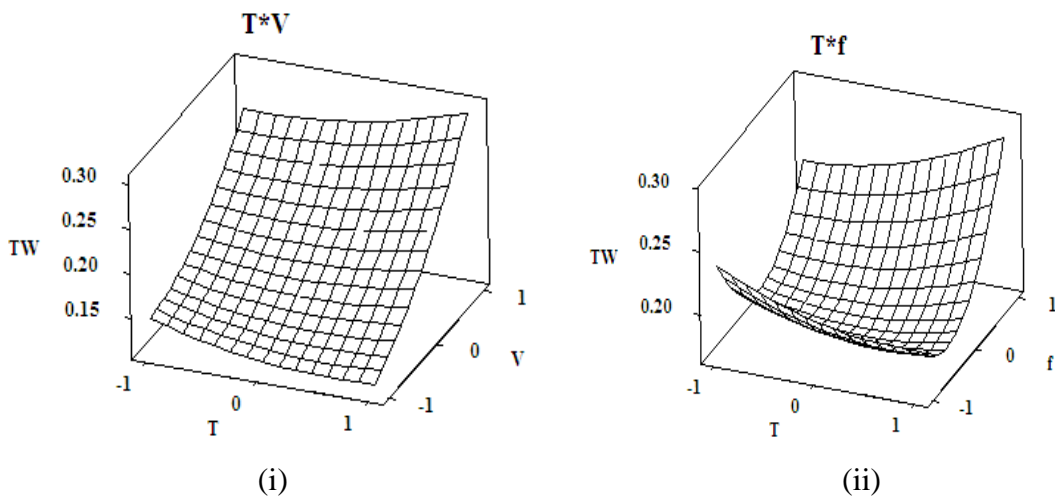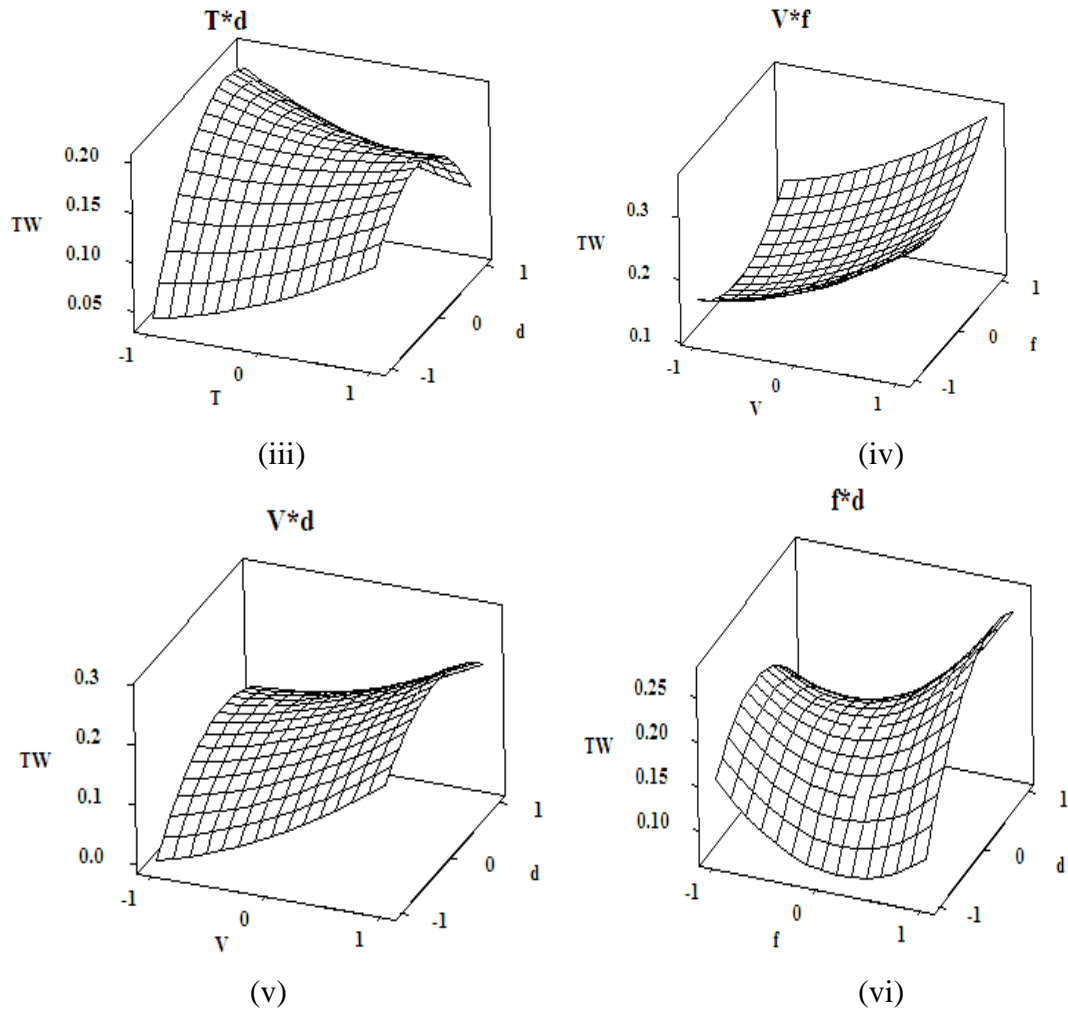
Figure 3. 12 Interaction plots for tool wear

Observation values are shown in Figure 3.3. Residual plot for TW is shown in Figure 3.4. Residual plots utilised for descriptions of the data which analysed for determining whether the model fits the data to meet the assumptions of the analysis. The data points obtained appearance as an approximate straight line which shows the consistency of the data. The shape of normal probability looks like Long tails (Figure 3.5).

Figure 3. 13 Run order plot
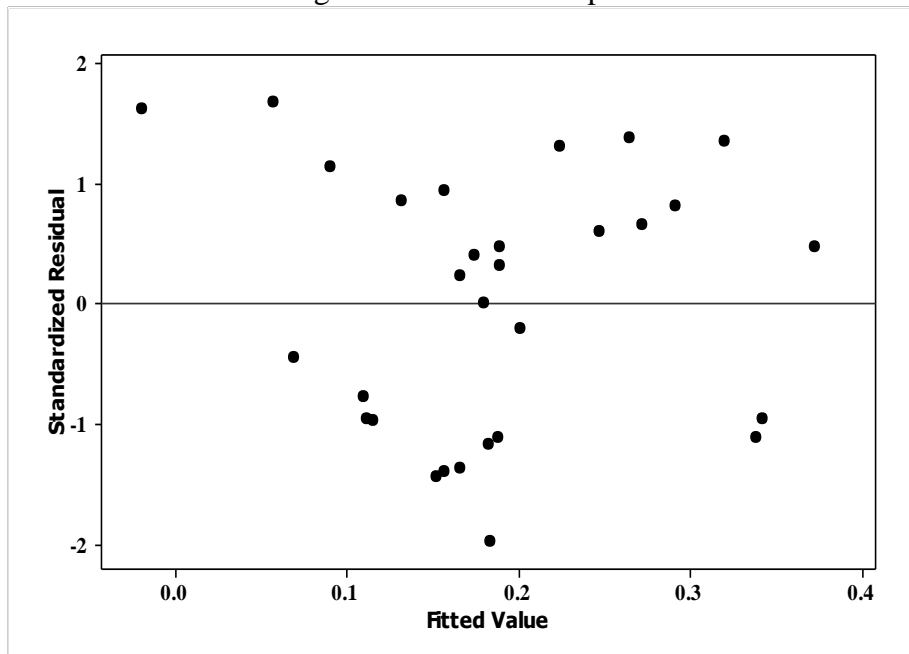
Figure 3. 14 Fit value plot
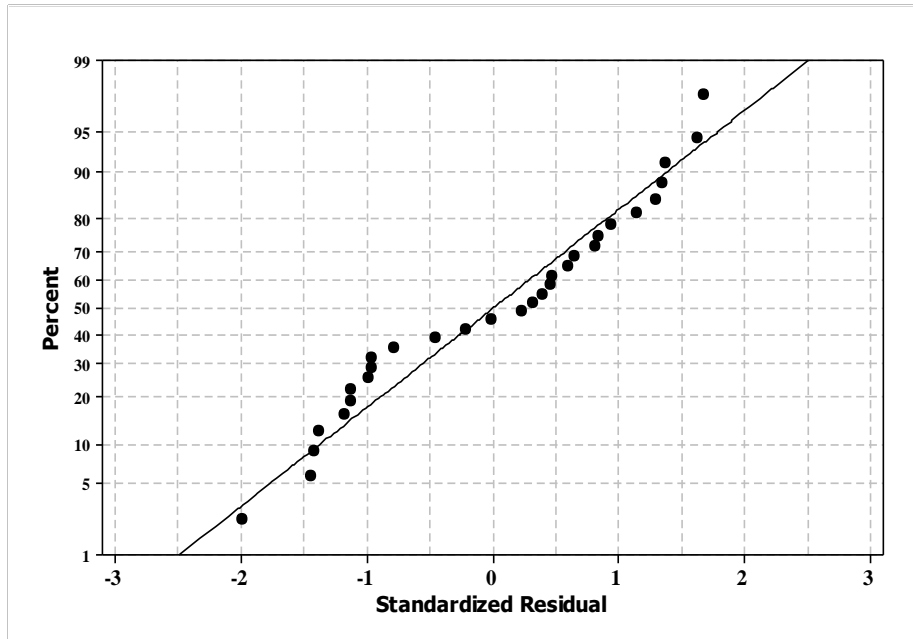
Figure 3. 15 Normal probability plot

3.3.2 Effects of process parameters on Surface roughness (Ra)

In order to see the effects of process parameters on Surface roughness, lower-the-better criterion is adopted. ANOVA test for surface roughness shows that feed and depth of cut are the two most significant factors for surface roughness as shown in Table 3.2 with 54.672% and 2.317% contribution respectively. Among the interactions temperature and cutting velocity, temperature and feed rate, velocity and feed and between feed and depth of cut are the significant interactions terms which effects Ra in an influensive manner at 95% confidence level. The effects of the process parameters can be seen from Figure 3.6. Due to increase in temperature, strain hardening ability and flow stress of material decreases which reduces the strength of material and requires less cutting force to cut material. Minimum Ra is obtained at 400°C. Ra is decreasing with increase in cutting velocity upto 45 m/min and further increases with cutting velocity. Minimum Ra is obtained at 45 m/min. Figure 3.7 shows effects of interactions between process parameters on Ra. The percentage contributions of process parameters for surface roughness are shown in Table 3.2. The value of R-sq for surface roughness is 97.26%. This indicates good predictability for response through presented model. The value of standard deviation of errors (S) is 0.467136. This shows insignificance of S factor and therefore indicates adequacy of model.

Table 3. 2 ANOVA test for Surface roughness

Source	DF	Seq SS	Adj SS	Adj MS	F	p	% Contribution
T	1	0.224	0.2236	0.2236	1.02	0.330	0.216162
V	1	0.121	0.1210	0.1210	0.55	0.470	0.116766
f	1	56.654	56.6545	56.6545	259.63	0.000*	**54.67161**
d	1	2.401	2.4010	2.4010	11.00	0.006*	**2.316986**
T×T	1	5.087	0.1075	0.1075	0.49	0.495	4.909
V×V	1	1.127	0.2147	0.2147	0.98	0.339	1.087565
f×f	1	13.609	11.8893	11.8893	54.48	0.000*	13.1328
d×d	1	0.151	0.1514	0.1514	0.69	0.420	0.145716
T×V	1	8.029	8.0287	8.0287	36.79	0.000*	7.748056
T×f	1	1.120	1.1204	1.1204	5.13	0.041*	1.08081
T×d	1	0.167	0.1669	0.1669	0.76	0.398	0.161156
V×f	1	2.668	2.6683	2.6683	12.23	0.004*	2.574643
V×d	1	2.507	2.5075	2.5075	11.49	0.005*	2.419277
f×d	1	0.003	0.0034	0.0034	0.02	0.902	0.002895
Total	29	103.626					
S = 0.467136			R-Sq = 97.26%			R-Sq (adj.) = 93.89%	
* = Significant terms							

Feed was noticed as the most pronounced factor on Surface roughness. Surface roughness slightly decreases with increase in feed to the value of 0.15 mm/rev, it tends to increase after that. Vibration was also observed as a cause which enhances the roughness of surface due to increase in feed. Surface roughness decreases upto depth of cut of 1.25mm and after that it increases. Minimum surface roughness is observed at depth of cut 1.25mm. Depth-of-cut interaction effect on surface roughness is more effective than its individual effect.

(i)

(ii)

(iii)

(iv)
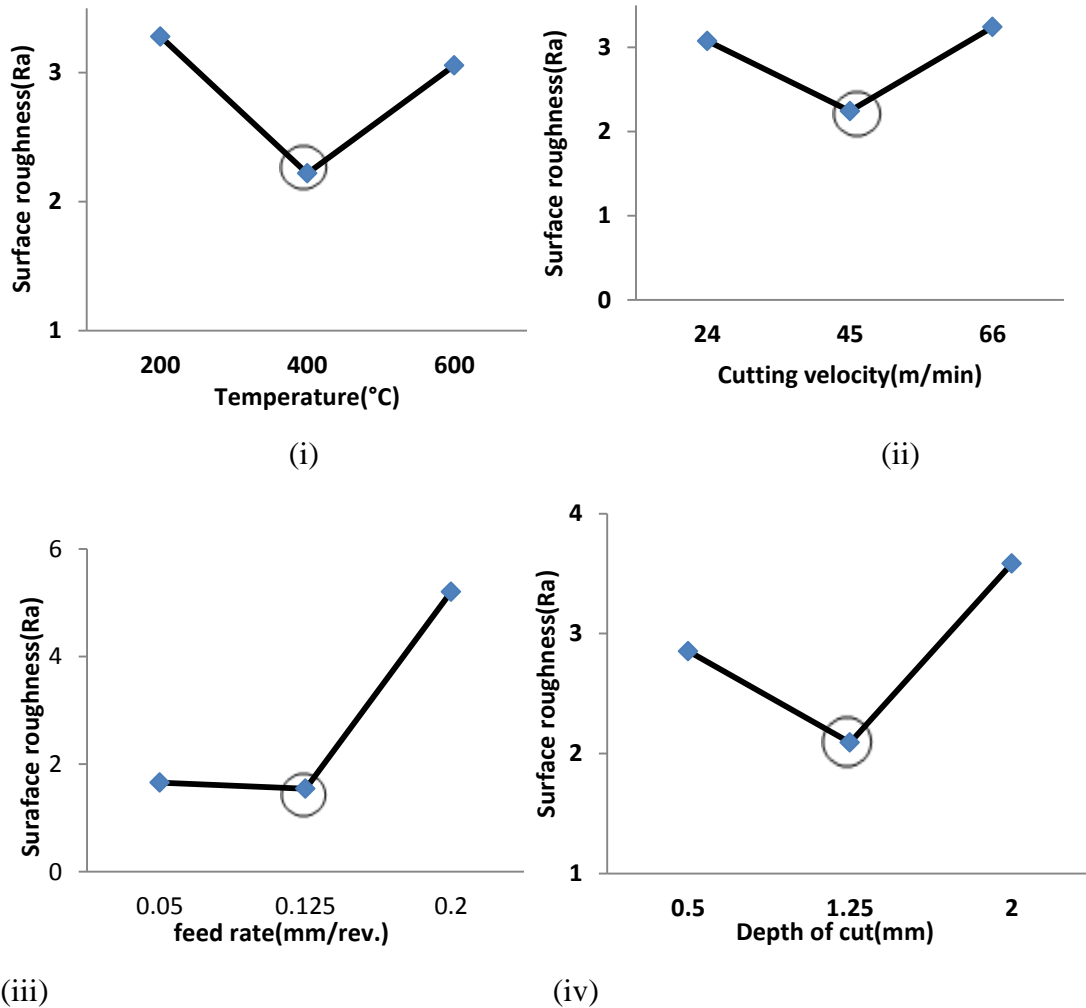
Figure 3. 16 Main effects plot for Surface Roughness

The second order equation is modelled for Ra is shown in Equation 3.3.

Ra = 1.52016 - 0.11144×T + 0.08200×V + 1.77411×f + 0.36522×d - 0.20582×T×T - 0.29082×V×V + 2.16418×f×f + 0.24418×d×d + 0.70838×T×V - 0.26462×T×f - 0.10213×T×d + 0.40838×V×f + 0.39588×V×d - 0.01462×f×d   (3.3)

Run order plot for each Ra is shown in Figure 3.8. Residual versus observation data reveals that the data are normally distributed and variables are influencing the Ra (Figure 3.9). It is concluded from normal probability plot that the points lie closer to straight line, indicates the data following a normal distribution as shown in Figure 3.10.

Figure 3. 17 Response surface plots representing the effects on Surface roughness
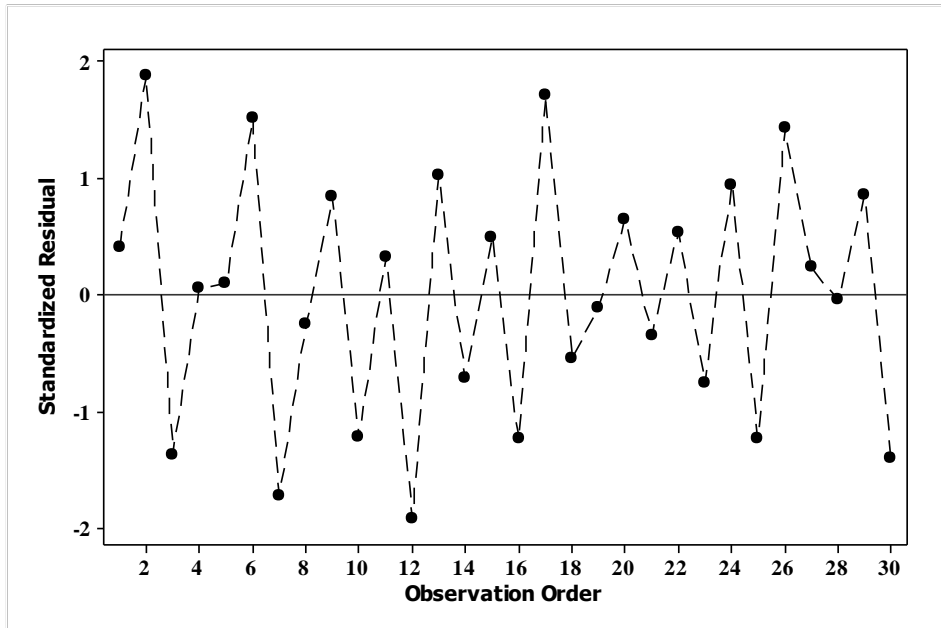
Figure 3. 18 Run order plot
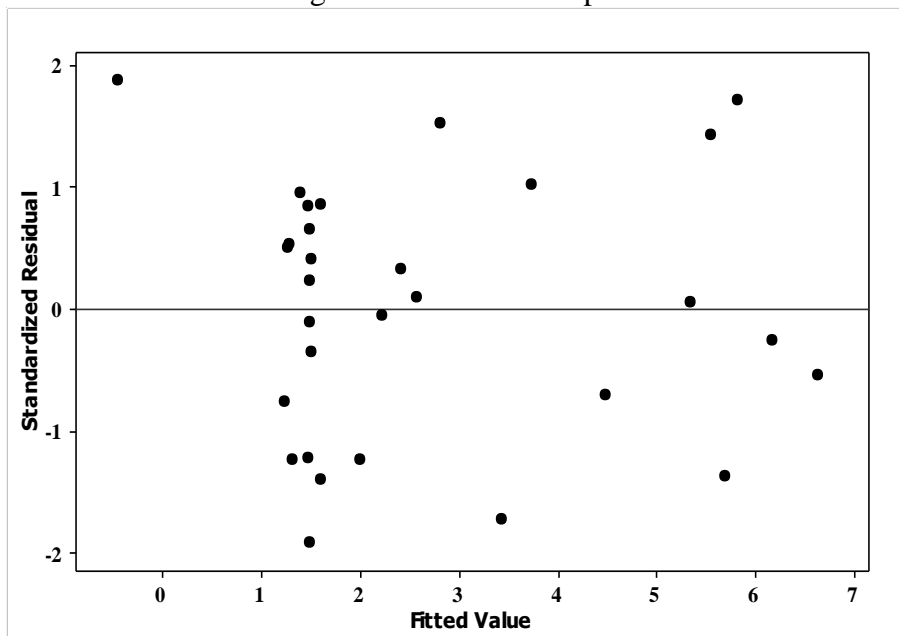
Figure 3. 19 Fit value plot
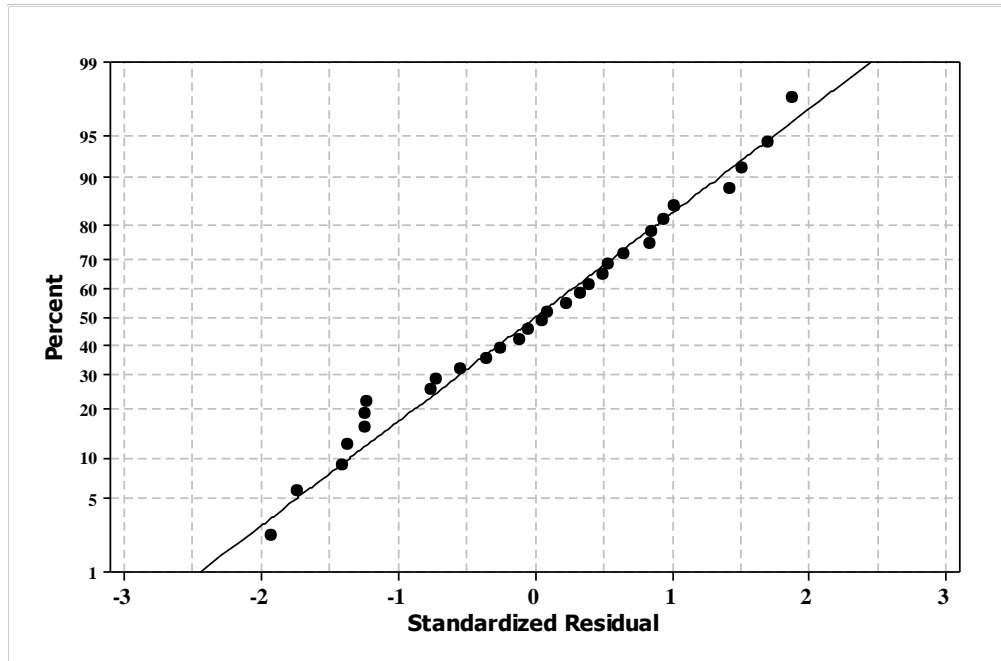
Figure 3. 20 Normal probability plot

3.3.3 Effects of process parameters on Chip reduction coefficient (ξ)

ANOVA test for chip reduction coefficient (ξ) is shown in Table 3.3. This table shows that the most significant factor as temperature followed by cutting velocity, feed and depth of cut. Value of R^2 is 75.33% which shows the better fitting of data with modelled equation. The value of S is 1.00176 which shows S as an insignificant factors for analysis.

Figure 3.11 shows the main effect plot for chip reduction coefficient which shows the optimum combination for minimum chip reduction coefficient. It is clearly observed that feed has the biggest factor on chip reduction coefficient. The optimum combination is 600°C, 66 m/min, 0.2 mm/rev and 1.25 mm depth of cut.

Table 3. 3 ANOVA test for chip reduction coefficient (ξ)

Source	DF	Seq SS	Adj SS	Adj MS	F	p	% Contribution
T	1	0.4010	0.4010	0.4010	0.40	0.538	0.758374
V	1	0.1218	0.1218	0.1218	0.12	0.733	0.230349
f	1	6.9269	6.9269	6.9269	6.90	0.021*	**13.1002**
d	1	3.1214	3.1214	3.1214	3.11	0.101	5.903212
T×T	1	0.0730	2.2434	2.2434	2.24	0.159	0.138058
V×V	1	0.0482	1.9129	1.9129	1.91	0.191	0.091156
f×f	1	3.9622	1.0894	1.0894	1.09	0.316	7.493338
d×d	1	10.5218	10.5218	10.5218	10.48	0.006	19.8989
T×V	1	3.9198	3.9198	3.9198	3.91	0.070*	**7.413151**
T×f	1	4.4098	4.4098	4.4098	4.39	0.056	8.339842
T×d	1	0.7398	0.7398	0.7398	0.74	0.406	1.399115
V×f	1	3.2773	3.2773	3.2773	3.27	0.094	6.198051
V×d	1	2.0598	2.0598	2.0598	2.05	0.176	3.895507
f×d	1	0.0588	0.0588	0.0588	0.06	0.812	0.111203
Total	29	52.8763					
S = 1.00176			R-Sq = 75.33%				R-Sq(adj) = 44.96%
* = Significant factor							

(i)   (ii)

(iii)   (iv)
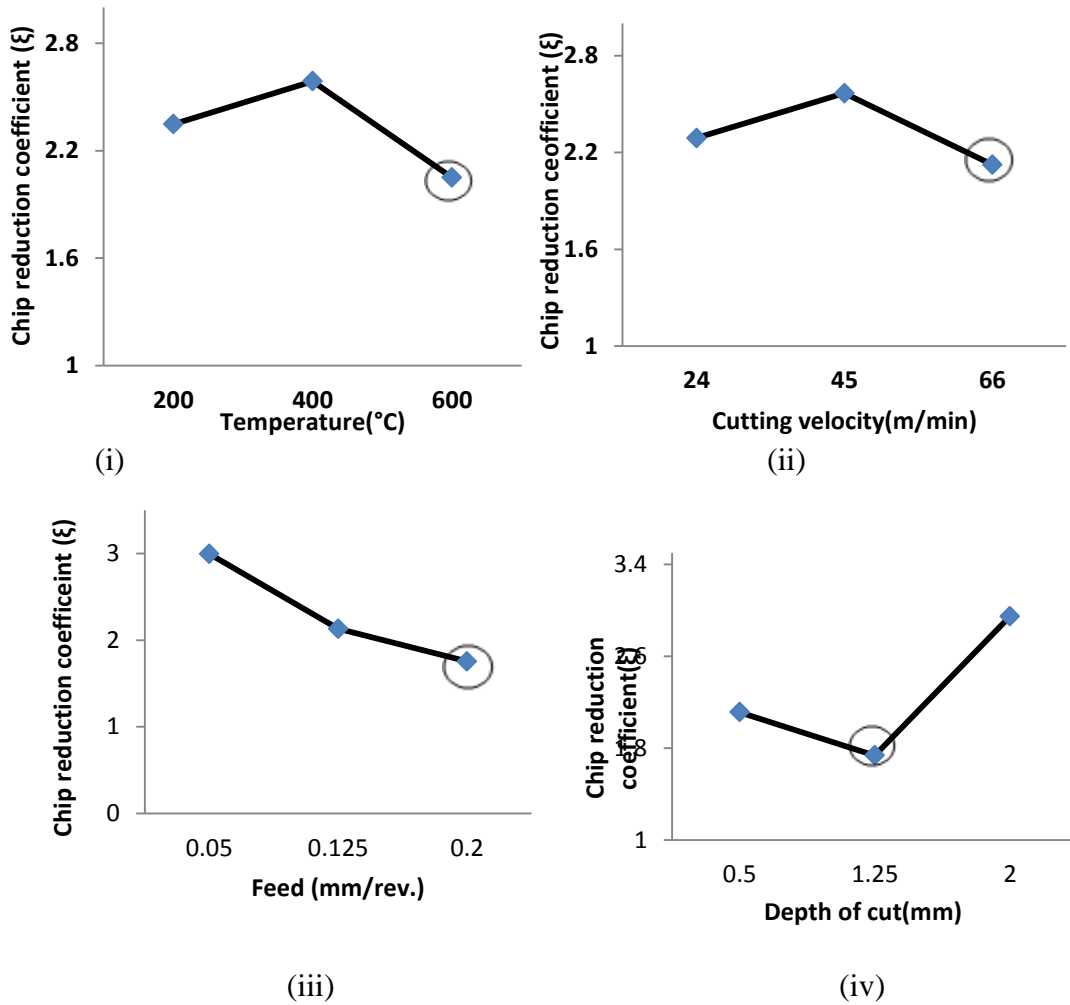
Figure 3. 21 Main effect plot for chip reduction coefficient

The mathematical model for chip reduction coefficient is shown by Equation 3.4. This developed model was used to understand the hot machining process in terms of cutting parameters.

$$\xi = 1.65941 - 0.14925 \times T - 0.08226 \times V - 0.62034 \times f + 0.41642 \times d - 0.94008 \times T \times T - 0.86809 \times V \times V + 0.65509 \times f \times f + 2.03592 \times d \times d + 0.49496 \times T \times V + 0.52499 \times T \times f - 0.21502 \times T \times d + 0.45258 \times V \times f - 0.35880 \times V \times d - 0.06065 \times f \times d \qquad (3.4)$$

All interaction factors plotted for chip reduction coefficient are shown in Figure 3.12. From Equation 3.4 we can conclude that the interaction between temperature and feed as the most significant factor followed by interaction between temperature and velocity and between cutting velocity and feed. The percentage contribution for each term is shown in Table 3.3 where cutting velocity has the maximum contribution percentage. Response value for each run is shown in Figure 3.13. Fit order plot has been given in Figure 3.14. Normal probability plot shown in Figure 3.15 indicates good normality distribution.
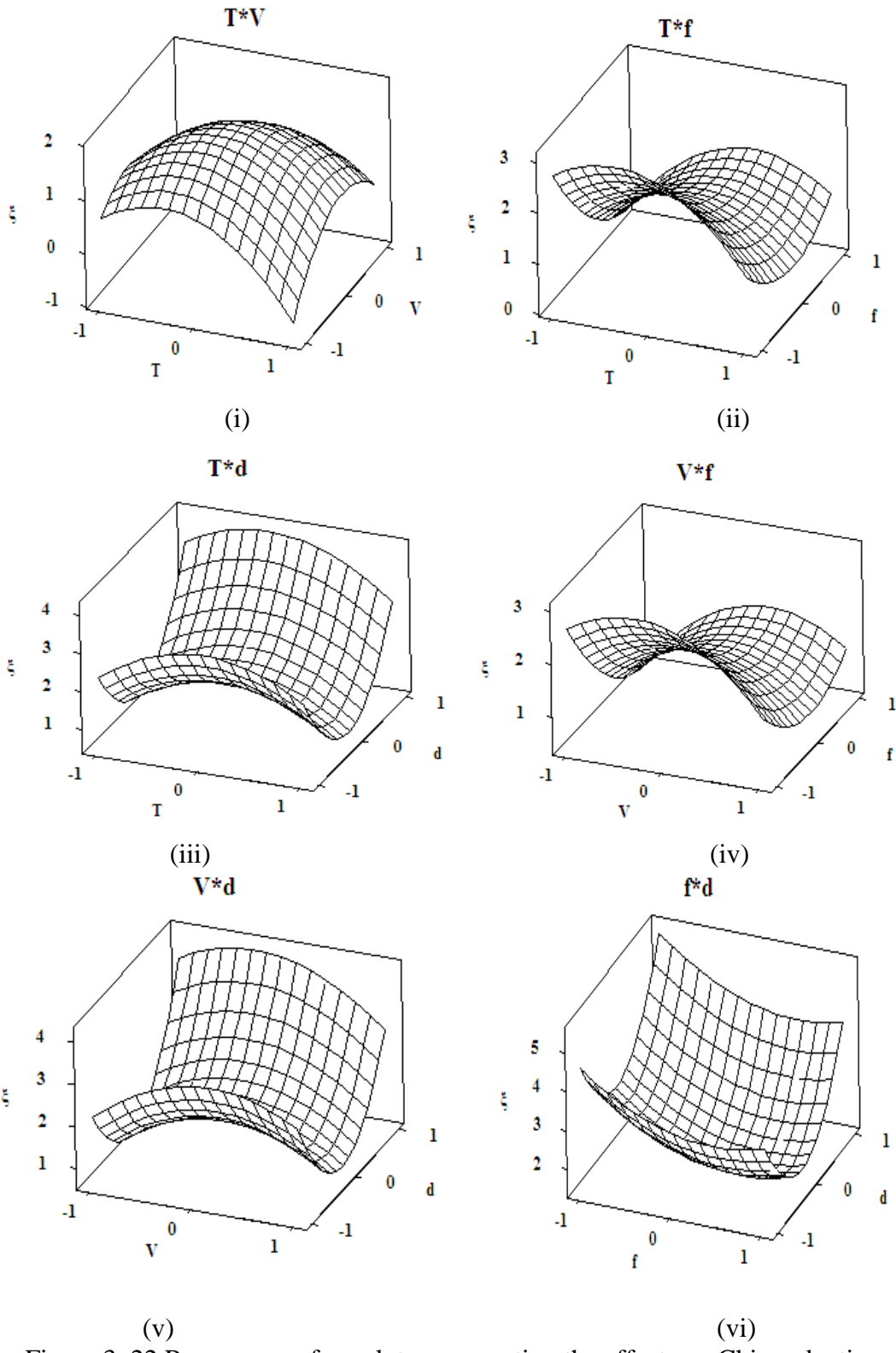
Figure 3. 22 Response surface plots representing the effects on Chip reduction coefficient
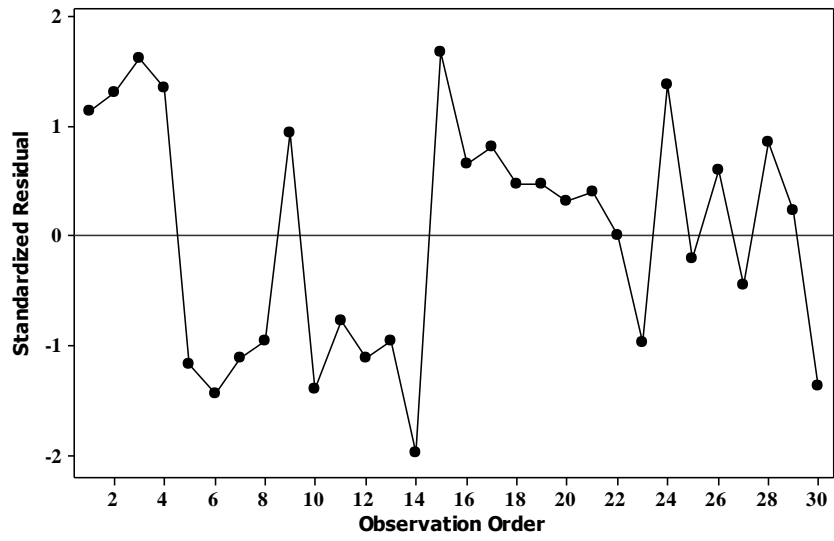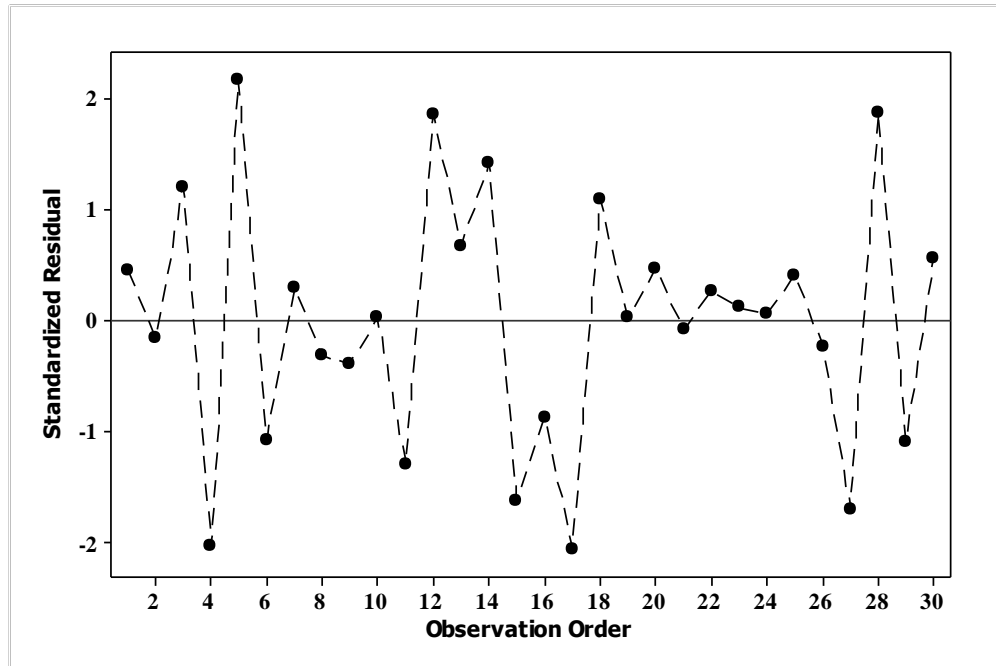
Figure 3. 23 Run order plot
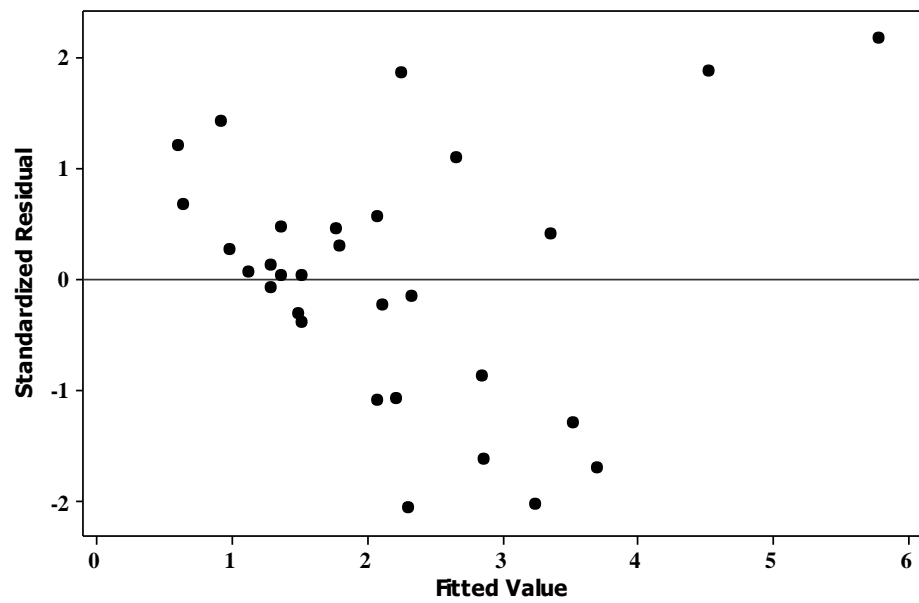
Figure 3. 24 Fit value plot
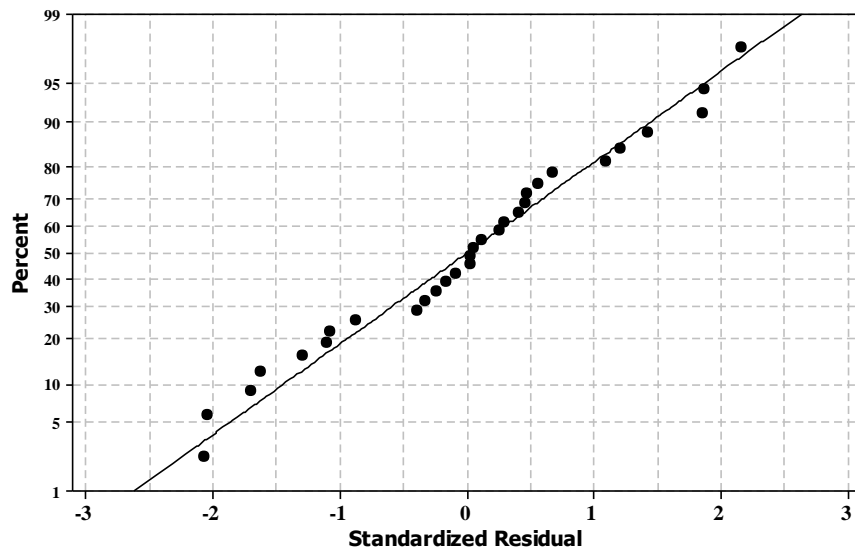
Figure 3. 25 Normal probability plot

3.3.4 Effects of process parameters on tool life (tl)

ANOVA test for tool life is shown in Table 3.4. It reveals the cutting velocity as the most significant factor. The percentage contribution of the process parameters and their interactions for tool life is shown in Table 3.4.

The influence of the cutting parameters on tool life is shown in Figure 3.16. In the present investigation, the tool life was determined by taking flank wear as the extension of flank wear. The tool life was determined by considering 0.3 mm as a flank wear limit. Present study reveals that cutting velocity is the most significant factor for effecting tool life. Maximum tool life obtained at 21.5 m/min of cutting velocity. The maximum tool life was obtained at medium temperature (400°C), low cutting velocity (8 m/min), low feed (0.05 mm/rev.) and medium level of depth of cut (0.75 mm). All the significant interaction between processes parameters on tool life are shown in Figure 3.17.

The second order equation mentioned for tool life (tl) is shown in Equation 3.5.

$tl = 43.7273 + 2.7222 \times T - 7.8333 \times V - 4.5000 \times f - 2.5556 \times d - 18.1364 \times T \times T + 9.8636 \times V \times V + 8.8636 \times f \times f - 28.6364 \times d \times d - 0.5000 \times T \times V - 1.8750 \times T \times f - 1.8750 \times T \times d + 1.3750 \times V \times f + 1.3750 \times V \times d + 1.7500 \times f \times d$ (3.5)

Table 3. 4 ANOVA test for tool life (tl)

Source	DF	Seq SS	Adj SS	Adj MS	F	p	% Contribution
T	1	133.39	133.39	133.39	1.30	0.275	1.59965
V	1	1104.50	1104.50	1104.50	10.77	0.006*	**13.24547**
F	1	364.50	364.50	364.50	3.55	0.082	4.371185
D	1	117.56	117.56	117.56	1.15	0.304	1.409812
T×T	1	2745.63	834.97	834.97	8.14	0.014*	***32.92636***
V×V	1	21.06	246.97	246.97	2.41	0.145	0.252557
f×f	1	3.64	199.43	199.43	1.94	0.187	0.043652
d×d	1	2081.64	2081.64	2081.64	20.29	0.001*	**24.9636**
T×V	1	4.00	4.00	4.00	0.04	0.847	0.047969
T×f	1	56.25	56.25	56.25	0.55	0.472	0.674566
T×d	1	56.25	56.25	56.25	0.55	0.472	0.674566
V×f	1	30.25	30.25	30.25	0.29	0.596	0.362766
V×d	1	30.25	30.25	30.25	0.29	0.596	0.362766
f×d	1	49.00	49.00	49.00	0.48	0.502	0.587622
Total	29	8338.70					
S = 10.1283			R-Sq = 84.01%				R-Sq(adj) = 64.32%
* = Significant factor							

The value of R-sq for tool life is 84.01% indicates good prediction for response from the presented model. The value of standard deviation of errors (S) for tool life is 10.1283 shows insignificance of the S factor indicates good prediction by model. Run order plot, fit value plot and normal probability plot are shown in Figure 3.18, 3.19 and 3.20 respectively.
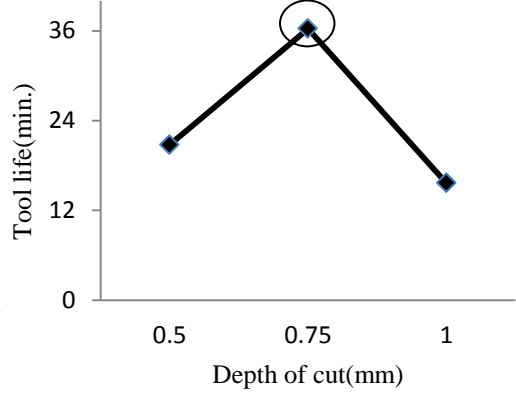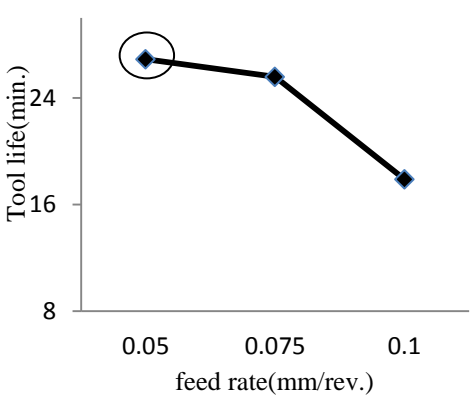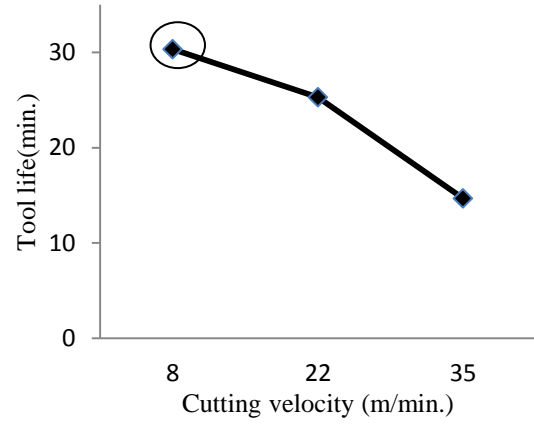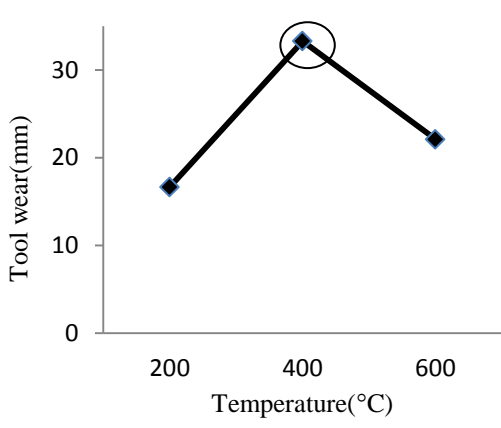
Figure 3. 26 Main effect plots for tool life

(iii)	(iv)
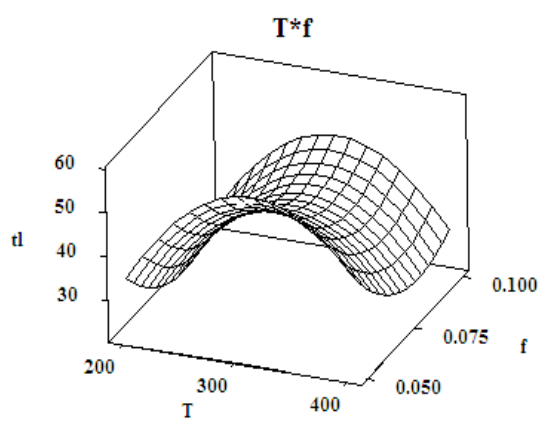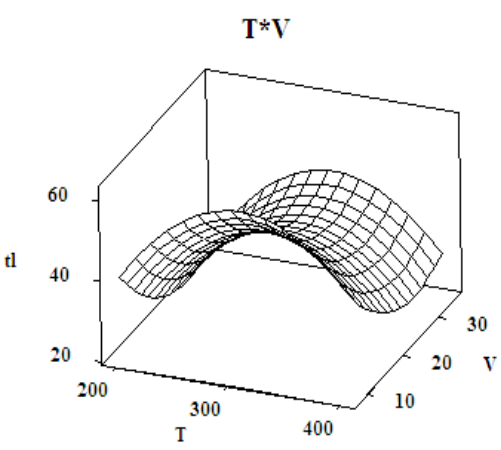
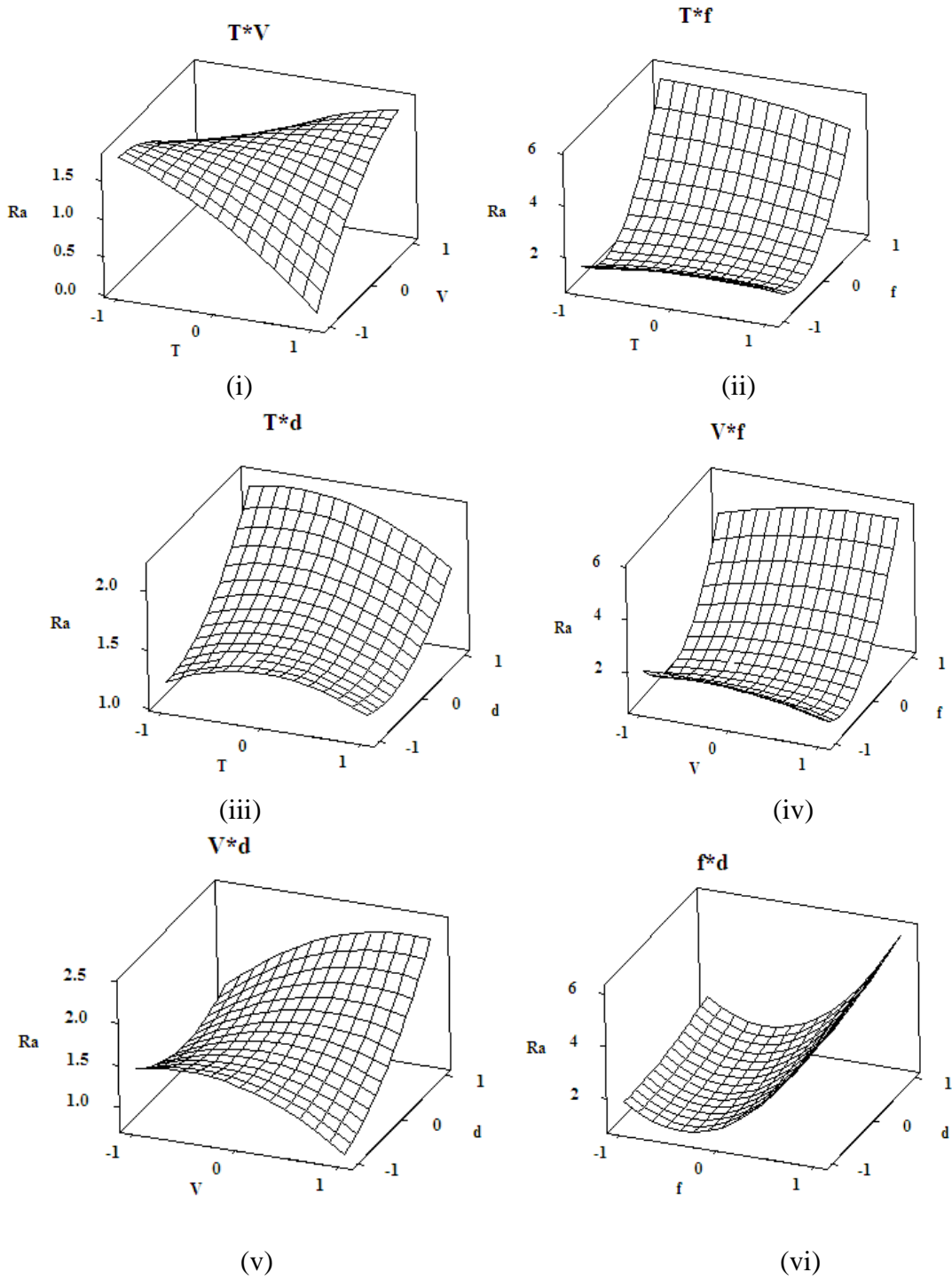|	
(v)	(vi)
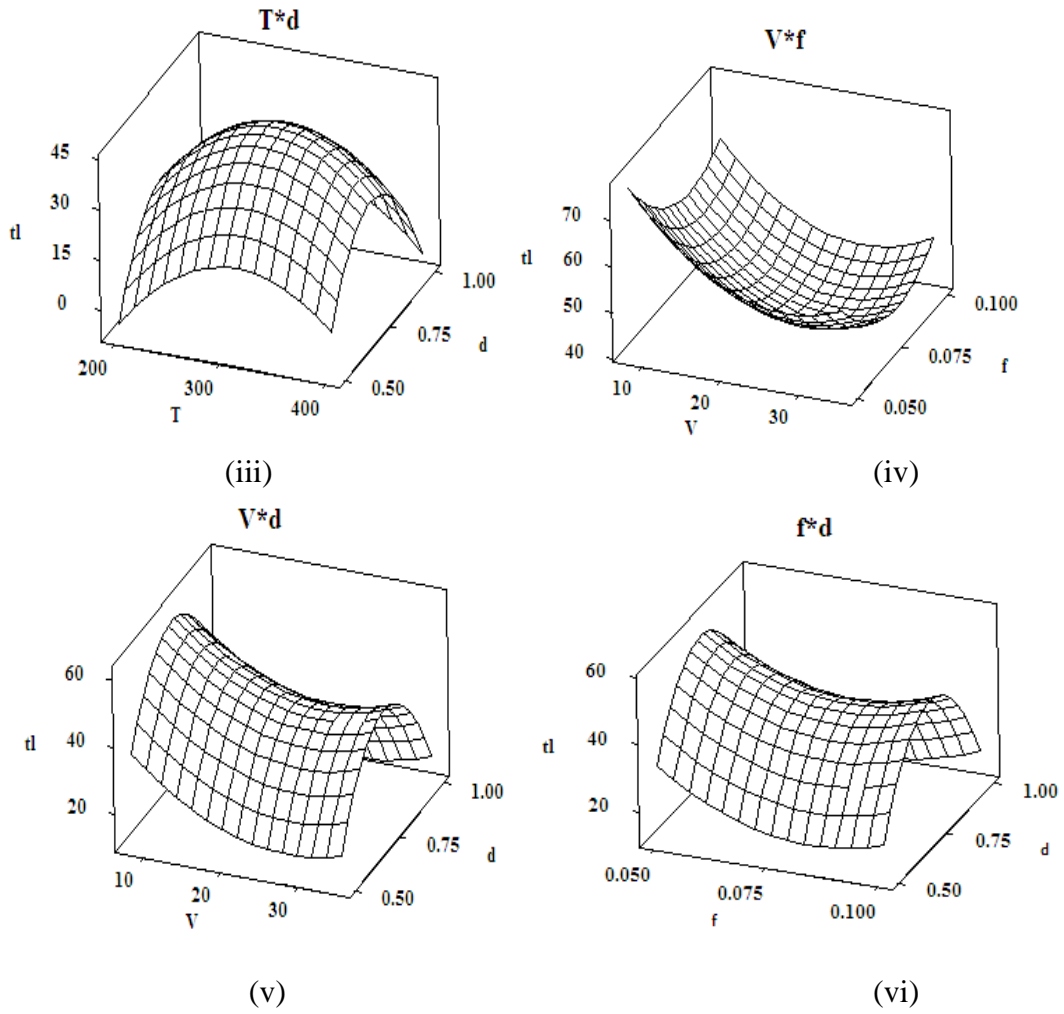
Figure 3. 27 Response surface plot representing effects on tool life
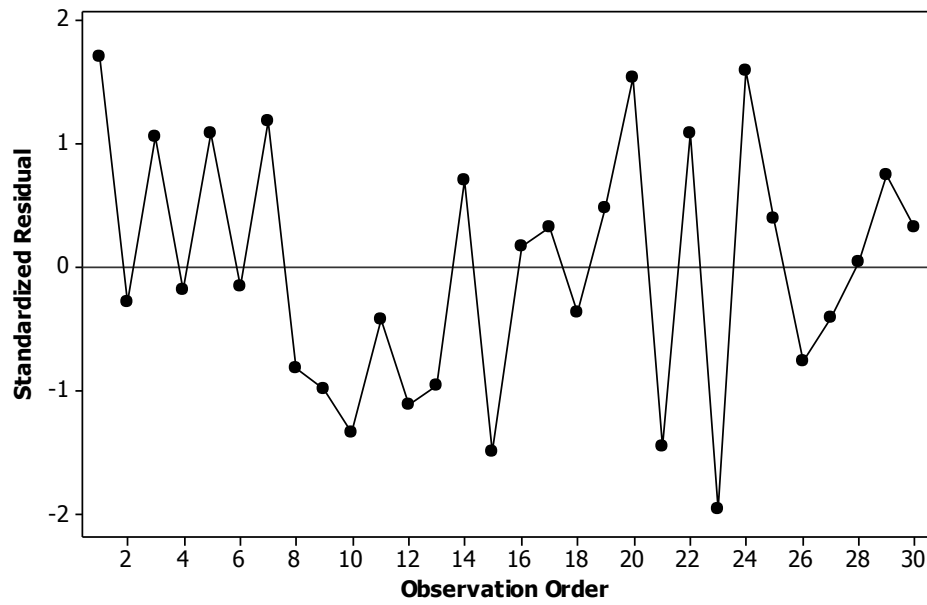
Figure 3. 28 Run Order plot
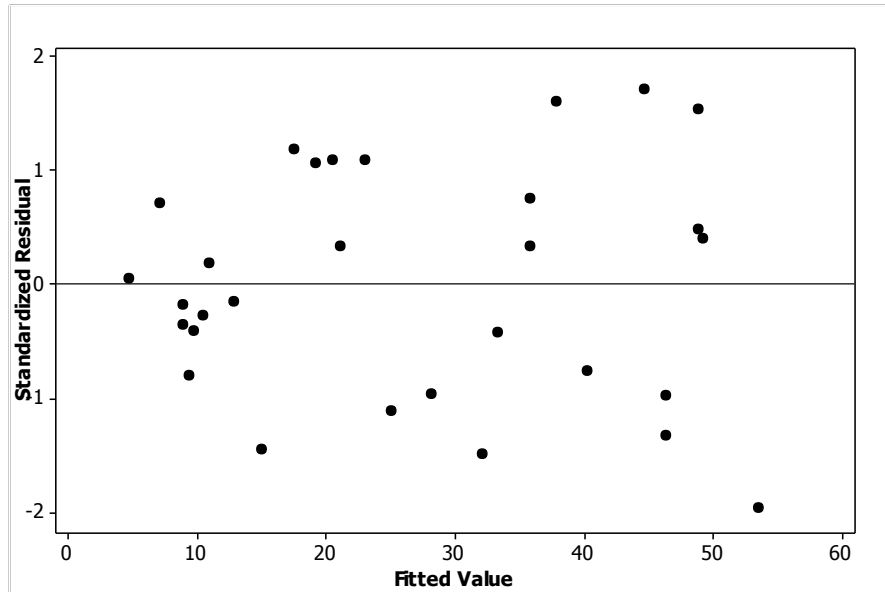
Figure 3. 29 Fit value plot
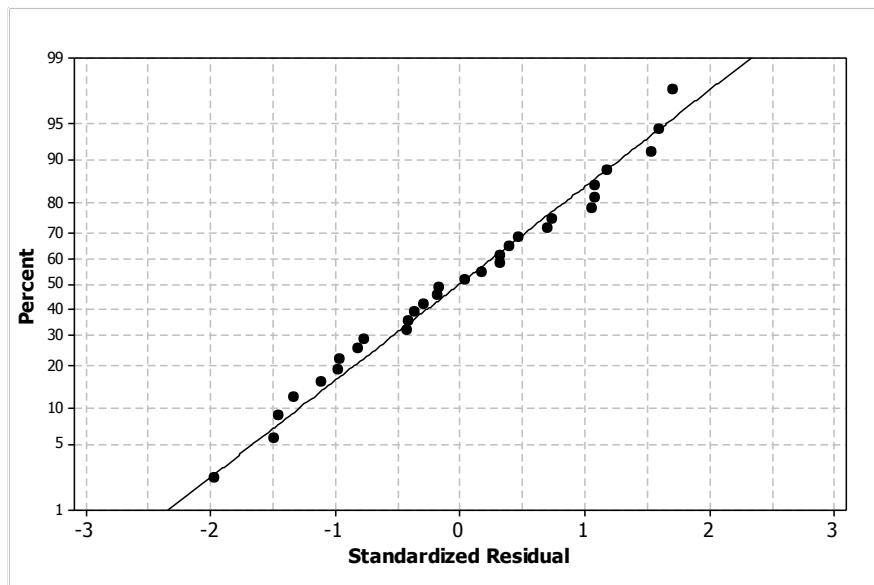
Figure 3. 30 Normal probability plot

3.3.5   Effects of process parameters on Power consumption (P)

The power consumption was calculated with the use of digital energy meter as shown in Figure (2.7). The power consumed to cut the workpiece is calculated as power consumption. ANOVA test for power consumption is shown in Table 3.5. It indicated that cutting velocity, feed and depth of cut are the significant parameters for power consumption having contribution of 76.7192%, 4.584347% and 1.175731% respectively. The second order equation for Power consumption is shown in Equation 3.6. Main effect plot for power consumption is shown in Figure 3.21. The minimum

power required at 200°C, 8 m/min, 0.05 mm/rev and at 0.5 mm for present investigation. The variation in Power with varying interactions between processes parameters are shown in Figure 3.22. Figure 3.23, 3.24 and 3.25 shows Run order plot, Fit order plot, and Normal probability plot respectively.

Table 3. 5 ANOVA test for power consumption (P)

Source	DF	Seq SS	Adj SS	Adj MS	F	P	% Contribution
T	1	684	685	685	2.09	0.172	0.380776
V	1	137813	137813	137813	421.63	0.000*	**76.7192**
F	1	8235	8235	8235	25.19	0.000*	**4.584347**
D	1	2112	2112	2112	6.46	0.025*	**1.175731**
T×T	1	2475	6	6	0.02	0.897	1.377809
V×V	1	7825	7540	7540	23.07	0.000*	**4.356104**
f×f	1	602	610	610	1.87	0.195	0.335128
d×d	1	16	16	16	0.05	0.829	0.008907
T×V	1	1122	1122	1122	3.43	0.087	0.624607
T×f	1	156	156	156	0.48	0.501	0.086844
T×d	1	12	12	12	0.04	0.849	0.00668
V×f	1	8556	8556	8556	26.18	0.000*	**4.763045**
V×d	1	2256	2256	2256	6.90	0.021*	**1.255894**
f×d	1	870	870	870	2.66	0.127	0.484321
Total	29	179633					
S = 18.0793			R-Sq = 97.63% R-Sq (adj) = 94.72%				
* = Significant factor							

Analysis of variance (ANOVA) was carried out on the experimental power consumption to identify significant factors.

The second order equation for power consumption is shown in Equation 3.6.

$P = 704.100 + 6.167×T + 87.500×V + 21.389 ×f + 10.833×d + 1.500×T×T -54.500×V×V + 15.500×f×f - 2.500×d×d -8.375×T×V +3.125×T×f + 875×T×d + 23.125×V×f + 11.875×V×d + 7.375×f×d$

(3.6)

The value of standard deviation of error (S) is 18.0793 which shows S factor as insignificant. The value for R-sq is 97.63% indicates as the predicted model for power consumption is significant for analysis.
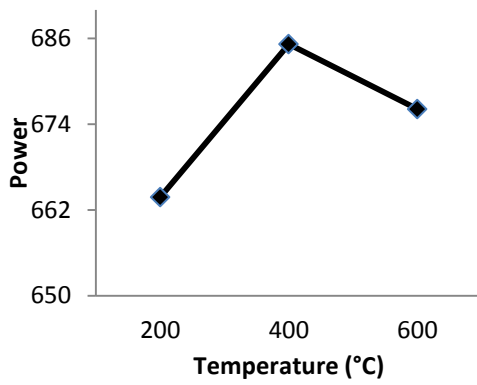
(i)
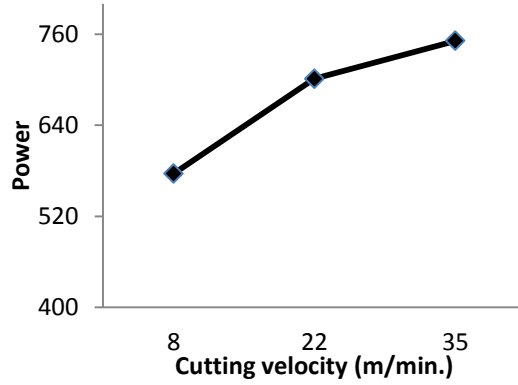
(ii)
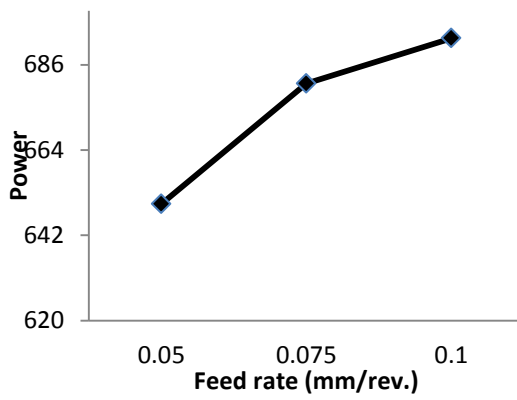
(iii)
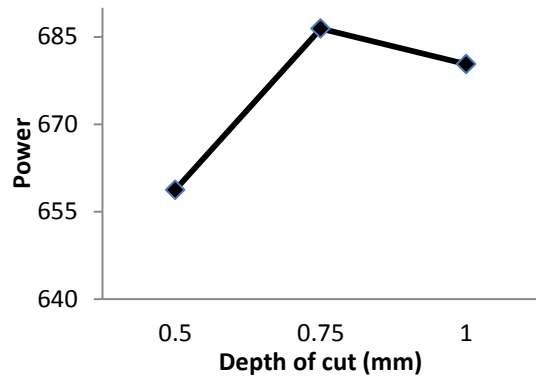
(iv)

Figure 3. 31 Main effect plot for Power consumption
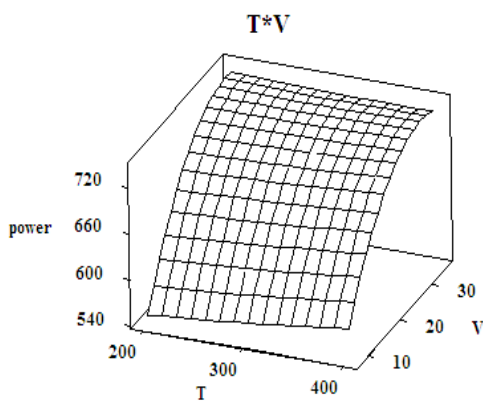
(i)
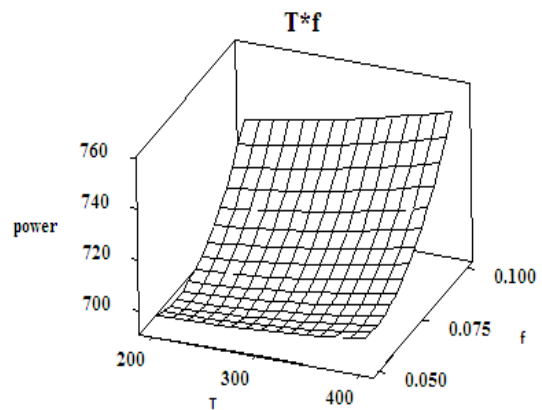
(ii)
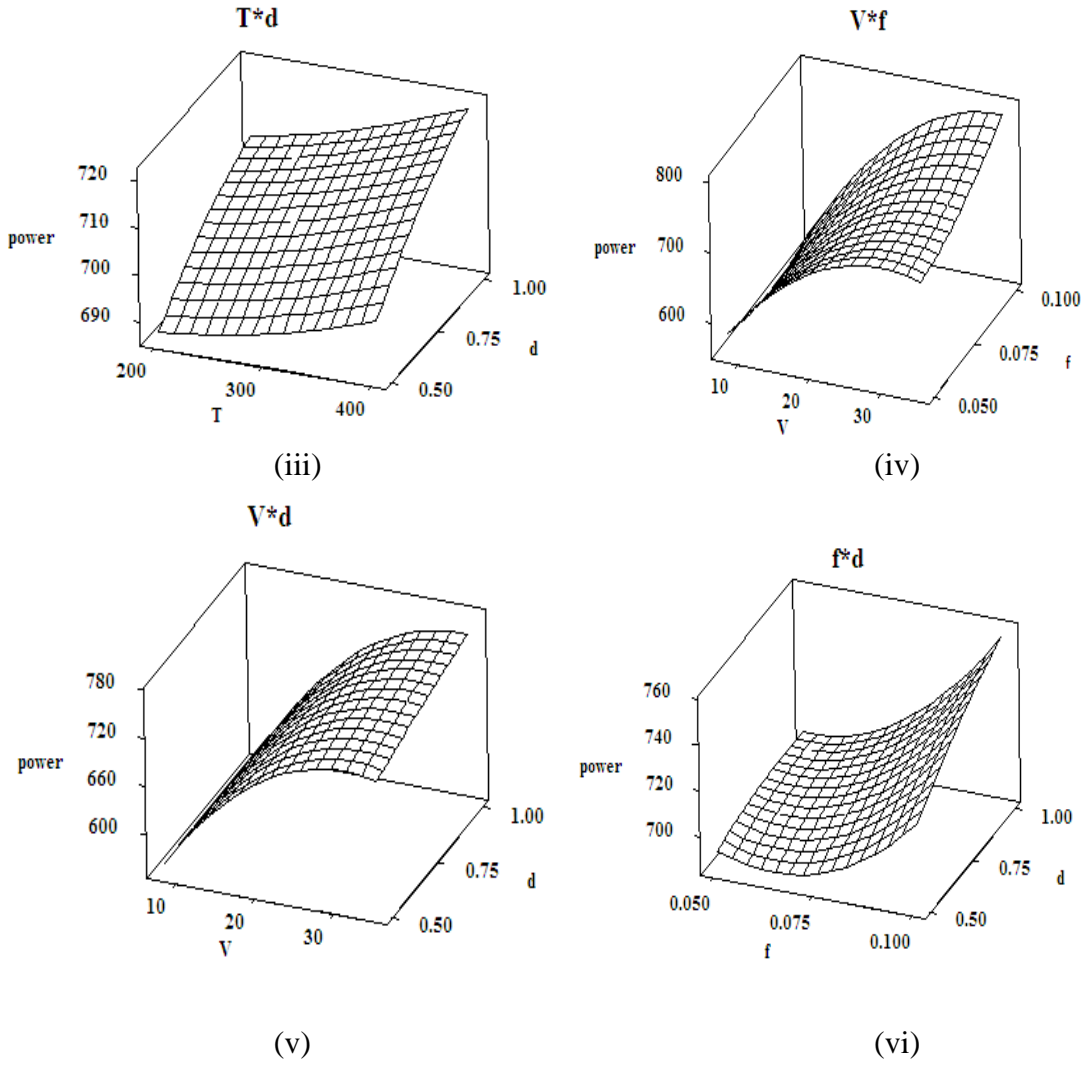
Figure 3. 32 Response surface plot representing the effects on for power
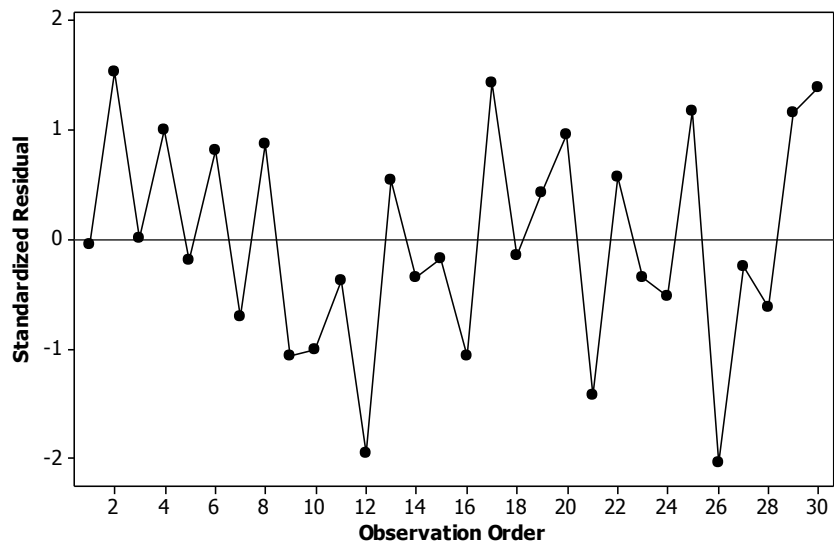
Figure 3. 33 Run order plot
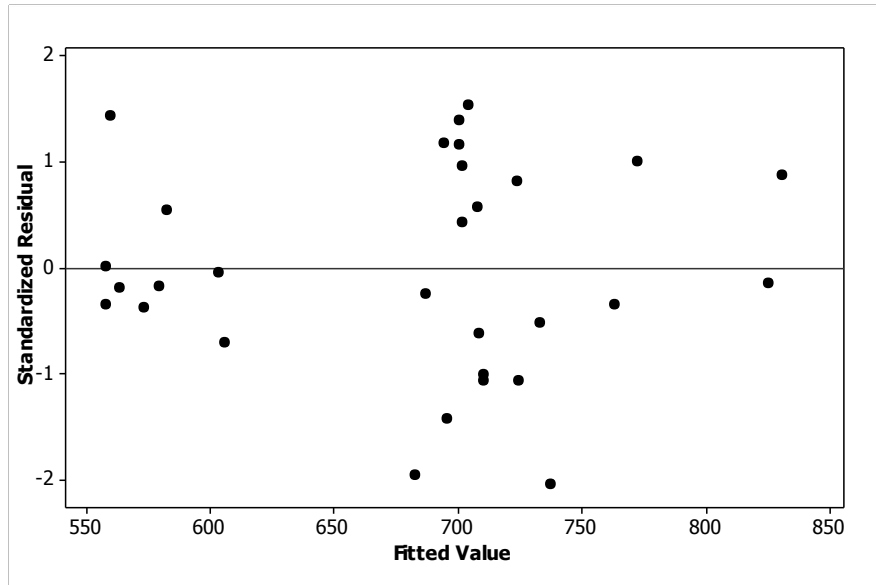
Figure 3. 34 Fit order plot
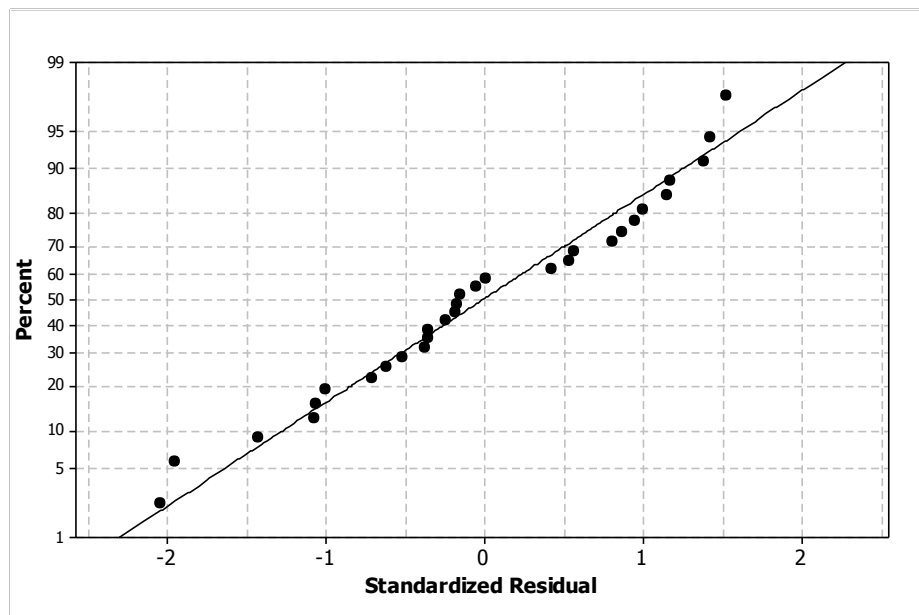
Figure 3. 35 Normal probability plot

3.4   Conclusion

The optimum setting for parameters as per RSM for minimum tool wear, minimum surface roughness, minimum power consumption and minimum chip reduction coefficient with maximum tool life were obtained. The optimum parameters are given as:

- Tool wear: 400°C, 24m/min., 0.125mm/rev. and 0.5mm depth of cut.
- Surface roughness: 400C, 45m/min., 0.125mm/rev. and 1.025mm depth of cut
- Chip reduction coefficient: 600C, 66m/min., 0.2mm/rev. and 1.25mm depth of cut
- Tool life: 400C, 8m/min., 0.05mm/rev. and 0.75mm depth of cut
- Power consumption: 200C, 8m/min, 0.05mm/rev and 0.5mm depth cut.

Chapter 4

PCA Based Multi-Response Optimization

PCA Based Multi-Response Optimization

4.1. Introduction

Previously, Taguchi method, response surface methodology, factorial design, etc. were used for designing experiments and for single response optimization. But, researchers focussed less on multi-response optimization techniques such as Grey relational analysis, Regression analysis method, artificial neural network, etc. In recent decades, grey relational analysis has become a good optimization technique to analyse the processes for multi response problems. GRA approaches are used for measuring the distance between response coefficients in a discrete manner. In GRA, white indicates the full information of the data and black represents the nil information of the data while grey represents incomplete information. When experiments is in ambiguous condition, then GRA approach is very helpful for satisfying the shortcomings. In present work, grey relational analysis (GRA) coupled with principal component analysis (PCA) based on response surface methodology (RSM) is applied for optimizing multi-performance characteristic which had not been applied in hot machining on uncoated carbide insert. It was noticed that in hot machining multi-response problems were solved by considering the equal weights to all the response for obtaining optimal combination. GRA-based solution is estimated by adopting non-weighted (equally weighted). PCA technique have property to transform several related variable to smaller number of uncorrelated principal components, which are in linear combination with original variables. Therefore, researchers found more beneficial to find optimal setting based on principal component instead of the on the original experimental data [34]. The problem is that equally weighted response will downgrades the performance [4, 60]. So, different weights assigned to all response which may cause a biased consideration and could be affecting response performance. Finally, determining the weights for each of the response variables become a research issue.

4.2. Optimization Procedure

The present work is accomplished by using two types of PCA based approaches i.e., PCA coupled with GRA and weighted principal component analysis (WPCA). PCA is

used for converting multi-responses into one response by using the concept of correlation between the responses and the multi-responses. The single response obtained is known as Process Performance Index (PPI). The steps for obtaining PPI values and MPI values are described in section 4.2.1 and 4.2.2 respectively. The experimental responses used were shown in Table 2.7.

4.2.1 PCA coupled with GRA

The evaluated PPI value in PCA coupled with GRA approach is known as Overall Quality Performance Index (OQPI). Higher the better criterion gives the optimal setting for the OQPI. The procedure for the optimization of multi-performance characteristics with grey relational analysis coupled with principal component analysis is shown as follows [34]:

1. Obtain the results for performance characteristics (tool wear, surface roughness and chip reduction coefficient).

2. Find the S/N ratio for all the three responses for j_{th} response variable and i_{th} trial. Basically, there are three types of S/N ratios – lower-the-better, higher-the- better and nominal-the-better. Equation used for respective S/N ratios are expressed as follows:

$$\eta_{ij} = -10\log\left(\frac{1}{n}\sum_{j=1}^{n} y_{ij}^{2}\right)$$
(4.1)

where, this equation used for lower-the-better performance characteristics

$$\eta_{ij} = -10\log\left(\frac{1}{n}\sum_{ij}^{n}\frac{1}{y_{ij}2}\right)$$
(4.2)

where, this equation used for higher-the-better performance characteristics

$$\eta_{ij} = -10\log\left(\frac{1}{ns}\sum_{j=1}^{n} y_{ij}2\right)$$
(4.3)

where, this equation used for nominal-the-better performance characteristics. (η_{ij}) is the S/N ratio, y_{th} is the experimental value of the jth response variable in ith trial. and s is the standard deviation.

3. Conduct PCA on S/N ratios. The uncorrelated principal component scores are formulated as in Equation 4.4.

$$PCS_{il} = a_{l1}\eta_{i1} + a_{l2}\eta_{i2} + \ldots + a_{lp}\eta_{ip} \tag{4.4}$$

where, PCS_{il} is uncorrelated principal component score corresponding to i_{th} experimental run and l_{th} eigen value. $a_{l1}^2 + a_{l2}^2 + \ldots + a_{lp}^2 = 1$, where a_{l1}, $a_{l2}\ldots$, a_{lp} is the elements of eigen vectors for corresponding to the l_{th} eigen values of the correlation matrix of the response variables.

4. Normalizing the principal component score.

It provides a comparable sequence. There are three different types if normalizations depends on the target of response, whether the lower is better (LB), higher is better (HB) and nominal is better (NB).

$$X_{ij} = \frac{PCS_i(k) - minPCS_i(k)}{maxPCS_i(k) - minPCS_i(k)} \tag{4.5}$$

where, this Equation (4.5) used for lower-the-better performance characteristic.

$$X_{ij} = \frac{maxPCS_i(k) - PCS_i(k)}{maxPCS_i(k) - minPCS_i(k)} \tag{4.6}$$

where, this Equation (4.6) used for higher-the-better performance characteristics

$$X_{ij} = 1 - \frac{\left| PCS_i - PCS_{0b}(k) \right|}{maxPCS_i(k) - minPCS_{0b}(k)} \tag{4.7}$$

where, this Equation (4.7) used for nominal-the-better performance characteristics. $X_i^*(k)$ represents the normalized value for the run of responses.

5. Evaluating the grey relational coefficients. Grey relational coefficient (γ) can be evaluated as follows:

$$\gamma_{il} = \frac{\Delta_{min} + \xi\Delta_{max}}{\Delta_{0,i}(k) + \xi\Delta_{max}} \tag{4.6}$$

where, $\Delta_{0,i}(k)$ is the deviation sequence. This is the absolute value of the difference between $X_0^*(k)$ and $X_i^*(k)$. ξ is known as distinguishing coefficient and its value range is between $0 \leq \xi \leq 1$. In this study its value is taken as 0.5. Δ_{max} and Δ_{min} are the maximum and minimum values of deviation.

6. The grey relational grade $\Upsilon(x_0, x_i)$ which can be evaluated by the following expression (4.7):

$$OQPI_i = \sum_{l=1}^{n} w_1 \gamma_{il} \qquad (4.7)$$

where, $\sum_{k=1}^{n} w_k \gamma_{il} = 1$, w_k is the percentage contribution given to the corresponding k_{th} grey relational coefficient, γ_{il} is the corresponding grey relational coefficient for l_{th} response.

4.2.2 Weighted Component Analysis (WPCA)

The evaluated PPI value in WPC approach is known as Multi performance index (MPI). In this WPC method, all components are taken into consideration in order to completely explain variation in all responses. The WPC method uses the explained variation as the weight to combine all principal components in order to form a multi-response performance index (MPI) [40]. The procedure of WPCA based on RSM to compute the optimal arrangements of the process parameters for hot machining of high manganese steel is described as follows [34]:

1. Data obtained from experimental investigation.
2. S/N ratio for each performance characteristics to be evaluated by Equation 4.1 which is based on lower the better criteria. Larger value of S/N ratio is desired for better performance.
3. All sequenced S/N ratio is substituted for normalization and evaluated by using Equation (4.5) and ranged between (0-1) intervals. Larger value of normalized result is desired for better performance.
4. The outcomes of the normalized values is then processed for principal component analysis (PCA) denoted by β_j. It can be obtained by using Equation (4.4).
5. The MPI values for each run are evaluated from Equation (4.8).

$$MPI_i = \sum_{l=1}^{p} w_1 \times \beta_{il} \qquad (4.8)$$

where, $\sum_{l=1}^{p} w_1 = 1$. For present work, the weights considered for three responses is as $MPI = 0.79322 \times \beta_1 + 0.15616 \times \beta_2 + 0.05062 \times \beta_3$.

4.3 Results and discussion

The results obtained from the algorithm of grey relational analysis coupled with principal component analysis and weighted principal component analysis is discussed.

4.3.1 PCA coupled with GRA

All the original sequences of S/N ratios and principal component scores (PCS) are shown in Table 4.1.

Table 4.1: S/N ratio for responses with evaluated PCS

Run Order	SN1	SN2	SN3	PCS1	PCS2	PCS3
1	17.0774	-4.0824	-6.1001	3.9546	-14.3589	11.1293
2	11.0568	35.9176	-7.0514	-24.3482	-24.9071	-15.8276
3	26.0206	-14.5671	-2.0074	16.4416	-18.1025	17.1997
4	8.4502	-14.5671	-6.6366	7.5010	-2.3033	16.3195
5	17.5885	-8.2995	-16.8447	-0.6281	-13.7844	21.7175
6	20.9151	-10.1030	-4.2725	10.3394	-15.3525	14.6796
7	17.0774	-9.5424	-5.8280	7.6488	-12.1586	14.5105
8	10.4287	-15.7066	-2.4443	11.7870	-3.4063	14.5328
9	13.1515	-5.1055	-1.5880	6.4631	-10.0868	7.6259
10	24.1522	0.0873	-3.7819	5.1929	-22.3611	8.4268
11	22.3837	-7.9588	-9.0357	6.1358	-17.8397	17.0413
12	10.7520	0.0000	-10.2750	-3.6257	-10.4546	9.9369
13	23.0980	-12.0412	-0.1036	15.1885	-16.3244	13.4817
14	20.1755	-12.6694	-4.5629	11.5443	-13.6666	16.3920
15	17.7211	-2.9226	-5.9640	3.5144	-15.4036	10.4258
16	10.4576	0.0000	-7.5334	-1.8190	-10.0207	7.9008
17	9.7090	-15.9176	-1.5909	12.2802	-2.6122	13.8871
18	8.1121	-16.2583	-10.2377	5.9774	-1.5336	19.9284
19	13.1515	-3.1672	-2.8840	4.3193	-10.9398	7.2856
20	13.5556	-4.8110	-4.9756	4.0547	-10.7775	9.9585
21	14.1549	-2.9226	-1.8404	5.2136	-11.8931	6.6168
22	14.8945	-3.2871	-1.3859	6.0041	-12.3968	6.7065
23	24.1522	0.0873	-2.7976	5.8760	-22.3020	7.7210
24	9.3704	-4.6090	-1.3859	5.0519	-6.8135	6.2521
25	14.4249	-4.0824	-11.2296	-0.4699	-12.2396	14.1732
26	11.0568	-15.5630	-5.8280	9.5513	-4.2415	17.0151
27	27.1309	-3.8625	-8.0967	5.7053	-23.7656	14.8195

28	14.9916	-6.8485	-15.3000	-1.3342	-11.8959	19.0388
29	14.7510	-5.9333	-0.4411	8.3118	-11.1503	7.7281
30	24.1522	0.0873	-8.3726	2.0069	-22.6365	11.7184

Table 4.2: Grey coefficients with normalized values for responses with OQPI values

Run Order	NORM1	NORM2	NORM3	GRC1	GRC2	GRC3	OQPI
1	0.3061	-0.5502	0.1804	0.4188	0.2439	0.3930	0.3916
2	1.0000	1.0000	0.9813	1.0000	1.0000	1.0000	**0.8210**
3	0.000	-0.0000	0.000	0.3333	0.3333	0.3458	0.3337
4	0.2192	-2.3219	0.0262	0.3904	0.1308	0.3519	0.3500
5	0.4185	-0.6346	-0.1342	0.4623	0.2342	0.3174	0.4235
6	0.1496	-0.4041	0.0749	0.3703	0.2626	0.3639	0.3538
7	0.2156	-0.8735	0.0799	0.3893	0.2107	0.3652	0.6200
8	0.1141	-2.1598	0.0792	0.3608	0.1366	0.3651	0.3271
9	0.2446	-1.1780	0.2845	0.3983	0.1867	0.4267	0.3672
10	0.2758	0.6258	0.2607	0.4084	0.5720	0.4185	0.4334
11	0.2527	-0.0386	0.0047	0.4009	0.3250	0.3469	0.3987
12	0.4920	-1.1239	0.2158	0.4960	0.1906	0.4039	0.4471
13	0.0307	-0.2613	0.1105	0.3403	0.2839	0.3733	0.3328
14	0.1201	-0.6519	0.0240	0.3623	0.2324	0.3514	0.3424
15	0.3169	-0.3966	0.2013	0.4226	0.2636	0.3994	0.3979
16	0.4477	-1.1877	0.2763	0.4751	0.1860	0.4238	0.4299
17	0.1020	-2.2765	0.0984	0.3577	0.1324	0.3701	0.3240
18	0.2565	-2.4350	-0.0811	0.4021	0.1271	0.3280	0.3584
19	0.2972	-1.0526	0.2946	0.4157	0.1959	0.4303	0.3829
20	0.3037	-1.0765	0.2152	0.4180	0.1941	0.4037	0.3837
21	0.2753	-0.9125	0.3144	0.4083	0.2073	0.4375	0.3788
22	0.2559	-0.8385	0.3118	0.4019	0.2138	0.4365	0.3745
23	0.2590	0.6172	0.2816	0.4029	0.5664	0.4257	0.4283
24	0.2792	-1.6590	0.3253	0.4096	0.1583	0.4415	0.3726
25	0.4146	-0.8616	0.0899	0.4607	0.2117	0.3678	0.4203
26	0.1689	-2.0370	0.0055	0.3756	0.1414	0.3470	0.3394
27	0.2632	0.8323	0.0707	0.4043	0.7488	0.3629	0.4551
28	0.4358	-0.9121	-0.0546	0.4698	0.2073	0.3336	0.4261
29	0.1993	-1.0217	0.2814	0.3844	0.1983	0.4256	0.3575
30	0.3539	0.6663	0.1629	0.4363	0.5998	0.3879	0.4595

The PCS values are further normalized and normalized values along with grey coefficients (GRC) are shown in Table 4.2. The grey relational coefficient is expressed as shown in Equation 4.6.

The Eigen values for respective Eigen vectors are listed in Table 4.3. The square of the Eigen value signifies the contribution of the corresponding responses to the principal component [35].

Table 4.3: Eigen vectors for corresponding Eigen values

Variables	Eigen values	Proportion	Eigen vectors		
			PC1	PC2	PC3
TW	1.1087	0.370	0.326	-0.915	0.239
Ra	0.9932	0.331	-0.642	-0.400	-0.655
Ξ	0.8981	0.299	0.694	0.060	-0.717

4.3.1.1 Effects on OQPI values

The effects of the process parameters on PPI can be seen from the main effects plot for OQPI shown in Figure 4.1. Highest point for the OQPI shows the optimal setting.

(i)

(ii)

(iii)

(iv)
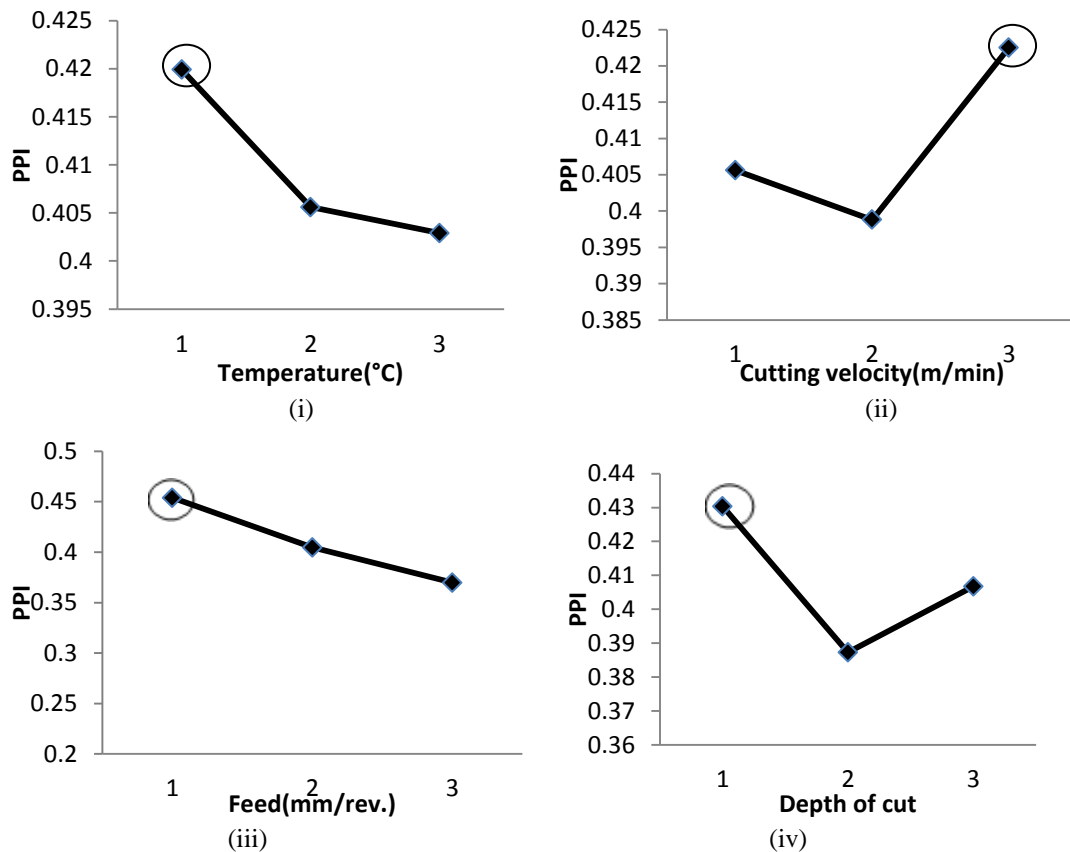
Figure 4.1: Main effect plots for OQPI

The predicted mean values obtained for each process parameters are shown in Table 4.4. The highest among all values shows the optimal parametric combination as the maximum value which is shown in bold. The ANOVA table for OQPI is shown in Table 4.5. ANOVA test reveals that feed is the most significant factor for OQPI whereas among interactions all interactions are significant except velocity with feed.

Table 4.4: Mean values for OQPI

Levels	T	V	f	d
1	**0.422**	0.406	**0.456**	**0.433**
2	0.406	0.397	0.401	0.391
3	0.407	**0.423**	0.364	0.407

Table 4.5: ANOVA for OQPI

Source	DF	Seq SS	Adj SS	Adj MS	F	P
T	1	0.001300	0.001300	0.001300	0.91	0.358
V	1	0.001280	0.001280	0.001280	0.90	0.361
f	1	0.031770	0.031770	0.031770	22.24	0.000*
d	1	0.002489	0.002489	0.002489	1.74	0.210
T×T	1	0.000157	0.000751	0.000751	0.53	0.481
V×V	1	0.001099	0.000110	0.000110	0.08	0.786
f×f	1	0.000006	0.000498	0.000498	0.35	0.565
d×d	1	0.005542	0.005542	0.005542	3.88	0.071
T×V	1	0.028344	0.028344	0.028344	19.84	0.001*
T×f	1	0.041685	0.041685	0.041685	29.18	0.000*
T×d	1	0.022483	0.022483	0.022483	15.74	0.002*
V×f	1	0.028291	0.028291	0.028291	19.80	0.0018
V×d	1	0.040003	0.040003	0.040003	28.00	0.000*
f×d	1	0.032741	0.032741	0.032741	22.92	0.000*
Lack-of-Fit	10	0.011182	0.011182	0.001118	0.45	0.849
Total	29	0.275835				
*= These factors are significant at 95% of confidence level						

The second order equation for OQPI is shown by Equation 4.11.

OQPI = 0.394450- 0.008497×T + 0.008431×V -0.042012×f -0.011759×d -0.017198×T×T + 0.006579×V×V -0.014008×f×f + 0.046725×d×d -0.042089×T×V + 0.051043×T×f + 0.037486×T×d - 0.042050×V×f -0.050002×V×d + 0.045236×f×d   (4.11)

4.3.1.2 Confirmatory test

After obtaining the optimal combination for responses, it is important to verify that obtained result is improved or not. There is a comparison of results given in Table 4.6 from initial setting to the optimal setting. It was analysed that value of tool wear decreased by 25.532%, surface finish increased by 98.56 % and chip reduction coefficient get reduced by 0.495%.

Table 4.6: Confirmation Table for OQPI

Levels	Initial setting T-3, V-1, f-1, d-1	Optimal setting T-1, V-3, f-1, d-1		
		Predicted	Experimental	Gain (%)
TW(mm)	0.14	0.28	0.188	-25.532
Ra(µm)	1.6	0.016	0.023	98.56
ξ	2.02	2.252	2.01	0.495
OQPI	0.392	1.00		

4.3.2 Weighted principal component analysis

The computed S/N ratio and normalized values are listed in Table 4.5. The evaluated principal component score and the multi performance index (MPI) values are shown in Table 4.6.

Table 4.5: S/N ratio and Normalized values

Run Order	SN1	SN2	SN3	NORM1	NORM2	NORM3
1	17.0774	-4.0824	-6.1001	0.47139	0.23336	0.64181
2	11.0568	35.9176	-7.0514	0.15483	1.00000	0.58499
3	26.0206	-14.5671	-2.0074	0.94162	0.03241	0.88628
4	8.4502	-14.5671	-6.6366	0.01777	0.03241	0.60976
5	17.5885	-8.2995	-16.8447	0.49826	0.15254	0.00000
6	20.9151	-10.1030	-4.2725	0.67318	0.11797	0.75098
7	17.0774	-9.5424	-5.8280	0.47139	0.12872	0.65806
8	10.4287	-15.7066	-2.4443	0.12180	0.01057	0.86018
9	13.1515	-5.1055	-1.5880	0.26497	0.21375	0.91134
10	24.1522	0.0873	-3.7819	0.84338	0.31328	0.78028
11	22.3837	-7.9588	-9.0357	0.75039	0.15907	0.46646

12	10.7520	0.0000	-10.2750	0.13880	0.31161	0.39243
13	23.0980	-12.0412	-0.1036	0.78795	0.08082	1.00000
14	20.1755	-12.6694	-4.5629	0.63428	0.06879	0.73363
15	17.7211	-2.9226	-5.9640	0.50524	0.25559	0.64994
16	10.4576	0.0000	-7.5334	0.12332	0.31161	0.55620
17	9.7090	-15.9176	-1.5909	0.08396	0.00653	0.91116
18	8.1121	-16.2583	-10.2377	0.00000	0.00000	0.39466
19	13.1515	-3.1672	-2.8840	0.26497	0.25090	0.83392
20	13.5556	-4.8110	-4.9756	0.28622	0.21940	0.70898
21	14.1549	-2.9226	-1.8404	0.31772	0.25559	0.89626
22	14.8945	-3.2871	-1.3859	0.35662	0.24861	0.92340
23	24.1522	0.0873	-2.7976	0.84338	0.31328	0.83908
24	9.3704	-4.6090	-1.3859	0.06616	0.22327	0.92340
25	14.4249	-4.0824	-11.2296	0.33192	0.23336	0.33541
26	11.0568	-15.5630	-5.8280	0.15483	0.01333	0.65806
27	27.1309	-3.8625	-8.0967	1.00000	0.23758	0.52255
28	14.9916	-6.8485	-15.3000	0.36172	0.18035	0.09227
29	14.7510	-5.9333	-0.4411	0.34907	0.19789	0.97984
30	24.1522	0.0873	-8.3726	0.84338	0.31328	0.50606

Table 4.6: PCS values on normalised values with MPI values

Run Order	PCS1	PCS2	PCS3	MPI
1	0.449269	-0.486160	-0.50037	0.255122
2	-0.185544	-0.506571	-1.03743	-0.278798
3	0.901236	-0.821370	-0.43165	0.564763
4	0.408158	0.007358	-0.45418	0.301918
5	0.064504	-0.516927	0.01917	-0.028587
6	0.664897	-0.618086	-0.45484	0.407866
7	0.527733	-0.443326	-0.44348	0.326930
8	0.629885	-0.064068	-0.59457	0.459536
9	0.581616	-0.273269	-0.73011	0.381718
10	0.615332	-0.850184	-0.56309	0.326825
11	0.466227	-0.722250	-0.25929	0.189000
12	0.117546	-0.228103	-0.45230	0.034724
13	0.898983	-0.693305	-0.58162	**0.575383**
14	0.671758	-0.563866	-0.41948	0.423565
15	0.451677	-0.525531	-0.51267	0.250261
16	0.226153	-0.204110	-0.57342	0.118489

17	0.655526	-0.024770	-0.63751	0.483838
18	0.273894	0.023679	-0.28297	0.206632
19	0.504040	-0.292773	-0.69893	0.318715
20	0.444483	-0.307108	-0.58364	0.275071
21	0.561491	-0.339179	-0.73409	0.355260
22	0.597493	-0.370342	-0.73968	0.378668
23	0.656138	-0.846657	-0.60525	0.357610
24	0.519069	-0.094440	-0.79251	0.356872
25	0.191160	-0.376931	-0.31401	0.076875
26	0.498615	-0.107517	-0.44355	0.356269
27	0.536124	-0.978678	-0.29128	0.257689
28	0.066174	-0.397576	-0.09784	-0.014547
29	0.666759	-0.339761	-0.74873	0.437929
30	0.425024	-0.866638	-0.36648	0.183252

4.3.2.1 Effects of process parameters on MPI

The main effect plot for MPI value is shown in Figure 4.2. The highest value reveals the optimal setting for cutting parameters as T1 V1 f3 d2.
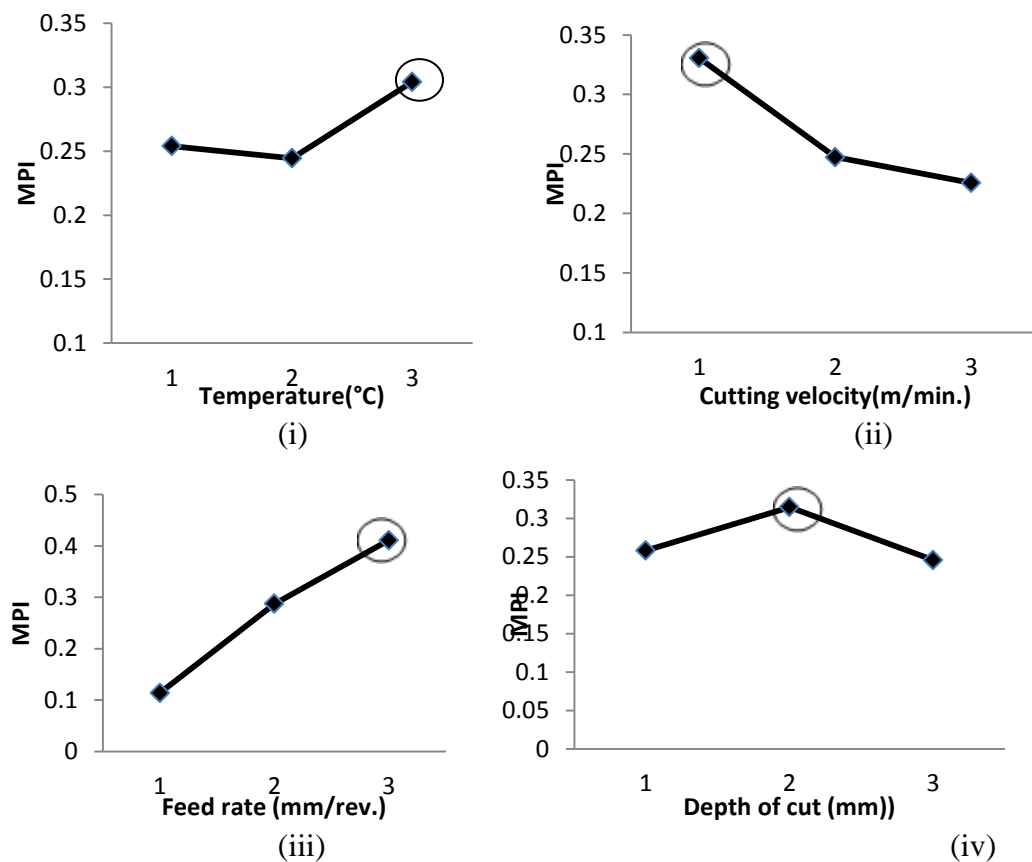
Figure 4.2 Main affects plots for MPI

The mean values for the cutting parameters are shown in Table 4.7.

ANOVA test for MPI is shown in Table 4.8. ANOVA test reveals that feed is the most significant factor.

Table 4.7 Mean values for MPI

Levels	T	V	F	d
1	0.262	**0.341**	0.110	0.281
2	0.281	0.281	0.300	**0.322**
3	**0.330**	0.223	**0.421**	0.230

Table 4.8 ANOVA test for MPI

Source	DF	Seq SS	Adj SS	Adj MS	F	P
T	1	0.01127	0.011272	0.011272	0.96	0.345
V	1	0.04946	0.049457	0.049457	4.22	0.061
f	1	0.39720	0.397202	0.397202	33.87	0.000*
d	1	0.00071	0.000709	0.000709	0.06	0.810
T×V	1	0.00006	0.000055	0.000055	0.00	0.946
T×f	1	0.13482	0.134819	0.134819	11.50	0.005*
T×d	1	0.00076	0.000759	0.000759	0.06	0.803
V×f	1	0.00193	0.001930	0.001930	0.16	0.692
V×d	1	0.09969	0.099689	0.099689	8.50	0.012*
f×d	1	0.05484	0.054835	0.054835	4.68	0.050*
Lack-of-Fit	10	0.11755	0.117550	0.011755	1.01	0.563
Total	29	1.00057				
*= These factors are significant at 95% of confidence level						

The second order equation for MPI is as follows:

MPI = 0.314641 + 0.025024×T -0.052418×V + 0.148549×f -0.006275×d + 0.086094×T×T + 0.076371×V×V -0.064298×f×f -0.159299×d×d + 0.001854×T×V -0.091794×T×f -0.006888×T×d - 0.010984×V×f + 0.078934×V×d -0.058542×f×d   (4.12)

4.3.2.2 Confirmatory test

Confirmation test compared the results of optimal setting (T3, V1, f3, d2) for MPI with the initial setting (T3, V1, f1, d1) of process parameters is shown in Table 4.9. The final changes obtained from confirmation test are decrease in tool wear is about 35.71%, surface roughness increment about 56.16% and chip reduction coefficient decreases about 18.32%.

Table 4.9 Confirmation Test for MPI

Levels	Initial setting T-3, V-1, f-1, d-1	Optimal setting T-3, V-1, f-3, d-2		
		Predicted	Experimental	Gain (%)
TW(mm)	0.14	0.07	0.09	35.71
Ra(µm)	1.60	4.00	3.65	-56.16
ξ	2.02	1.012	1.65	18.32
MPI	0.255	0.575383		

4.4 Conclusions

In this study, the application of grey relational analysis coupled with principal component analysis was used for optimizing the multiple performance characteristics on hot machining operation. The results are concluded as follows:

1. Grey relational analysis is used to solve the multi-performance characteristics optimization problems while principal component analysis was coupled to give weightage to the performance characteristics to analyse the relative importance to each characteristics.

2. The feed rate is the most significant factor which affects performance characteristics with its contribution percentage 12.819%.

3. The optimal setting of the process parameters obtained from applying principal component analysis coupled with grey analysis is T1-V3-f1-d1. Confirmation experiment has been done to verify the reduction in tool wear by 0.048, decrease in surface roughness by 1.577 and chip reduction coefficient by 0.01.

4. For optimizing multiple variables, it is not necessary that all the responses could get their desired values. Statistical techniques provide best combination for all the process parameters simultaneously.

5. The statistical technique which provide more desired values. In present case, WPCA found to give better result as it provide less tool wear. Both methods are suitable for multi optimization depends on the desired values obtained.

Chapter 5

Optimization of process parameters using Fuzzy TOPSIS

Optimization of process parameters using Fuzzy TOPSIS

5.1   Introduction

Many efforts have been done by researchers to predict and to optimise the cutting parameters for consistent response. An operator has to decide the appropriate tool and cutting parameters on the basis of skill, intuition and experience. Many Multiple Attribute Decision Making (MCDM) methods have been proposed and used, the Technique for Order Performance by Similarity to Ideal Solutions (TOPSIS) gains much attraction because of its simplicity and easy to access.

Fuzzy model consists of a number of conditions for fuzzy regulations-called fuzzy rules that establish the relationship between a value in the underlying domain and fuzzy space. The basic function of rules is to represent the strategically adopted for optimizing the problem. Making of rules is the most difficult task in fuzzy system as there are no systematic tool based rules. In fuzzy sets, the information is in uncertain manner, therefore, the application of fuzzy set theory for multi-objective evaluation methods proven to be an effective approach. First state the membership function for the decision matrix to weighted normalized decision matrix of fuzzy numbers and then defuzzyfy for crisp values. Then it extends from fuzzy group decision making to the TOPSIS Method for determining the rank order for all strategies by evaluating the distance to both ideal solution and anti-ideal solution based on ordering of the numbers simultaneously. TOPSIS method is a popular approach for multiple criteria decision making (MCDM) and has been widely used by the researchers. Fuzzy TOPSIS is a method that can help in objective and systematic evaluation of alternatives on multiple criteria. TOPSIS is based upon the concept that the chosen alternative should have the shortest distance from the Positive Ideal Solution (PIS), i.e., the solution that maximizes the benefit criteria and minimizes the cost criteria; and the farthest from the Negative Ideal Solution (NIS), i.e., the solution that maximizes the cost criteria and minimizes the benefit criteria.

In fuzzy TOPSIS, the fuzziness in the decision data and group decision-making

process is considered. First, linguistic values are expressed in triangular membership function to assess weights and ratings of selection criteria. Second, a hierarchy multiple-model based on fuzzy set theory is expressed and fuzzy positive-ideal and negative-ideal solutions are used to evaluate each closeness coefficient. In addition, mathematical model is established for tool life and power consumption using fuzzy TOPSIS based RSM method.

5.2   Methodology

The approach was utilised positive and negative ideal concept for decision making in the fuzzy environment. In fuzzy sets theory, it is applied for transformation of linguistic terms into fuzzy numbers. It is a common practice in literature to initiate the ratings scale from 1 to 10. Here, a scale of 1 to 9 is applied for rating the criteria and the alternatives as shown in Table 5.1. Intervals are selected, to have a constant representation between 1 and 9 for the fuzzy triangular numbers applied for the five linguistic variables. Narrow interval indicates lower fuzziness in the data for evaluation. Ratings are assigned for the linguistic terms. The ratings assigned to the alternatives corresponding to respective criterion for decision matrix is denoted by D. Best alternative is that which has less distance from ideal solution(maximises benefit criteria and minimizes cost criteria) and farthest from negative ideal solution (maximises cost criteria and minimises benefit criteria). Here, ideal solution is which gives maximum tool life and minimum power consumption. TOPSIS method is a technique used for order preference by similarity to ideal solution and proposed by Hwang and Yoon (1891).

Table 5.1: Linguistic terms for ratings

Fuzzy number	Alternative assessment	QA weights
(1, 1, 3)	Very poor	Very low
(1, 3, 5)	Poor	Low
(3, 5, 7)	Fair	Medium
(5, 7, 9)	Good	High
(7, 9, 9)	Very good	Very high

Linguistic terms were denoted by using triangular fuzzy set called as membership function. The output of the experimental data has been fed as input in Fuzzy Inference

System (FIS). The Fuzzy Inference System (FIS) consist of four input variables and two output variables as shown in Figure 5.1. 30 fuzzy rules have been explored for fuzzy reasoning as listed in Table 5.2. The output in form of crisp value has been defined as Multi-Performance Characteristic Index (MPCI). Lastly, the optimal combination for process parameters found out by optimizing relative closeness coefficient index (C+) in RSM. For evaluating MPCI value, three membership functions are assigned for the input variables and five membership functions assigned for output variables as shown in Figure 5.2 and 5.3 respectively.
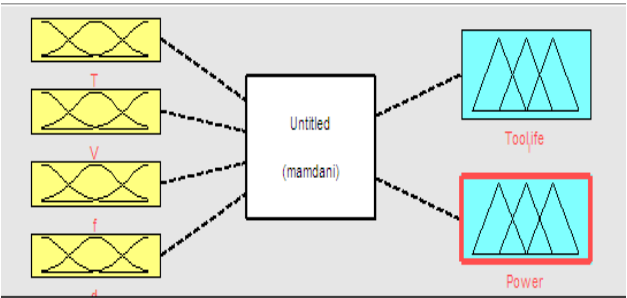
Figure 5.1: Assigned Fuzzy model
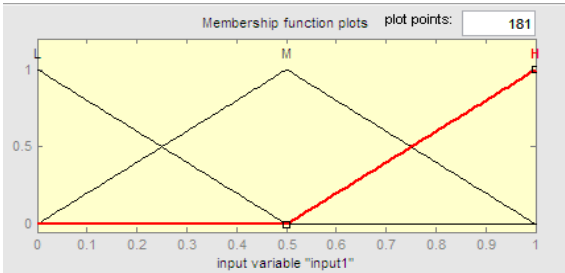
Figure 5.2: Membership functions for inputs

Five membership functions have been assigned for MPCI as shown in Figure 5.3.
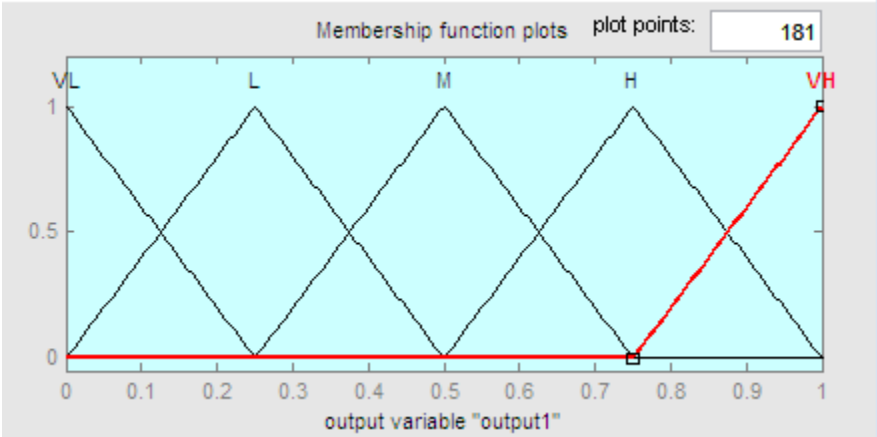
Figure 5.3: Membership functions for outputs

An algorithm for solving the MCDM problem using our proposed fuzzy TOPSIS model is as follows:

Steps 1: Construct Fuzzy matrix, Subjective assessments are to be made by decision maker to determine the decision matrix $D = \{X_{ij}, I = 1,2,.....m; j = 1,2,..........n\}$, using the linguistic terms. The decision matrix is expressed by Equation 5.1:

$$D_{30 \times 2} = \left[x_{ij} \right] \tag{5.1}$$

where, $\left[x_{ij} \right]$ are the actual values of experiments. i and j shows the number of experimental runs and number of attributes respectively.

Step 2: Normalize the fuzzy decision matrix using Equation 5.2. However, the purpose of linear scales transform normalization function used in this study is to preserve the property that the ranges of normalized triangular fuzzy numbers to be included in [0-1].

$$R_{ij} = \frac{x_{ij}}{\sqrt{\sum_{i=1}^{30} x_{ij}^2}} \tag{5.2}$$

where, R_{ij} is the normalized decision matrix. The normalized weighted fuzzy decision matrix R_{ij} is constructed as shown in Table 32.

Step 3: Evaluate the weighted normalised matrix using Equation 5.3. weighted normalised matrix is obtained by multiplying the normalized decision matrix with the weight assigned to the corresponding responses:

$$V_{30 \times 2} = \left[v_{ij} \right] \tag{5.3(a)}$$

where, $V_{ij} = R_{ij} \times w_j$

The weights are obtained by using standard deviation method. The standard deviation method calculates the weights (Eq. 5.3(b))

$$w_j = \frac{\sigma_j}{\sum_{k=1}^{M} \sigma_k} \tag{5.3(b)}$$

where, σ_j is the standard deviation.

Step 4: Establish FPIS (A^+) and FNIS (A^-)

$$A^+ = \left(v_1^+, v_2^+\right) \tag{5.4}$$

where, $v_j^+ = \max \{v_{ij}\}$, I = 1, 2, 3….30; j= 1, 2

$$A^- = \left(v_1^-, v_2^-\right) \tag{5.5}$$

where, $v_j^- = \min\{v_{ij}\}$, i = 1,2,….30; j = 1,2

Step 5: Determination of the distance measures.

The distance from the FPIS can be computed form following Equation 5.6.

$$S_i^+ = \sqrt{\sum_{j=1}^{n}\left(v_{ij} - v_j^+\right)^2} \tag{5.6}$$

The distance from the FNIS can be computed from following Equation 5.7.

$$S_i^- = \sqrt{\sum_{j=1}^{n}\left(v_{ij} - v_j^-\right)^2} \tag{5.7}$$

where, i =1, 2…..30

Step 6: Closeness coefficient index value can be evaluated for each alternative from Equation 5.8.

$$C_i^+ = \frac{S_i^-}{S_i^+ + S_i^-}, \ i = 1, 2, ..., m; \ 0 \le C_i^+ \le 1 \tag{5.8}$$

Step 7: Ranking for alternatives

The rank has been given according to the increasing value of the C+. Highest value for C+ has the higher ranking and the lower value for the C+ has the lower ranking. The highest value for C+ shows best alternative and closest to FPIS and farthest from FNIS.

Weighted normalized values obtained from Equation 5.3 are listed in Table 5.3.The FPIS and FNIS values are shown in Table 5.4. The distance of each value from the FPIS and FNIS are evaluated and listed in Table 5.5. The closeness coefficients for all the runs are evaluated by using Equation 5.8 and listed in Table 5.6.

Table 5.2 30 Fuzzy based rules

Run Order	T	V	f	d	MPCI1	MPCI2
1	H	L	L	L	0.5000	0.196
2	L	H	L	L	0.0876	0.822
3	L	L	H	L	0.7500	0.804
4	H	H	H	L	0.5000	0.500
5	L	L	L	H	0.0966	0.804
6	H	H	L	H	0.5000	0.500
7	H	L	H	H	0.2500	0.500
8	L	H	H	H	0.1030	0.209
9	M	M	M	M	0.5020	0.500
10	M	M	M	M	0.5020	0.500
11	L	L	M	L	0.5450	0.483
12	H	H	M	L	0.5000	0.500
13	H	L	H	L	0.5000	0.500
14	L	H	H	L	0.5000	0.500
15	H	L	L	H	0.5000	0.500
16	L	H	L	H	0.5000	0.500
17	L	L	H	H	0.2500	0.209
18	H	H	H	H	0.0800	0.837
19	M	M	M	M	0.5020	0.500
20	M	M	M	M	0.5020	0.500
21	L	M	M	M	0.5280	0.500
22	H	M	M	M	0.4150	0.398
23	M	L	M	M	0.4910	0.491
24	M	H	M	M	0.0946	0.808
25	M	M	L	M	0.5020	0.500
26	M	M	H	M	0.6110	0.808
27	M	M	M	L	0.5020	0.500
28	M	M	M	H	0.0946	0.808
29	M	M	M	M	0.5020	0.500
30	M	M	M	M	0.5020	0.500

Table 5.3 Weighted normalized matrix

v1	v2
0.114324	0.005537
0.020030	0.097389
0.171486	0.093171
0.114324	0.036034
0.022087	0.093171
0.114324	0.036034
0.057162	0.036034
0.023551	0.006296
0.114782	0.036034
0.114782	0.036034
0.124613	0.033625
0.114324	0.036034
0.114324	0.036034
0.114324	0.036034
0.114324	0.036034
0.114324	0.036034
0.057162	0.006296
0.018292	0.100976
0.114782	0.036034
0.114782	0.036034
0.120726	0.036034
0.094889	0.022831
0.112266	0.034748
0.021630	0.094100
0.114782	0.036034
0.139704	0.094100
0.114782	0.036034
0.021630	0.094100
0.114782	0.036034
0.114782	0.036034

Table 5.4 Ideal and negative ideal solution for tool life and power consumption

	V+	V-
Tool life	0.171486	0.020030
Power	0.100976	0.005537

Table 5.5 Evaluated distance measures

S+	S-
0.057162	0.135391
0.177132	0.003986
0.087634	0.153393
0.064788	0.115930
0.173204	0.008679
0.064788	0.115930
0.118322	0.075686
0.147937	0.094826
0.064385	0.116309
0.064385	0.116309
0.054644	0.125859
0.064788	0.115930
0.064788	0.115930
0.064788	0.115930
0.064788	0.115930
0.064788	0.115930
0.114326	0.102348
0.180491	0.000000
0.064385	0.116309
0.064385	0.116309
0.059216	0.121286
0.078525	0.109424
0.066032	0.114967
0.174069	0.007644
0.064385	0.116309
0.094093	0.121607
0.064385	0.116309
0.174069	0.007644
0.064385	0.116309
0.064385	0.116309

Table 5.6 Closeness coefficients

Run Order	C+
1	0.703137
2	0.022006
3	0.636415
4	0.641496
5	0.047719
6	0.641496
7	0.390120
8	0.390611
9	0.643679
10	0.643679
11	**0.697267**
12	0.641496
13	0.641496
14	0.641496
15	0.641496
16	0.641496
17	0.472360
18	0.000001
19	0.643679
20	0.643679
21	0.671936
22	0.582201
23	0.635179
24	0.042064
25	0.643679
26	0.563778
27	0.643679
28	0.042064
29	0.643679
30	0.643679

5.3 Results and Discussion

5.3.1 Effects of process parameters on closeness coefficient index (C+)

The alternative having the largest closeness coefficient is the best choice and according to that the ranking has been given in the descending order of the closeness coefficient. The maximum value of C+ shows the optimal setting for process parameters. ANOVA Table 5.8 shows the significant factors and interactions of process parameters for both the performance characteristics simultaneously. The significant terms are temperature (T), depth of cut (d) and interaction between temperature (T) and feed rate (f). Among them cutting velocity (V) and feed (f) are the insignificant parameters which do not affect performance in an influensive manner. The preferred alternative having the highest ranking have maximum value 0.697267 of closeness coefficient. The main effect plot for C+ is shown in Figure 5.4. It is clearly indicated that the optimal setting for machining parameters for present experiment is T = 600°C (level 3), V = 21.5m/min (level 2), f = 0.075mm/rev (level 2) and d = 0.05mm (level 1). Table 5.7 represents optimal parametric setting and maximum mean value for each process parameters. Optimal result has been validated by accomplishing confirmatory test.

(i)   (ii)

(iii)   (iv)
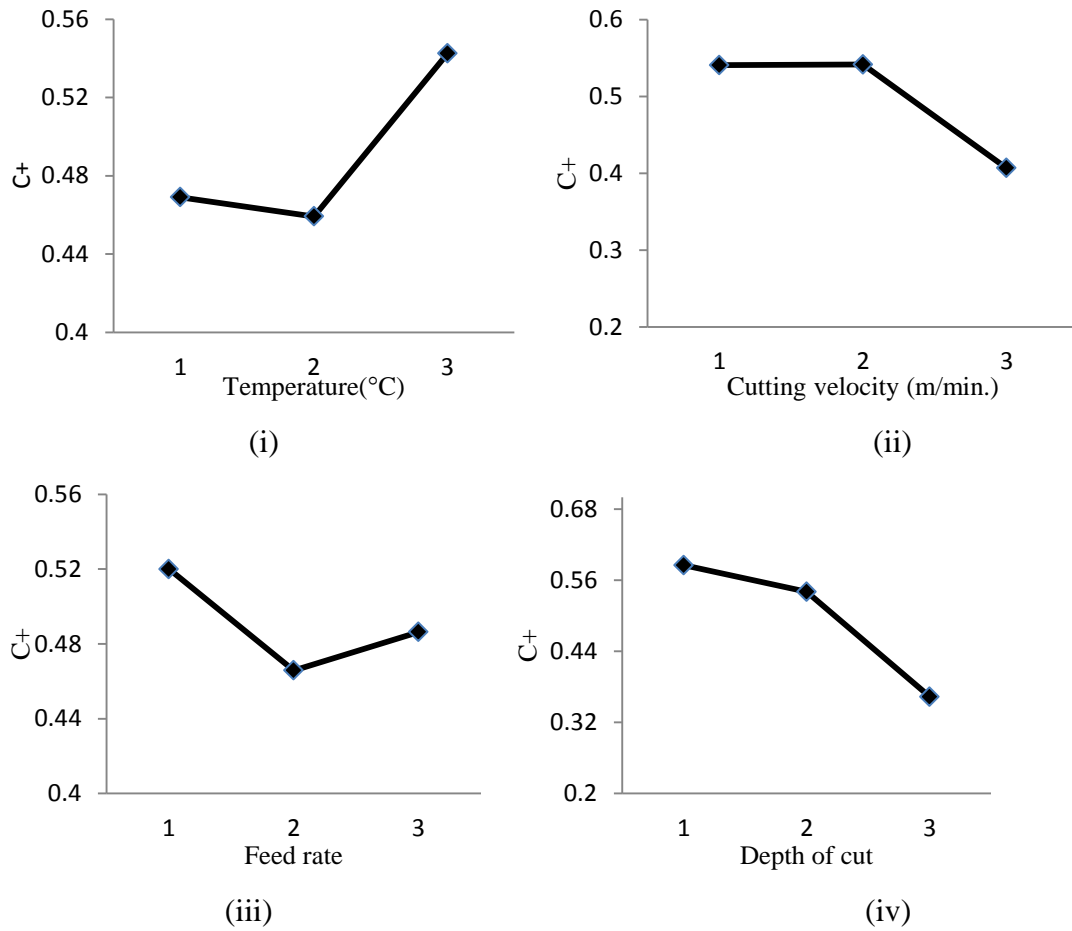
Figure 5.4: Main effects plot for Closeness coefficient index (C+)

Table 5.7: Response values for mean of Closeness coefficient index

Levels	T	V	f	d
1	0.4682	0.5312	0.5043	**0.5622**
2	0.5253	**0.5641**	**0.5273**	0.5613
3	**0.5322**	0.4324	0.4632	0.3582

Present work represents the selection of optimal level of process parameters in hot machining by considering the experimental results in terms of linguistic variables (based on experience and skills) in respect to avoid vagueness in data for maximizing tool life and reducing power consumption. Fuzzy TOPSIS favours to convert multi-response to single response optimization which makes ease to obtain optimal level for performances characteristics. Confirmation test (Table 5.9) reveals that there is an improvement in responses simultaneously.

Table 5.8: ANOVA for C+

Source	DF	Seq SS	Adj SS	Adj MS	F	p
T	1	0.16475	0.164755	0.164755	8.73	0.011*
V	1	0.02701	0.027007	0.027007	1.43	0.253
f	1	0.04793	0.047928	0.047928	2.54	0.135
d	1	0.14144	0.141438	0.141438	7.50	0.017*
T×T	1	0.01059	0.013019	0.013019	0.69	0.421
V×V	1	0.08915	0.054908	0.054908	2.91	0.112
f×f	1	0.00467	0.015151	0.015151	0.80	0.387
d×d	1	0.04523	0.045229	0.045229	2.40	0.146
T×V	1	0.00050	0.000499	0.000499	0.03	0.873
T×f	1	0.23479	0.234794	0.234794	12.44	0.004*
T×d	1	0.00000	0.000002	0.000002	0.00	0.991
V×f	1	0.00061	0.000608	0.000608	0.03	0.860
V×d	1	0.01154	0.011543	0.011543	0.61	0.448
f×d	1	0.02836	0.028358	0.028358	1.50	0.242
Total	29	1.08562				
*= These factors are significant at 95% confidence level						

Table 5.9: Confirmation table for closeness coefficient index (C+)

Levels	Initial setting T-3, V-1, f-1, d-1	Optimal setting T-3, V-2, f-2, d-1		
		Predicted	Experimental	Gain (%)
tl (min)	54	31	40	25.926
P(W)	603	570	538	10.779
C+	0.703137	0.697267		

5.4   Conclusion

1. The multi responses have been converted into single optimum setting of the process parameters which is known as relative closeness coefficient (C+). Highest level value of the C+ gives the optimum setting.

2. It was noticed that the optimal combination for the process parameters obtained as T= 600°C (level 3), V= 21.5m/min (level 2), f = 0.075 mm/min (level 2) and d= 0.5 mm (level 1).

3. Confirmation test has been done, and it is revealed that there is increase in tool life and decrease in power consumption by 25.926% in tool life and 10.779 % in power consumption.

Chapter 6

Prediction of temperature distribution using Finite Element Analysis

Chapter 6

Prediction of temperature distribution using Finite Element Analysis

6.1 Introduction

Traditionally, the turning operation has been used to reduce the diameter of cylindrical work piece. This is done by rotating the work piece about the machine's spindle and cutting the workpiece material with the cutting tool which is fed in the perpendicular direction. Repetition of such type of experiments require more initial investment, therefore Finite element method (FEM) is the only solution to overcome this high cost. In consequence, temperatures in the tool, chip and work piece, as well as cutting forces, plastic deformation (shear angles and chip thickness), chip formation can be determined faster by using FEM than using costly and time consuming experiments. FEM analysis is widely used for calculating stress, strain, cutting forces, temperature distributions in the primary, secondary and at tertiary cutting zones, etc.

From the past fifty years metal cutting researchers have developed many modelling techniques including analytical techniques, slip-line solutions, empirical approaches and finite element techniques. In recent years, the finite element analysis has particularly become the main tool for simulating metal cutting processes. The modelling and simulation of metal cutting have become very important in order to decrease the cost of experimental investigations. Plasticity based analytical modelling are used in predicting the mechanics of temperatures at the interface zone. These methods utilize and rely on work material constitutive models to simulate deformation conditions in metal cutting. Therefore, identification of constitutive material model parameters considering high-strain rate deformation characteristics is crucial.

In addition, this research includes the analysis for the results and graphs from simulation machining such as temperature versus time. The comparison has been made between simulation and experimental result.

6.2 FEM Description

DEFORM 3D is used for present analysis and the major input requisites is shown in

Appendice C. FEM consists of mainly three sections:

i. Pre-processor: The input data for materials and its conditions are fed into pre-processor.

ii. Simulator: Simulation done according to the data feeding for numerical calculations for turning operation.

iii. Post- processor: Used to view simulation data after the simulation has been run. Basic function is to read the database files from the simulation engine and representing the results in graphical and pictorial forms. It facilitates to view geometry field data such as temperature, stress, strain, forces direction, etc.

The procedure to achieve interface temperature is shown as flow chart represented by Figure 6.1.
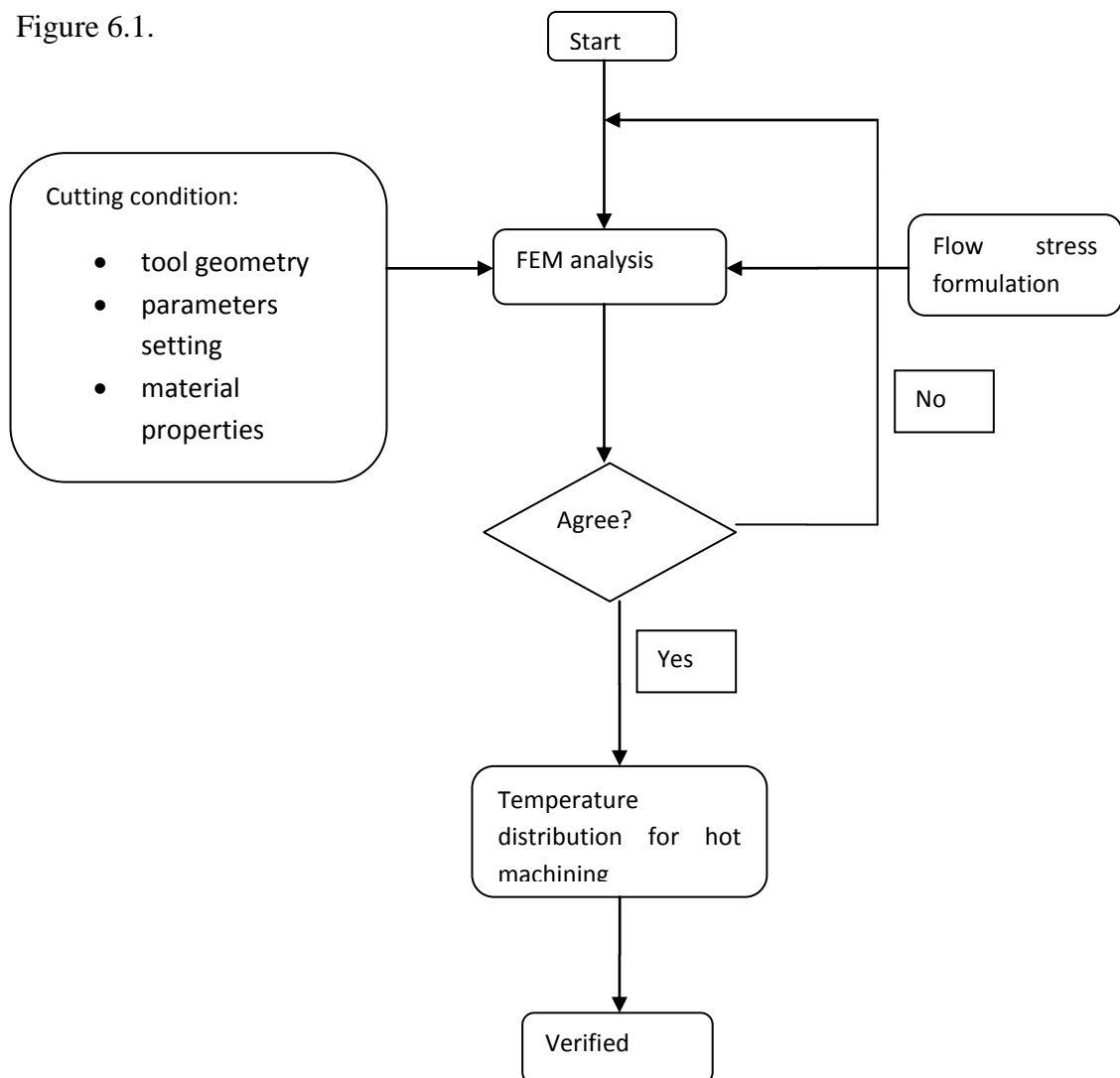

Figure 6.1 Process flow chart for FEM simulation

For analyzing the effects of the cutting parameters on the temperature at chip tool interface Taguchi design was used. According to Taguchi design, nine runs have been done to which cutting parameters has to vary at different levels. The experimental runs are represented by Table 2.9. The initial data, namely, the process parameters and conditions, work and cutting tool material properties, cutting speed, depth of cut, feed rate, environment temperature before modelling and simulation, other assumptions, etc. are to be fed as input in pre-processor.

6.2.1   Material models/design and methodology

Environment:

- Temperature-20 °C
- Convective coeffcieint-0.4 W /m^2°C
- Tool workpiece interface: shear friction factor- 0.6
- Heat transfer coefficient: 10000 W/m^2°C
- Tool – SNMG 120408 TTR 08 (Uncoated Tungsten Carbide P 30 Insert)

The geometry for SNMG is not available in DEFORM software. Therefore, geometry for cutting insert has been made in SOLID WORKS modelling software and then it was imported by converting it into *.stl* file. The shape of the tool is specified in a special sequence, called tool signature. According to Orthogonal Rake System (ORS):

$$\lambda - \gamma_0 - \alpha_0 - \alpha_0' - \phi_e - \phi - r \qquad\qquad (6.1)$$

λ (Inclination angle)   : 6˚

γ_0 (Orthogonal rake angle)   : 6˚

ϕ_e (End clearance angle)   : 6˚

ϕ (Side clearance angle   )   : 6˚

α_0 (Auxiliary cutting edge angle)   : 15˚

α_0' (Principal/ side cutting edge angle)   : 75˚

r (Nose radius)   : 0.8 mm

PSBNR 2525 M12 right hand tool holder has been used for turning operation.

Side cutting edge angle (SCEA) =6 ˚

Back rake angle (BR) = -6 ˚
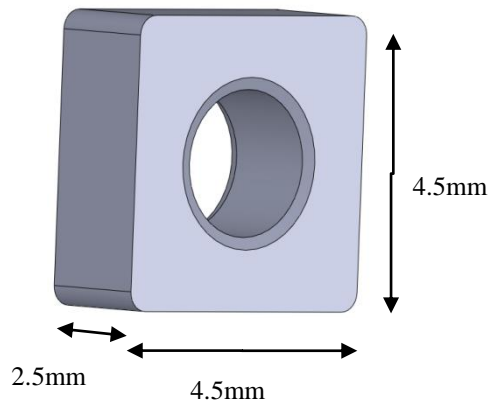
Side rake angle (SR) = -6 ˚

Figure 6.2 Solid works fig of tool with measurement

Table 6.1 Commercially available high manganese steel: Plastic type [68]

Properties		Units
Thermal conductivity	46.8	W/m-K
Hardness	42	HRC
Specific heat capacity	0.502	J/g-°C
Density	7.75	g/cc
Modulus of elasticity	201-209	GPa
Poisson Ratio	0.27-0.30	-
Shear Modulus	81.0-82.0	GPa
Tensile strength	1678	MPa

Here, in simulation SI unit conversion is used. Due to severe deformation at shear zone the Lagrangian formulation was used for thermo-mechanical finite element model of the plane-strain orthogonal metal cutting with a continuous chip formation produced by plane-faced uncoated carbide tools.

Here, a FE model of the whole workpice is used to evaluate temperature distribution in workpiece. Therefore, the time for an individual rotation of workpiece is less and simultaneously feed travel for one rotation is less. The rotational workpiece forces are significantly less than the cutting forces and therefore cutting forces are neglected for deformation in simulation. To facilitate the removal of material, it is meshed with respect to the tool path. Two kinds of shapes are available such as curved model and simplified model. As a circular shape is made up of infinite straight lines same as circular cylindrical shape is also made up of infinite straight paths having L length for

movement. In present work, simplified model is used for turning operation. The solid model of the insert is shown in Figure 6.2. The cutting tool material is taken as uncoated tungsten carbide (WC). Isometric view of the initial tool/workpiece mesh configuration, where +Y is the cutting direction, X is the feed direction and Z is the depth of cut direction.

It is very important to build the material models in order to get accuracy in simulation results. Material properties are further essential inputs to FEM analysis. The available mechanical and physical properties of work piece and tool materials are fed to pre-processor and finally develop the FE model. The unsteady state three-dimensional heat-conduction equation can be written as [69]:

$$\frac{\partial^2 T}{\partial x^2} + \frac{\partial^2 T}{\partial y^2} + \frac{\partial^2 T}{\partial z^2} + \frac{q(x,y,z,t)}{k_T} = \frac{1}{\alpha_T}\frac{\partial T}{\partial t} \qquad (6.2)$$

where, K_T is the thermal conductivity, T the temperature, α_T the thermal diffusivity coefficient, ρ the density, Cp the heat capacity, t the time and T∞ the medium temperature. This equation is subjected to the following boundary conditions in the regions exposed to the environment: [70].

$$-k\frac{\partial T}{\partial n} = h(T - T_\infty) \qquad (6.3)$$

where, h is the heat transfer coefficient.

FE model assumptions:

1. Due to less temperature difference between tool and chip, therefore the value considered for h (heat transfer coefficient) should be constant.
2. The end boundaries far from the heat affected zone (HAZ) remains at room temperature (20°C).

Methodology adopted for simulation of hot machining operation is L9 orthogonal array for analysing temperature distribution. The flow stress, σ, depends on effective strain ε, strain rate $\dot{\varepsilon}_0$ &, and temperature, T, of the high strain rate deformations

exerted in the cutting zone [71]. The workpiece material is considered to be modelled by the Johnson Cook (JC) model as shown in equation below:

$$\sigma = A + B\,p^{n} + C\ln\left(\frac{\dot{p}}{\dot{\varepsilon}_{0}}\right)\left[1 - \left(\frac{\theta - \theta_{R}}{\theta_{m} - \theta_{R}}\right)^{m}\right]$$
(6.5)

where, p designates the equivalent strain, $\overset{0}{p}$ equivalent strain rate and A, B, C, n, m are the constants yield strength (MPa), hardening modulus (MPa), strain rate sensitivity coefficient, hardening coefficient and thermal softening coefficients respectively. The properties of the materials are entered in the programme as per Table 6.1.

During meshing tool insert has 30000 elements and number of elements for workpiece has been taken as 25% of feed. The tool is considered as rigid body and its material is taken as Tungsten carbide (WC). The automatic generation for the mesh was not adopted due to constant meshing gives impreciseness in predicted result. A finer meshing obtained at the insert tip and in the workpiece where tool comes first with contact to workpiece. Therefore, a fine meshing is required to obtain accurate result. Initially, the workpice was meshed equally throughout the material by 1401 ISO-parametric quadrilateral elements. For all cutting simulations conducted in this study, the Coulomb friction law is used. The friction modelling used can be represented by Equation 6.6.

$$\tau = \mu\sigma_{n}$$
(6.6)

where, τ denotes frictional stress, μ and σ_{n} denotes coefficient of friction and normal stress respectively.

6.2.4 Boundary condition

The displacement and thermal boundary conditions are applied to the work piece and cutting tool.

Workpiece: For a consistent cutting operation the workpiece material is fixed from all sides (X, Y, Z directions).

Tool: Cutting tool is considered as a rigid body and movement in +Y direction. The position of the tool with respect to workpiece is shown in Figure ....
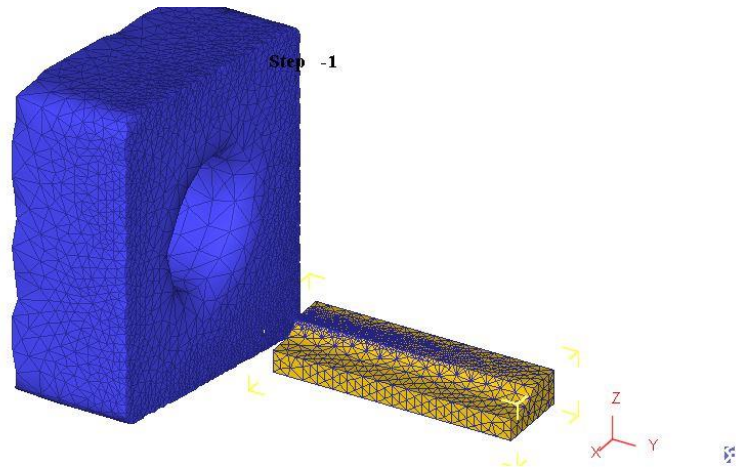
Figure . Tool position

6.3   Result and discussion

It was noticed that maximum temperature was found at the interface. The highest temperature of the workpiece surface, about 470°C, was located at a distance nearby the interface, this was due to high heat generation in the contact region between tool and work piece. Figure 6.3 reveals the simulated graphics for each run. It shows that the maximum temperature obtained at the interface of the tool and workpiece. The temperature far from interface has low temperature compared to the interface due to high heat generation at the interface. The largest deformation was occurred at the primary shear zone followed by the secondary shear zone. It causes high stress and heat generation. Effects of cutting parameters at chip tool interface temperature are discussed as follows:

(i) Effect of the workpiece temperature on temperature distribution

Workpiece temperature is the most important factor for analysing temperature distribution. Due to heating the workpiece at elevated temperature the resistance power for machining get reduced.

(ii) Effect of the cutting speed on Temperature distribution

Chip-tool interface temperature is directly related to cutting speed. It may possibly due to increase of cutting speed friction increases and this induces an increase in temperature in the shear zone.

(iii) Effect of the cutting feed on Temperature distribution

The increase in feed rate, section of chip increases and consequently increases friction. Due to increase in friction temperature also increases.

(iv) Effect of the depth of cut on Temperature distribution

It was observed that by increasing depth of cut, the cutting temperature also increases. With increase in depth of cut, the section of chip increases which increases friction at chip-tool increases that what leads to increase in temperature.

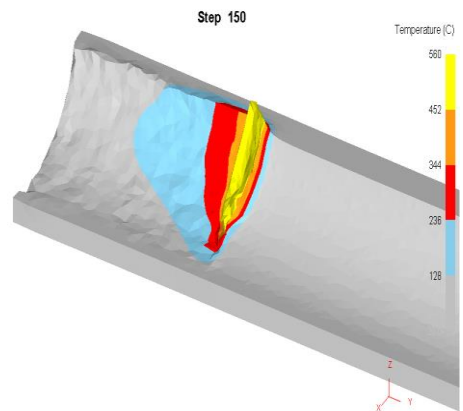Result obtained from the simulation for high manganese in hot turning operation are summarised as follows:
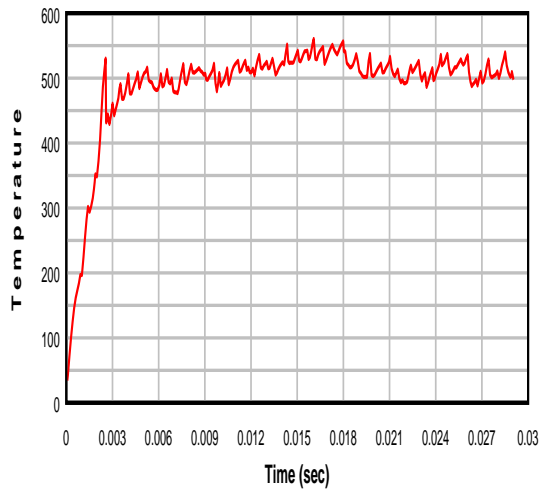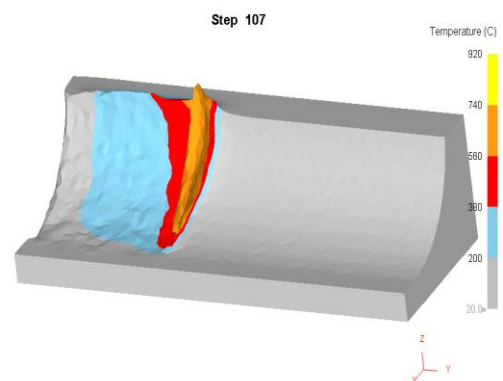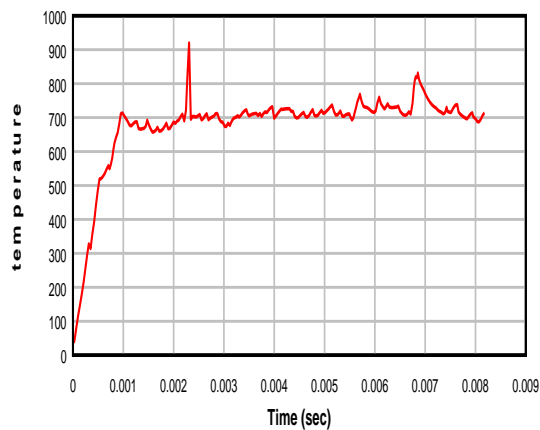

Figure (i)

Figure (ii)
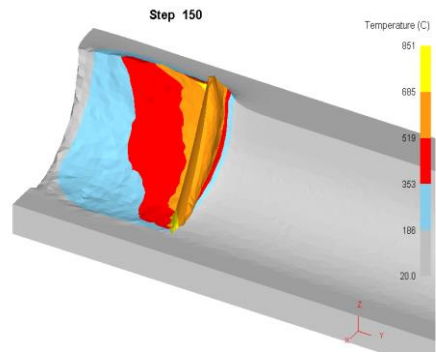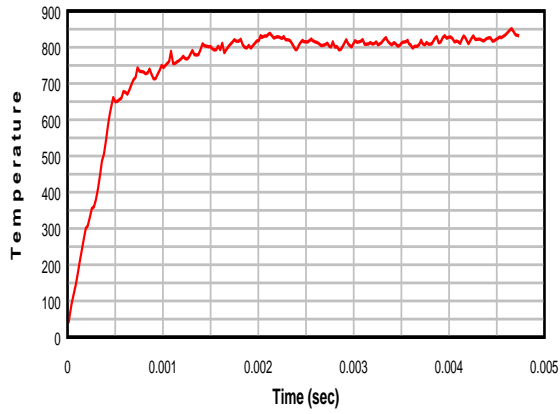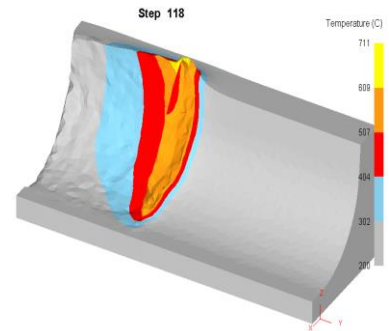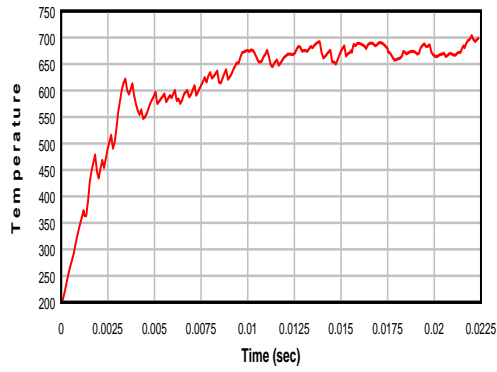
Figure (iii)
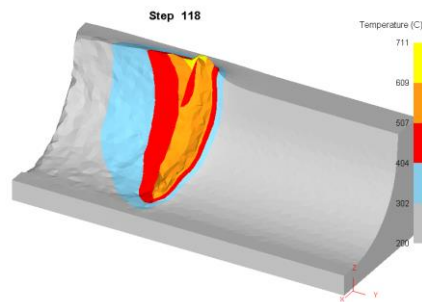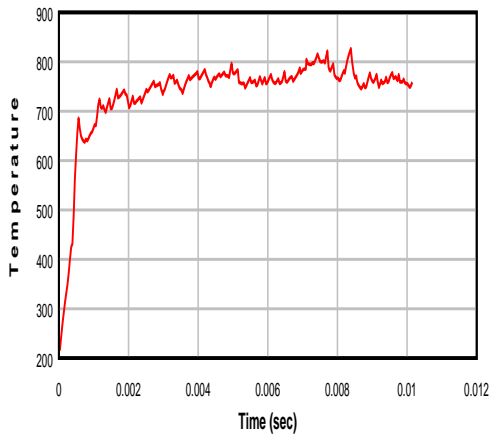
Figure (iv)

Figure (v)
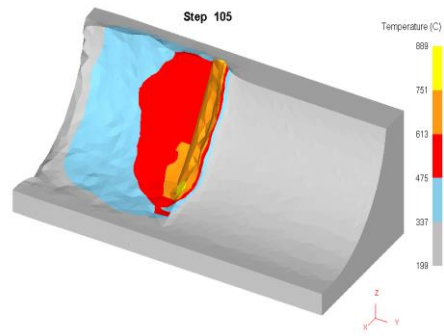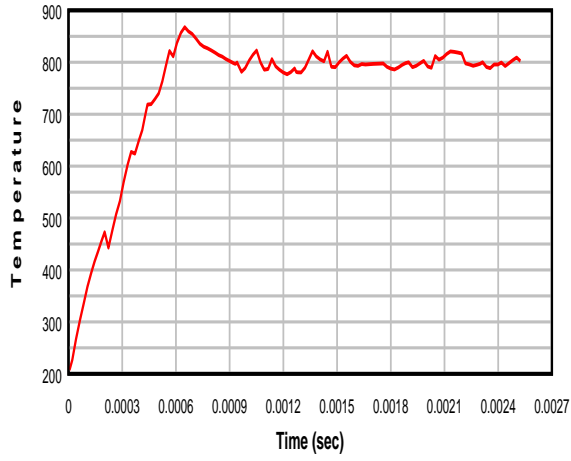
Figure (vi)
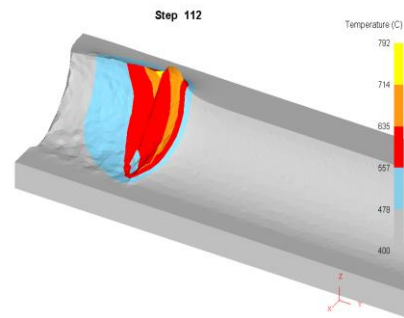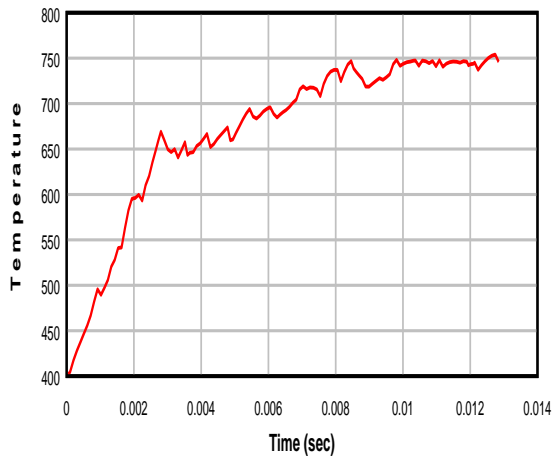
Figure (vii)
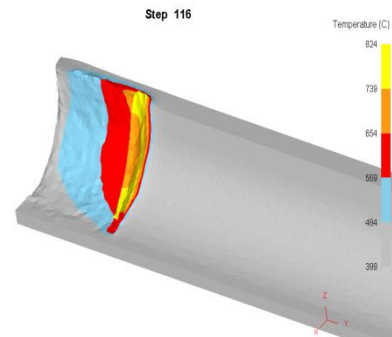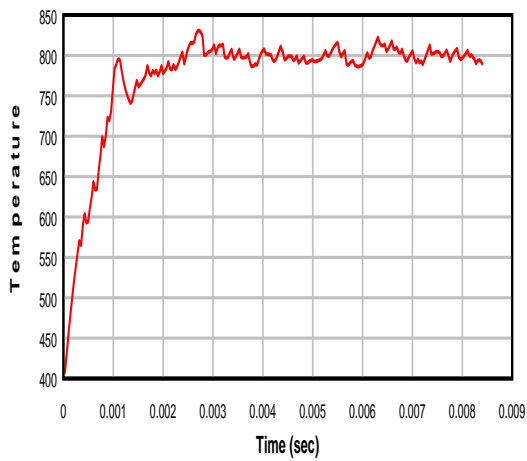
Figure (viii)
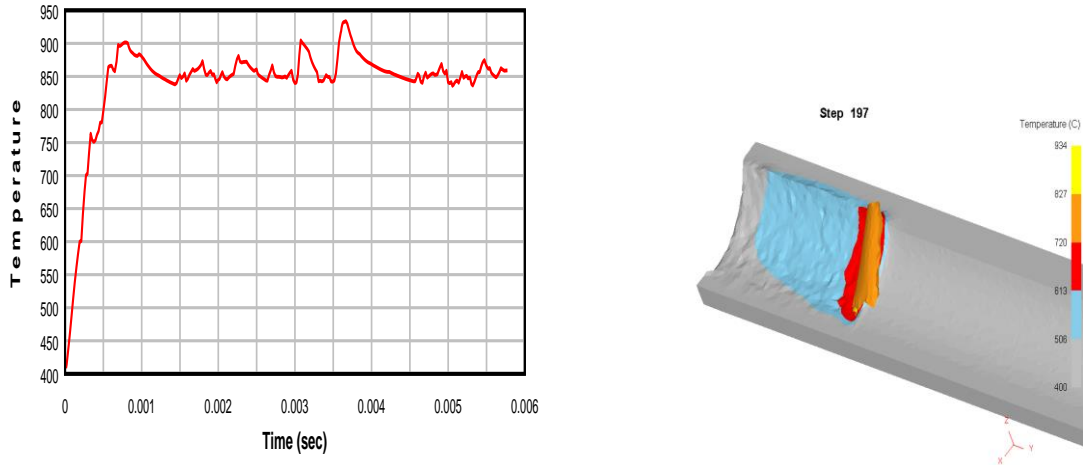
Figure (ix)

Figure 6.3 Temperature vs Time

6.4 Comparison of Simulated results with experimental results

Tool surface nodes are continuously tracked for chip tool interface. For validation, comparison has been done between predicted result and experiment result for temperature distribution. Experimental values obtained are shown in Table 2.9. The error between the experimental result and predicted results are evaluated using Equation 22. Error present in the temperature measurement is shown in Table 6.2.

$$\text{Percentage of error} = \frac{\left|X_{def} - X_{exp}\right|}{X_{exp}} \times 100 \qquad (6.7)$$

where, X_{def} is the DEFORM simulated value and X_{exp} is the experimental value. The percentage errors between the experimental and predicted results are less than 8.44 %, except in case of run 4 and 9 having 13.43% and 20.99% error respectively.

Table 6.2 Comparison of temperature distribution at chip tool interface for L9 experiments

Runs	Simulated temperature (^{o}C)	Experimental temperature(^{o}C)	Percentage error %
1	244	225	8.44
2	269	264	1.89
3	328	306	7.12
4	532	469	13.43

5	492	476	3.36
6	455	435	4.59
7	559	558	0.18
8	633	615	2.93
9	634	524	20.99

6.6   Conclusion

3D turning is simulated by using FEM code of DEFORM 3D software. The following conclusions can be made from the present study:

1. FEM predicted temperature is found to be well validated with the experimental interface temperature.

2. The maximum temperature was found at the vicinity (primary shear zone) of the shear zone.

Proposed model may give better accurate results if h was considered because it depends on pressure and temperature.

Chapter 7

Conclusion and Scope for Future

Conclusion and Scope for Future

7.1   Conclusions

The following conclusions are made from the present work:

1. Experimental investigation of hot machining operation of high manganese steel has been carried out using gas flame heating technique. The temperature of workpiece is varied from 200°C to 600°C.

2. It is observed that tool wear, surface roughness, chip reduction coefficient and power decreases with increase in temperature of workpiece in heated condition.

3. It is observed that there is maximum reduction of 53.26% tool wear, 68.35% surface roughness and 72.13% of chip reduction coefficient at 600°C compared to machining at room temperature for high manganese steel.

4. It is also observed that microhardness increases from the centre to the edge of the sample. It is also seen that mocrohardness increases with increase in cutting velocity.

5. Experimental investigation has been carried out to predict tool wear, surface roughness, chip reduction coefficient, tool life and power consumption using response surface methodology.

6. From response surface methodology it is evident that cutting velocity is significant factor for tool wear, tool life and power consumption, while feed and depth of cut is significant for surface roughness and feed is significant for chip reduction coefficient.

7. The performance characteristics (tool wear, surface roughness and chip reduction coefficient) has been analysed with the use of statistical technique such as principal component analysis (PCA) coupled with grey relational analysis (GRA) and weighted principal component analysis (WPCA) approach is found to be more efficient.

8. The best combination of process parameters has been obtained using Fuzzy TOPSIS (Technique for Order of Preference by Similarity to Ideal Solution) for tool life and power consumption simultaneously as 600°C, 21.5m/min, 0.075mm/rev and 0.5mm depth of cut.

9. Finite element analysis based on DEFORM 3D was used successfully to analyse interface temperature at tool and workpiece. Maximum 615°C is obtained at 400°C, 32m/min, 0.05mm/rev. and 1.0mm depth of cut and 633°C interface temperature is obtained from FEM modelling.

7.2   Scope for future work

1. Experimental investigation of hot-machining operation of other hard materials can be carried out.
2. FEM modelling of the process can be carried out to determine cutting forces for hot machining operation.
3. Experimental investigation can be carried out using other heating techniques.

References:

[1]   G Madhavulu and B. Ahmed, Hot Machining Process for improved Metal Removal Rates in turning operations, Int. J. of Mater. Process Technol. 44 (1994) 199-206.

[2]   M. Dwami, M. Zadshakoyan, Investigation of Tool Temperature and Surface Quality in Hot machining of Hard to Cut, Int. J. of World Academy of Science and Technology, 46 (2008) 10-27.

[3]   N. Tosun, L. Ozler, Optimization for hot turning operations with multiple performance characteristics, Int. J. Adv. Manuf. Technology, 23 (2004) 777-782.

[4]   C. H. Che-Haron, A. Jawaid, The effect of machining on surface integrity of titanium Alloy Ti–6%Al–4%V, J. of Materials Processing Technology. 166 (2005) 188–192.

[5]   C. F. Ho, Hot machining of alloy steels, 1976, The University of Hong Kong.

[6]   L. Ozler, A. Inan, C. Ozel, Theoretical and experimental determination of tool life in hot machining of austenitic manganese steel, Int. J. of Machine Tools & Manufacture 41 (2001) 163-172.

[7]   N. Tosun, L. Ozler, Optimization for hot turning operations with multiple performance characteristics, Int. J. Adv. Manuf. Technology, 23 (2004) 777-782.

[8]   P. C. Sharma, Machining- Fundamental and recent advances, 2008.

[9]   M. Baili, V. Wagner, G. Dessein, An experimental investigation of hot machining with induction to improve Ti-5553 machinability, Applied mechanics and Materials, 62, (2011) 67-76.

[10]   T. Kitagawa, K. Maekawa, Plasma hot machining for new engineering materials, Int. Conference on the behaviour of materials in machining, Stratford-upon-Avon, U.K., 139 (1990) 251-267.

[11]   M. T. Rajopadhye, N. S. Telsang, Dhole, Experimental set up for hot machining process to increase tool life with Torch flame, IOSR Journal of Mechanical and Civil Engineering (IOSR-JMCE), (2009) pp. 58-62.

[12]   Z. Y. Wang, K. P. Rajurkar, J. Fan, S. Lei, Y. C. Shin, G. Petrescu, Hybrid machining of Inconel 718, Int. J. of Machine Tools & Manufacture. 43 (2003) 1391–1396.

[13]   L. Popa, Complex Study of Plasma Hot Machining (PMP), Nonconventional Technologies Review 2012 Romanian Association of Nonconventional Technologies Romania, (2012) 26-33.

[14]   S. R. Deshmukh, B. K. Borkar, Tool Life Analysis by using FEA of Multilayer Coated Carbide Insert, Int. J. of Engineering Research & Technology (IJERT), 2(6) (2013) 3408- 3417.

[15]   Raczkovi, Tool life of cutting tool in case of hard turning, Hungarian J. of Industrial Chemistry Veszprem, (38(2) 2010) 133-136.

[16]   N. A. Talib, Studying the effect of cutting speed and feed rate on tool life in the turning processes, Diyala J. of Engineering Sciences, (2010) 181-194.

[17]   D. K. PAL and S. K. Basu, Hot Machining of Austenitic Manganese Steel by Shaping, Int. J. of Mach. Tools and Manufacture, 11 (1969) 45-61.

[18]   E. Kuljanic, M. Sortino, G. Totis, F. Prosperi, Evaluation Of Commercial Tools For Machining Special-Alloy Hadfield Steel, (2010) 96- 99.

[19]   J. Kopac, Hardening phenomena of Mn-austenite steels in the cutting process, J. of Materials Processing Technology, 109 (2001) 96-104.

[20]   Y. Jeon, Park, H.W. Lee, C. M. Current Research Trends in External Energy Assisted Machining, Int. J. of Precision Engineering and Manufacturing, 14 (2013) 337-342.

[21]   S. Raganthan, T. Senthivelan, Optimizing the process parameters on tool wear of WC insert when hot turning of AISI 316 stainless steel, Int. J. of Materials and Manufacturing, 5 (2010) 24–35.

[22]   S. Ranganathan, T. Senthilvelan, Multi-response optimization of machining parameters in hot turning using grey analysis. Int. J of Adv. Manufacturing and Technology, 56 (2011) 455-462.

[23]   K. P. Maity, P. K. Swain, An experimental investigation of hot-machining to predict tool life, Int. J. of Materials processing Technology, 198 (2008) 344-349.

[24]   A. K. Sahoo, T. Mohanty, Optimization of multiple performance characteristics in turning using Taguchi's quality loss function: An experimental investigation, Int. J. of Industrial Engineering Computations, 4 (2013) 325–336.

[25]   M. A. Lajis, A. K. M. N. Amin, A.N.M. Karim, H.C.D.M. Radzi, T.L. Ginta, Hot Machining of Hardened Steels with Coated Carbide Inserts, American J. of Engineering and Applied Sciences, 2 (2) (2009) 421-427.

[26]   K. C. Lo, N.N.S. Chen, Factors affecting tool life in hot machining of alloy steels. Int. J. of Machine Tool Design, 14 (1977) 161-173.

[27]   B. Fnides, M. A. Yallese, T. Mabrouki, J. F. Rigal, Application of response surface methodology for determining cutting force model in turning hardened AISI H 11 hot work tool steel, Int. J. of Indian Academy of Sciences, 36 (2011) 109–123.

[28]   L. Ozler, A. Inan, C. Ozel, Theoretical and experimental determination of tool life in hot machining of austenitic manganese steel, Int. J. of Machine Tools & Manufacture 41 (2001) 163-172.

[29]   N. Tosun, L. Ozler, A study of tool life in hot machining using artificial neural networks and regression analysis method, 2002, Journal of Materials Processing Technology, 124, 99-104

[30]   R. Rai, A. Kumar, S. Shrikantha, S. Rao., Development of a surface roughness prediction system for machining og hot chromium steel (AISI H11) based on Artificial neural network, APRN J. of Engineering and Applied Sciences 5(15) (2010) 53-59.

[31] M. A. Lajis, A. K. M. N. Amin, A. N. M. Karim, Surface Integrity in Hot Machining of AISI D2 Hardened Steel, Int. J. of Advanced Materials Research, 500 (2012) 44-50.

[32] S. Ranganathan, T. Senthilvelan, G. Sriram, Evaluation of Machining Parameters of Hot Turning of Stainless Steel (Type316) by Applying ANN and RSM, Int. J. of Materials and Manufacturing Processes, 25 (2010) 1131–1141.

[33] S. Ranganathan, T. Senthilvelan, Multi-response optimization of machining parameters in hot turning using grey analysis, Int. J. ManufTechol, 55 (2011) 455-462.

[34] R. Chakravorty, S. K. Gauri, S. Chakraborty, Optimization of Correlated Responses of EDM Process, Int. J. of Materials and Manufacturing processes, 27 (2012) 337-347.

[35] M. K. Pradhan, Estimating the effect of process parameters on MRR, TWR and radial overcut of EDMed AISI D2 tool steel by RSM and GRA coupled with PCA, 2013, Int. J. of Advanced Manufacturing Technology, 68 (2013) 591-605.

[36] A. N. Siddiquee, Z. A. Khan, Z. Mallik, Grey relational analysis coupled with principal component analysis for optimisation design of the process parameters in in-feed centreless cylindrical grinding, Int. J. of Advanced Manufacturing Technology, 46 (2010) 983–992.

[37] H. S. Lu, C. K. Chang, C. T. Chung, Grey relational analysis coupled with principal component Analysis for optimization design of the cutting parameters in high-speed end milling, Int. J. of Advanced Manufacturing Technology, (2009) 3808-3819.

[38] N. Tosun, L. Ozler, Optimization for hot turning operations with multiple performance characteristics, Int. J. of Advanced Manufacturing Technology, 23 (2004), 777-782.

[39] D. L. Olson, Comparison of Weights in TOPSIS Models, Int. J. of Mathematical and Computer Modelling, (2004).

[40] G.A.M.S. Wimatsari, K.G.D. Putra, P. W. Buana, Multi-Attribute Decision Making Scholarship Selection Using A Modified Fuzzy TOPSIS, Int. J. of Computer Science, 10(1) (2013) 309-317.

[41] J. Jiang, Y. Chen, Y. Chen, K. Yang, TOPSIS with fuzzy belief structure for group belief multiple criteria decision making, Expert Systems with Applications, 3 (2011) 9400–9406.

[42] I. Chamodrakas, N. Alexopoulou, D. Martakos, Customer evaluation for order acceptance using a novel class of fuzzy methods based on TOPSIS, Expert Systems with Applications, (2009) 7409- 7415.

[43] S. M. Holland, Principal component analysis (PCA), Department of Geology, University of Georgia Athens GA, 2008.

[44] W. Xu, X. Liu, J. Song, J. Sun, L. Zhang, Finite element simulation and experimental research on electric hot machining, Int. J. of Advanced Manufacturing Technology, (2012).

[45]   T. Tamizharasan, N. Kumar, Optimization of cutting insert geometry using deform 3d-numericak simulation and experimental validation, Int. J. of Simulation modelling, 11(2) (2012) 65-76.

[46]   I. Tanase, V. Popovici, G. Ceau, G. N. Predincea, cutting edge temperature prediction using the process simulation with deform 3d software package, Proceedings in Manufacturing Systems, 7(4) (2012).

[47]   Y. R. Bhoyar, P. D. Kamble, Finite Element Analysis on Temperature Distribution of Turning Process, Int. J. of Modern Engineering Research (IJMER), 3(1) (2013) 541-546.

[48]   A. G. Jaharah, Y. Hendri, C. H. Che-Hassan, R. Ramli, Z. Yaakob, Simulation of Turning Process of AISI 1045 and Carbide Tool Using Finite Element Method, Proc. Of the 7th WSEAS Int. Conf. on Computational Intelligence, Man-Machine Systems and Cybernetics (CIMMACS '08), (2008) 152-158.

[49]   C. Ezilarasan,V. S. Senthilkumar, A. Velayudham, Theoretical predictions and experimental validations on machining the Nimonic C-263 super alloy, Int. J. of Simulation Modelling Practice and Theory, 40 (2014) 192-207.

[50]   S. D. Ghodam, Review of Effects of Temperature Distribution on Tool Life in Turning Process by using Finite Element Analysis, Int. J. of Scientific Engineering and Research (IJSER), 1(2) (2013) 84-87.

[51]   R. Komanduri, Z. B. Hou, A review of the experimental techniques for the measurement of heat and temperatures generated in some manufacturing processes, Int. J. of Tribology International, 34 (2001) 653-682.

[52]   Y. Huang, S. Y. Liang, Cutting Temperature Modelling Based on Non-Uniform Heat Intensity and Partition Ratio, Int. J. of Machining Science and Technology, 9 (2005) 301-323.

[53]   F. Klocke, H. Kratz, Advanced Tool Edge Geometry for High Precision Hard Turning, Aachen University.

[54]   E. Uhlmann, M. G. Schulenburg, R. Zettier, Finite Element Modelling and Cutting Simulation of Inconel 718, Int. J. of CIRP Annals- Manufacturing Technology, 56 (2007) 61-64.

[55]   S. J. Yaseen, Theoretical study of temperature distribution and heat flux variation in turning process, Int. J. of Engineering Sciences, 5(3) (2012) 299-313.

[56]   L. B. Abhang, M. Hameedullah, Chip-Tool Interface Temperature Prediction Model for Turning Process, Int. J. of Engineering Science and Technology, 2(4), (2010) 382-393.

[57]   A. A. Kawi, Temperatures behaviour of some alloy steels in turning process under different operating Conditions, Int. J. of Engineering Science and Technology, (2011) 4(3).

[58] W. Grzesik, M. Bartoszuk, P. Niesłony, Finite element modelling of temperature distribution in the cutting zone in turning processes with differently coated tools, Int. J. of Materials Processing Technology, 164–165 (2005) 1204–1211.

[59] J. Petru, R. Cep, M. Grepl, L, Petrkovska, Effect of high feed milling on the microstructure and microhardness of surface layer, Proceedings of the 22nd International DAAAM Symposium, 22 (2011) 999-1000.

[60] D. G. Thakur, B. Ramamoorthy, L. Vijayaraghavan, Effect of High Speed Cutting Parameters on the Surface Characteristics of Superalloy Inconel 718, Proceedings of the World Congress on Engineering 2010 London, U.K. 3 (2010).

[61] H. Autenrieth, B. Okolo, V. Schulze, A. Wanner, Surface Workhardening and Residual Stresses Induced By Micro Cutting Processes, International Centre for Diffraction Data, (2009) pp. 608-615.

[62] O. Sarikaya, Effect of some parameters on microstructure and hardness of alumina Coatings prepared by the air plasma spraying process, Int. J. of Surface and Coatings Technology, 190 (2005) 388-393.

[63] D. Jaiswal, Analysing the Effect of Parameters in Multipass Submerged arc Welding Process, Int. J. of Theoretical and Applied Research in Mechanical Engineering (IJTARME), 2(2) (2013) 2319 – 3182.

[64] S. A. Alrabii, L. Y. Zumot, Chip Thickness and Microhardness Prediction Models during Turning of Medium Carbon Steel, Int. J. of Applied Mathematics, (2007).

[65] G. Krolczyk, P. Nieslony, S. Legutko, Microhardness and Surface Integrity in Turning Process Of Duplex Stainless Steel (DSS) for Different Cutting Conditions, Int. J. of Materials Engineering and performances, 23(3) (2013) 859–866.

[66] Alan Stone, Aston Metallurgical Services, Inc., and Daniel H. Herring, The Herring Group, Inc, Practical Considerations for Successful Hardness Testing, Int. J. of Mterials Testing & Characterisation, (2006) pp. 83- 85.

[67] A. I. Khuri, S. Mukhopadhyay, Response surface methodology, John Wiley & Sons, 2, (2010).

[68] J. E. Bringas, Handbook of Comparative World Steel Standards, 2nd edition, 2004.

[69] A. Molinari, A. Moufki, A new thermo mechanical model of cutting applied to turning operations. Part I. Theory, International Journal of Machine Tools & Manufacture, 2005, vol. 45, pp.166–180.

[70] K. Raja, Cutting tool temperatures in interrupted cutting, the effect of feed-direction modulation. Journal of Manufacturing Processes, 2009, 28 May.

[71] T. Ozel, Y. Karpat, Identification of constitutive material model parameters for high-strain rate metal cutting conditions using evolutionary computational algorithms, Materials and manufacturing processes, 22 (2007) 659-667.
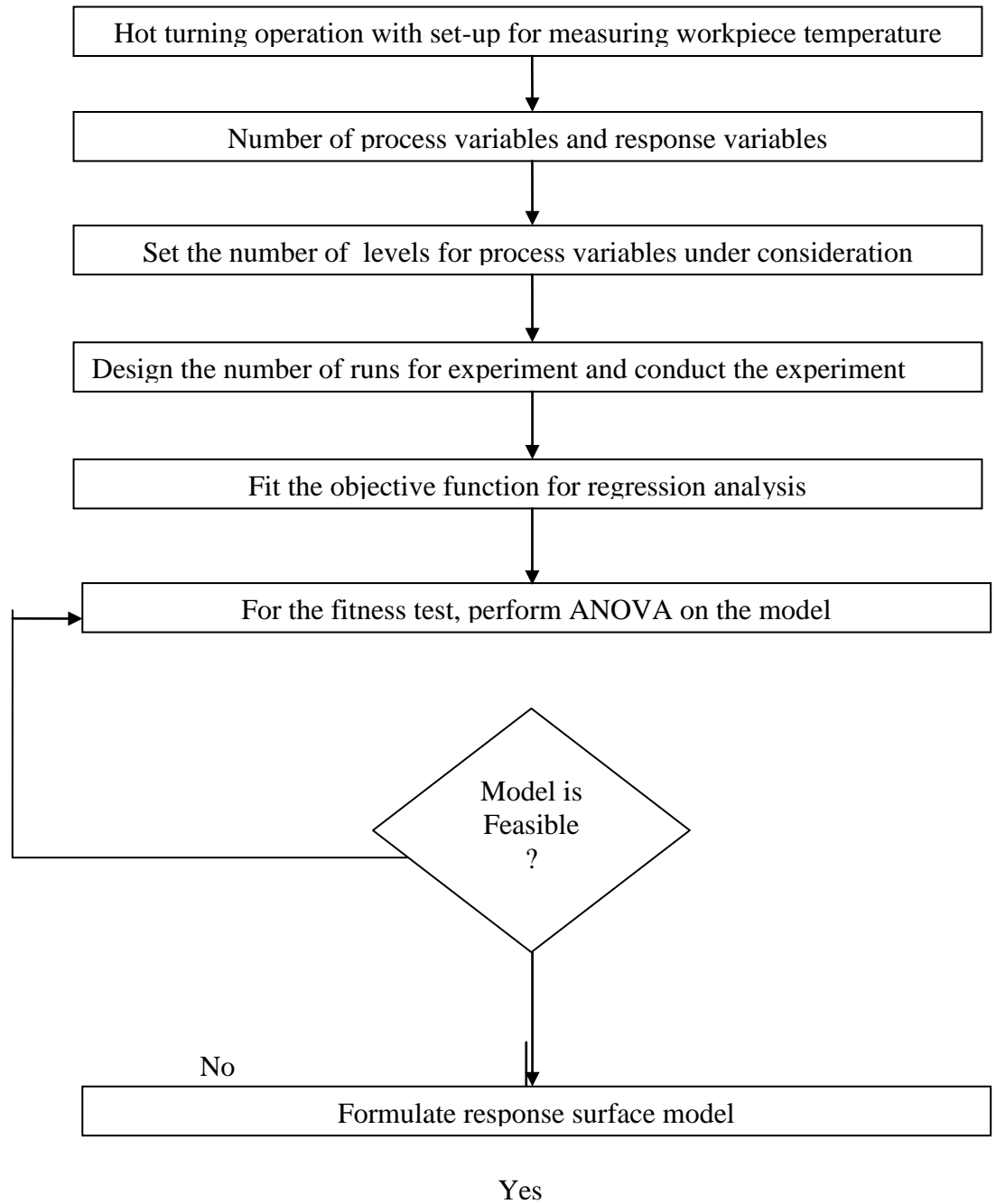
Appendice A

Hot turning operation with set-up for measuring workpiece temperature

↓

Number of process variables and response variables

↓

Set the number of levels for process variables under consideration

↓

Design the number of runs for experiment and conduct the experiment

↓

Fit the objective function for regression analysis

↓

For the fitness test, perform ANOVA on the model

Model is
Feasible
?

No

Formulate response surface model

Yes

Figure A1 Flow chart for RSM design

Appendice B

ANOVA test

The purpose of finding sum of squares (SS) is to find out variation which is explained by each factor. The sources of variation were obtained by finding its "sum of squares". The sum of all the "sums of squares" is equals to the total sum of squares for all the variations. The test works by comparing the variation due to each factor to the 'common cause variation'. Sum of Squares (SS) is the sum of squared distances. SS_{Total} is defined as the total variation in the data and SS Regression is defined as the portion of the variation explained by the model, while SS Error is defined as the portion not explained by the model and is attributed to error. The calculations are:

$$SS_{Regression}=\sum(\hat{y}-y)^2$$
$$SS_{Error}=\sum(y-\hat{y})^2 \tag{B.1}$$

$$SSTotal=SSregression+SSError$$
$$=(\hat{y}-y)^2+S(y-\hat{y})^2$$
$$=S(y-\hat{y})^2 \tag{B.2}$$

where, y = observed response, $\hat{y}$ = fitted response, and y = mean response. The sequential sums of squares depend on the order of the terms that are entered into the model.

Degree of Freedom (DOF)

DOF indicate the number of independent part of information involved in the response data needed to calculate the sum of squares. The degrees of freedom for each component of the model are shown by the following equations:

$$DFRegression=p-1$$
$$DF\ Error = n-p$$
$$Total=n-1 \tag{B.3}$$

where, n = number of observations and p = number of terms in the model.

Mean Square

From ANOVA test, the term Mean Square (MS) refers for estimation of population variance based on the variability among a given set of measures. The calculation for the mean square for the model terms is defined by following equation:

$$MS = \frac{AdjSS}{DF}$$
(B.4)

- F-value

F-value gives the distance measurement between the individual distributions. The increment in F-value gives decrement in p-value. F-test is a test used to determine the significant factors and significant interactions. The formula of F for the model terms is defined as in following equation:

$$F = \frac{MS}{MS(Error)}$$
(B.5)

Larger values of F support rejecting the null hypothesis that there is not a significant effect.

- p-value

The p-value is used for hypothesis testing to decide whether to reject or to fail to reject a null hypothesis. Generally, the cut-off value for the p-value is considered as 0.05. The null hypothesis is rejected when the p-value of a test statistic is less than 0.05

- Model Adequacy

The adequacy of model should be checked before concluding the result. The adequacy of model is checked by following steps:

➢ Verify that none of the least square regression assumptions are violated. The ordinary R^2 is

$$R^2 = \frac{SS_{regression}}{SS_{total}}$$
(B.6)

➢ R^2 (R-sq): Coefficient of determination

It indicates the variation in the response explained by the model. The higher the R^2 value, the better the model fits the data. It can be evaluated by following Equation (B.7):

$$R^2 = 1 - \frac{\text{SS Error}}{\text{SS Total}}$$

(B.7)

Adjusted R^2 (R-sq (adj)):

Adjusted R^2 accounts for the number of factors in the model. It can be evaluated by Equation (B.8).

$$R^2 = 1 - \frac{\text{MS(Error)}}{\text{SS total} / \text{DF Total}}$$
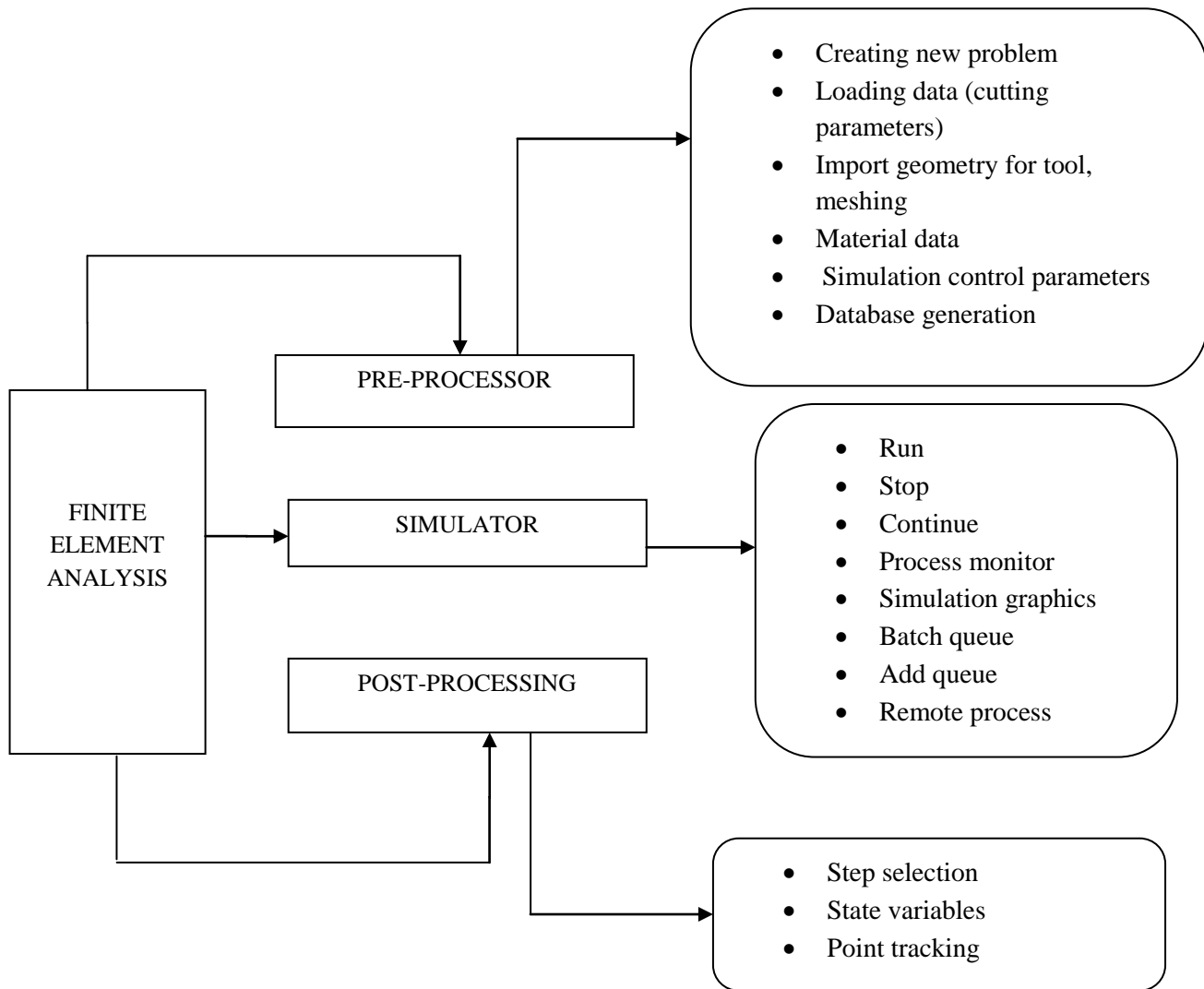
(B.8)

Appendice C

Figure C 1 Flow chart for FEM analysis

Bio data

Shalini Singh

E-mail: shalinisingh4190@gmail.com

Mobile no.: 9776457214

Education:

The author, Shalini Singh graduated in mechanical Engineering from Uttar Pradesh Technical University (UPTU) in 2011. Then she joined M. Tech. (Research) programme in 2012.

Personal information:

Date of birth: 04/01/1990

Nationality: Indian

Address: C-4 Afeem Kothi Colony

Patel nagar, Civil lines, Fatehpur

Dist.- Fatehpur, U.P., Pin -212601

List of publications

Journals

1. K. P. Maity and S. Singh, Multi-response Optimization In Hot Machining Operation Using Principal Component Analysis, J. of Materials and Manufacturing. (Communicated)
2. K. P. Maity and S. Singh, Multi-response optimization in hot machining operation using fuzzy TOPSIS. Advances in manufacturing. (Communicated)
3. K. P. Maity and S. Singh, Multi-response optimization of hot turning operation using Fuzzy TOPSIS, J. of the Brazilian Society of Mechanical Sciences and Engineering. (Communicated)

International Conferences

1. K. P. Maity and Shalini Singh, Experimental Investigation of Hot Machining by using RSM coupled with Grey Relational Analysis, Int. Conference on Engineering (NUiCONE 2013), November 13, Ahmadabad, Gujarat.
2. S. Singh and K. P. Maity, Multi-response optimization of machining parameters in hot turning using PCA coupled with TOPSIS, Int. conference on design and manufacturing (IDMC 14), March 14, NIT Rourkela, Odisha.